Effects of selected natural products on human immunocompetent cells

Inauguraldissertation

zur Erlangung der Würde eines Doktors der Philosophie

vorgelegt der Philosophisch-Naturwissenschaftlichen Fakultät

der Universität Basel

von

Amy Marisa Zimmermann-Klemd

Basel, 2020

Genehmigt von der Philosophisch-Naturwissenschaftlichen Fakultät auf Antrag von

Prof. Dr. Carsten Gründemann

Prof. Dr. Matthias Hamburger

Prof. Dr. Jörg Heilmann

Basel, den 17. März 2020

Prof. Dr. Martin Spiess

Dekan

Attribution-NonCommercial-NoDerivatives 4.0 International
(CC BY-NC-ND 4.0)

You are free to: Share — copy and redistribute the material in any medium or format

The licensor cannot revoke these freedoms as long as you follow the license terms.

Attribution — You must give appropriate credit, provide a link to the license, and indicate if changes were made. You may do so in

NonCommercial — You may not use the material for commercial purposes.

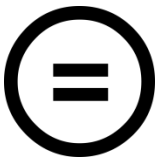

NoDerivatives — If you remix, transform, or build upon the material, you may not distribute the modified material.

No additional restrictions — You may not apply legal terms or technological measures that legally restrict others from doing anything the license permits.

Notices: You do not have to comply with the license for elements of the material in the public domain or where your use is permitted by an applicable exception or limitation.

No warranties are given. The license may not give you all of the permissions necessary for your intended use. For example, other rights such as publicity, privacy, or moral rights may limit how you use the material.

Source: https://creativecommons.org/licenses/by-nc-nd/4.0/ date: 21.01.2020

Table of contents

List of abbreviations I

Summary III

Zusammenfassung VI

1. Aim of work 1

2. Introduction 5

2.1. The human immune response 6

2.1.1. The innate immune response 6

2.1.2. The adaptive immune response 8

2.2. T cell signaling pathways 12

2.3. Autoimmune diseases 14

2.3.1. Treatment of autoimmune diseases 17

2.4. Natural product-based drug discovery 20

2.5. Reverse pharmacology approach 24

2.6. Cell-based *in vitro* test systems 26

2.7. Flow cytometry-based analysis 27

2.8. High-performance liquid chromatography (HPLC)-based activity profiling 29

3. Results and discussion 31

3.1. Sesquiterpene lactones from Artemisia argyi: absolute configuration and immunosuppressant activity 32

3.2. Immunosuppressive activity of *Artemisia argyi* extract and isolated compounds 43

3.3. *Boswellia carteri* extract and 3-O-acetyl-alpha-boswellic acid suppress T cell activation and function 57

3.4. Influence of traditionally used Nepalese plants on wound healing and immunological properties using primary human cells *in vitro* 66

4. Conclusion and outlook 76

5. Acknowledgments 84

Curriculum vitae 87

List of abbreviations

A. argyi	*Artemisia argyi*
ADAP	Adhesion and degranulation promoting adaptor protein
ADCC	Antibody-dependent cellular cytotoxicity
AICD	Activation-induced cell death
AIRE	Autoimmune regulator
AP-1	Activator protein 1
APC	Antigen presenting cell
BAFF	B cell activating factor
B. carteri	*Boswellia carteri*
Bcl-10	B cell lymphoma/leukemia 10
BCR	B cell receptor
B. longifolia	*Bassia longifolia*
CARMA1	CARD-containing MAGUK protein 1
CTLA-4	Cytotoxic T-lymphocyte-associated protein 4
CRAC	Calcium release-activated channel
DAG	Diacylglycerol
DAMPs	Damage associated molecular patterns
DC	Dendritic cell
DCM	Dichloromethane
DNA	Deoxyribonucleic acid
DMSO	Dimethyl sulfoxide
dsRNS	Double-stranded ribonucleic acid
ECD	Electronic circular dichroism
ELS	Evaporative light scattering
ER	Endoplasmic reticulum
Erk	Extracellular signal-regulated kinase
FCM	Flow cytometry
FDA	Food and Drug Administration
FEZF2	FEZ family zinc finger 2
Fsc	Forward scatter
G. arborea	*Gmelina arborea*
GFP	Green fluorescent protein
HMGB1	High-Mobility Group Protein B1
HPLC	High-performance liquid chromatography
HTS	High-throughput screenings
IC_{50}	Half maximal inhibitory concentration
IFN-γ	Interferon-γ
Igs	Immunoglobulins
IκB	Inhibitor of κB
IKK	IκB kinase
IL-1	Interleukin-1
IL-2	Interleukin-2
IL-4	Interleukin-4
IL-5	Interleukin-5
IL-6	Interleukin-6
IL-8	Interleukin-8
IL-9	Interleukin-9
IL-10	Interleukin-10

IL-13	Interleukin-13
IP3	Inositol trisphosphate
ITAM	immunoreceptor tyrosine-based activation motif
ITK	IL-2 inducible T cell kinase
Jakinhibs	Janus kinases inhibitors
JNK	Jun kinase
LAT	Linker for activation of T cells
LCK	Lymphocyte-specific protein tyrosine kinase
LPS	Lipopolysaccharides
MALT1	Mucosa-associated lymphoid tissue lymphoma translocation protein 1
MAPK	Mitogen-activated protein kinase
MS	Mass spectrometry
mTECs	Medullary thymic epithelial cells
mTor	Mammalian target of rapamycin
NFAT	Nuclear factor of activated T cells
NF-κB	Nuclear factor kappa-light-chain-enhancer of activated B cells
NK cell	Natural killer cell
NMR	Nuclear magnetic resonance
NOD-like receptors, NLRs	Nucleotide-binding oligomerization domain-like receptors
ORAI1	Calcium release-activated calcium channel protein 1
PAMPs	Pathogen-associated molecular patterns
PD-1	Programmed cell death protein 1
PD-L	PD-ligand
PIP_2	Phosphatidylinositol 4,5-bisphosphate
PKC-θ	Protein kinase C-θ
PLCγ1	Phospholipase Cγ1
PMTs	Photomultiplier tubes
PRRs	Pattern recognition receptors
RIG-like receptors, RLRs	Retinoic acid-inducible gene-I-like receptors
SLP76	SH2-domain-containing leukocyte protein of 76 kDa
SOCE	Store operated calcium entry
SR	Scavenger receptors
Ssc	Side scatter
STAT	Signal transducer and activator of transcription
STIM1	Stromal interaction molecule 1
TAP	Transporter associated with antigen processing
TCM	Traditional Chinese medicine
TCR	T cell receptor
TDC	Thymic dendritic cell
Tfh	Follicular T helper cells
TGF-β	Transforming growth factor β
TLR	Toll-like receptor
TNF α	Tumor necrosis factor α
Tregs	Regulatory T cells
UV	Ultraviolet
VCD	Vibrational circular dichroism
ZAP70	ζ -chain-associated protein kinase 70

Summary

The identification of new lead compounds, and the development of novel drugs for the treatment of autoimmune diseases, are of great importance, since today's available pharmaceuticals often have substantial limitations. Glucocorticoids and drugs that inhibit the deoxyribonucleic acid (DNA) synthesis (e.g. cyclophosphamide) often cause severe side effects, while state-of-the-art biologicals usually impose a heavy financial burden. Plant extracts are a good starting point for the development of immunosuppressive leads, since they are evolutionarily optimized to serve numerous biological functions. The track record of natural product drug discovery for immunosuppressive leads has been distinguished by blockbuster drugs, such as cyclosporin A or tacrolimus; however, a well-planned, multidisciplinary research approach is required for screening plant extracts, characterizing their effects, clarifying targets, and isolating bioactive compounds.

Enhanced T cell proliferation is a feature of autoimmune diseases such as rheumatoid arthritis or multiple sclerosis; therefore, as a starting point, this study investigated the T cell proliferation inhibitory potential of a library of 435 extracts, prepared from plants used in traditional Chinese medicine (TCM). The immunosuppressive activity of the extracts was assessed by a proliferation-based assay utilizing physiologically-relevant anti-CD3 and anti-CD28 stimulated primary human T lymphocytes. It showed that an *Artemisia argyi* (Asteraceae, *A. argyi*) ethyl acetate extract and a *Boswellia carteri* (Burseraceae, *B. carteri*) dichloromethane (DCM) extract were active, reflected by a half maximal inhibitory concentration (IC_{50}) of 16.2 µg/mL for the *A. argyi* extract and 27.0 µg/mL for *B. carteri* extract. The observed inhibitory effect on T cell proliferation was based on a specific intervention of T cell signaling via an interleukin-2 (IL-2)-dependent mechanism, rather than induced apoptosis or necrosis. Further characterizations revealed a reduced expression of the T cell activation markers CD25 and CD69, as well as a decreased production of IL-2 and interferon-γ (IFN-γ), by the *A. argyi* extract; the *B. carteri* extract also suppressed the IL-2 and IFN-γ secretion. Moreover, treatment with *B. carteri* extract resulted in a reduced degranulation capacity of stimulated T cells.

Both extracts were subjected to high-performance liquid chromatography (HPLC)-mass spectrometry (MS)-based activity profiling. A T cell proliferation assay identified 8-acetyl-artanomaloide, arteglasin A, jaceosidin, 1R-canin, and (4S,5S,6S,7S)- and (4R,5R,6S,7S)-seco-tanapartholides as active constituents of *A. argyi*. The proliferation assay showed that for *B. carteri*, 3-O-acetyl-8,24-dienetirucallic acid, 3-O-acetyl-7,24-dienetirucallic acid, 3-oxo-8,24-dienetirucallic acid and 3-O-acetyl-α-boswellic acid suppressed the proliferation of stimulated T lymphocytes.

To validate the target of the active *A. argyi* and *B. carteri* compounds, monitoring of the T cell signaling cascade was performed, starting with the IL-2 transcription factor activator protein 1 (AP-1), the nuclear factor kappa-light-chain-enhancer of activated B cells (NF-κB), and the nuclear factor of activated T cells (NFAT). Suppression of the NF-κB and NFAT activity, with IC_{50} values between 2.0 and

9.3 µM for NF-κB and 1.6 and 9.3 µM for NFAT, was detected for the *A. argyi* sesquiterpene lactones. 3-O-acetyl-alpha-boswellic acid was found to be the most promising candidate among the *B. carteri* compounds, as reflected by an IC_{50} value of 5.6 µM for NFAT activity suppression. For *A. argyi* the T cell signaling cascade monitoring was extended to the calcium flux in anti-CD3 stimulated Jurkat T cells. The results indicated a suppression of the calcium flux by 30 µg/mL *A. argyi* extract; however, no influence on the calcium flux of stimulated Jurkat T cells could be shown for the *A. argyi* compounds, suggesting that the crude plant extract may affect the signaling on a more upstream level than the single compounds, isolated thus far.

This study also evaluated the potential wound healing and immune modulating capacities of extracts from nine plants that are traditionally used in Nepal to improve wound healing. An ethyl acetate extract of *Gmelina arborea* (Lamiaceae, *G. arborea*) positively influenced the wound-healing capacity of human keratinocytes and fibroblasts.

For satisfactory wound healing, a balance between pathogen clearance by inflammatory feedback loops, and regulatory mechanisms to prevent fatal inflammatory responses, is essential; thus, the influence of the extracts on inflammation parameters was addressed. The *G. arborea* ethyl acetate extract, and an ethyl acetate extract from *Bassia longifolia* (Sapotaceae, *B. longifolia*), concentration-dependently inhibited the proliferation of stimulated T cells. This proliferation inhibition was not related to induced apoptosis or necrosis. The observed suppression of T cell proliferation could be linked to a decreased secretion of IL-2, which is essential for the proliferation and differentiation of T lymphocytes. Furthermore, the degranulation capacity of stimulated T cells was shown to decrease in response to treatment with either *B. longifolia* or *G. arborea* extract, emphasizing the anti-inflammatory potential of both extracts. Dendritic cells (DCs) play an important role in wound closure, since they increase the cell migration rate of keratinocytes by secreting interleukin-8 (IL-8). A slightly enhanced IL-8 secretion by DCs was detected after treatment with ethyl acetate extracts of either *G. arborea* or *B. longifolia*.

Zusammenfassung

Die Identifikation neuer Leitstrukturen und die Entwicklung neuer Medikamente zur Behandlung von Autoimmunerkrankungen ist von großer Wichtigkeit, da derzeit auf dem Markt verfügbare Präparate zum Teil beträchtliche Einschränkungen aufweisen. Glucocorticoide und Medikamente, welche die DNA Synthese hemmen (wie z.B. Cyclophosphamid) besitzen zum Teil starke Nebenwirkungen, die hochmodernen Biologika bedeuten hingegen eine hohe finanzielle Belastung.

Da Pflanzenstoffe evolutionär optimiert sind, um vielerlei biologische Funktionen zu erfüllen, sind Pflanzenextrakte ein guter Ausgangspunkt für die Entwicklung neuer immunsuppressiver Medikamente. Blockbuster-Medikamente, wie Cyclosporin A und Tacrolimus, sind Teil der Erfolgsgeschichte der Naturstoffforschung zur Entwicklung anti-entzündlicher Präparate. Allerdings ist für die Selektion vielversprechender Pflanzenextrakte, die Charakterisierung ihrer Wirkung, die Aufklärung von Targets, sowie die Isolation bioaktiver Inhaltsstoffe ein gut durchdachter, multidisziplinärer Forschungsansatz essenziell.

In dieser Arbeit wurden 435 Extrakten von Heilpflanzen der Traditionell Chinesischen Medizin im Hinblick auf eine mögliche immunsuppressive Aktivivät untersucht. Bei Autoimmunerkrankungen, wie rheumatoider Arthritis oder multipler Sklerose, ist die Zellteilung der T-Zellen gesteigert. Die immunsuppressive Aktivität der Extrakte wurde daher, initial, mittels Proliferations-basierter Analyse anhand von physiologisch relevanten, anti-CD3 und anti-CD28 stimulierten humanen T-Lymphozyten evaluiert. Für einen *Artemisia argyi* (Asteraceae, *A. argyi*) Ethylacetat-Extrakt (IC_{50}: 16,2 µg/mL) sowie einen *Boswellia carteri* (Burseraceae, *B. carteri*) Dichloromethan-Extrakt (IC_{50}: 27,0 µg/mL) konnte eine anti-proliferative Wirkung beobachtet werden. Es konnte weiter gezeigt werden, dass diese immunsuppressive Aktivität nicht auf der Induktion von Apoptose oder Nekrose basiert. Eine genauere Charakterisierung der immunsuppressiven Effekte zeigte eine Suppression der Expression der Aktivierungsmarker CD25 und CD69, sowie eine erniedrigte IL-2- und IFN-γ-Produktion durch Behandlung humaner T-Zellen mit *A. argyi*-Extrakt. Der *B. carteri*-Extrakt supprimierte ebenfalls die Sekretion von IL-2 und IFN-γ. Außerdem inhibierte der Extrakt die Degranulationsfähigkeit stimulierter T-Zellen.

Für beide Extrakte wurde ein HPLC-MS-basiertes Aktivitätsprofil erstellt. Somit konnten mittels T-Zell-Proliferations-Test 8-Acetyl-Artanomaloid, Arteglasin A, Jaceosidin, 1R-Canin und (4S,5S,6S,7S)- und (4R,5R,6S,7S)-Seco-Tanapartholid als aktive Komponenten aus *A. argyi* identifiziert werden. Für *B. carteri* konnte gezeigt werden, dass 3-Acetoxytirucallicsäure, O-Acetyl-Elemolicsäure, 3-Oxo-tirucallicsäure und 3-O-Acetyl-Alpha-Boswelliasäure die Proliferation stimulierter T-Zellen inhibierten.

Zur Validierung des Targets der aktiven Einzelstoffe aus *A. argyi* und *B. carteri* wurde ein Monitoring der T-Zell-Signaltransduktionskaskade, angefangen bei den Transkriptionsfaktoren des *iL-2* Gens, AP-

1, NF-κB und NFAT, durchgeführt. Für die Sesquiterpenlactone aus *A. argyi* konnte eine Suppression der NF-κB und NFAT-Aktivität, mit IC_{50} Werten zwischen 2,0 und 9,3 µM für NF-κB und 1,6 und 9,3 µM für NFAT, verzeichnet werden. Für *B. carteri* stellte sich 3-O-Acetyl-Alpha-Boswelliasäure als vielversprechendster Kandidat heraus, der die NFAT-Aktivität mit einer IC_{50} von 5,6 µM inhibierte. Für *A. argyi* wurde das Monitoring auf die Untersuchung des Calcium-Fluxes in stimulierten Jurkat T-Zellen erweitert. Die Behandlung mit 30 µg/mL *A. argyi*-Extrakt führte dabei zu einer Unterdrückung des Calcium-Fluxes in stimulierten Jurkat T-Zellen. Für die Einzelstoffe aus *A. argyi* konnte jedoch kein Einfluss auf den Calcium-Flux in stimulierten Jurkat T-Zellen nachgewiesen werden. Die Ergebnisse lassen vermuten, dass der *A. argyi-G*esamtextrakt die T-Zell-Signaltransduktion auf einer höheren Stufe beeinflusst, als die aus dem Extrakt isolierten Einzelstoffe.

Die vorliegende Arbeit umfasst weiterhin auch die Evaluierung möglicher wundheilungsfördernder und immunmodulierender Effekte von neun Pflanzen, die traditionell in Nepal zur Verbesserung der Wundheilung verwendet wurden. Ein *Gmelina arborea* (Lamiaceae, *G. arborea*) Ethylacetat-Extrakt verbesserte die Wundheilungskapazität humaner Keratinozyten und Fibroblasten.

Für eine adequate Wundheilung ist die Balance zwischen der Eliminierung von Krankheitserregern durch entzündliche Feedbackschleifen, sowie regulatorischer Mechanismen zur Prävention von schwerwiegenden Entzündungsreaktionen von großer Bedeutung. Aus diesem Grund wurde der Einfluss der nepalesischen Pflanzenextrakte auf verschiedene Entzündungsparameter untersucht. Der *G. arborea*-Extrakt und ein *Bassia longifolia* (Sapotaceae, *B. longifolia*) Ethylacetat-Extrakt inhibierten die Zellteilung stimulierter humaner T-Zellen konzentrationsabhängig. Diese Inhibition ist nicht auf die Induktion von Apoptose oder Nekrose zurückzuführen, konnte jedoch mit einer verminderten Sekretion von IL-2 in Verbindung gebracht werden. Bei IL-2 handelt es sich um ein Zytokin, welches eine wichtige Rolle für die Proliferation und Differenzierung von T-Lymphozyten spielt. Es konnte außerdem ein inhibitorischer Einfluss von *B. longifolia* und *G. arborea* auf die Degranulationsfähigkeit von T-Zellen gezeigt werden. Da DCs mittels IL-8 Sekretion die Zellmigration von Keratinozyten steigern können, sind sie ebenfalls von Bedeutung für die Wundschließung. In dieser Arbeit konnte eine leichte Erhöhung der IL-8 Sekretion durch die Behandlung DCs mit *G. arborea* Ethylacetat-Extrakt oder *B. longifolia* Ethylacetat-Extrakt nachgewiesen werden.

1. Aim of work

Excessive immune reactions are a major challenge for modern medicine, either by themselves causing a problem, in the case of autoimmunity, or by accompanying other medical conditions and processes, such as wound healing; thus, immune modulatory treatments are now indispensable for treating pathological conditions.

Despite the achievements of modern medicine concerning the development of innovative medications, continuous research on novel drugs is vital for overcoming current and future limitations. Problems of available medications can be side effects, nonresponding, the development of bacterial or viral resistances, or high costs (Allison, 2000; Aslam et al., 2018; Daubert et al., 2017; Mathur and Hoskins, 2017; Río et al., 2009).

Natural products provide a sound basis for the development of novel and innovative drugs, including blockbuster drugs, such as β-lactams or paclitaxel (Desai et al., 2006; Deshpande et al., 2004; Newman and Cragg, 2016; Singla et al., 2002). Nevertheless, natural product research has become the preserve of startup companies and academic research groups, because the fast turnaround and tight deadlines of modern screening programs have deterred major pharmaceutical companies from undertaking such research (Hamburger, 2019).

The overall aim of this study was to establish a cell-based screening platform for the initial investigation of natural products, based on a database of plants that have been used in TCM for thousands of years. Since autoimmune diseases are characterized by an increase of T cell proliferation, inhibition of the T lymphocyte proliferation was used as a marker for immunosuppressive activity. This first part of the work aimed to identify plant extracts with immunosuppressive potential that invite further investigation with regard to drug development. An ethyl acetate extract of *Artemisia argyi (*Asteraceae*, A. argyi*) and a DCM extract from *Boswellia carteri* (Burseraceae, *B. carteri*) were further analyzed in this work.

The second part of the project addressed the characterization of the impact of plant extracts, which tested positive in the preliminary screening, on the function of human T cells. Upon activation, T lymphocytes fulfill several important functions, including degranulation and cytokine secretion. In this part of work, the impact of *A. argyi* extract and *B. carteri* extract on the activation and functions of human T lymphocytes, namely degranulation capacity and cytokine secretion, was examined.

The third part of this work was performed in collaboration with the Department of Pharmaceutical Sciences in Basel and dealt with the identification of bioactive compounds from the investigated plant extracts, using an approach that combined microfractionation with a T cell proliferation assay.

The final part of this study covered the target validation for the plant extracts and active compounds by monitoring the T cell signaling cascade downstream of the target, using state-of-the-art biological assays for cellular systems.

Another project included in this work addressed the immune modulatory and wound-healing potential of nine extracts from plants traditionally used in Nepal to treat wounds and cuts. The potential to ameliorate wound healing was initially investigated with classical scratch assays using human keratinocytes and human fibroblasts, while the procedure to detect anti-inflammatory potential was carried out as described previously for the TCM project. The results qualified the ethyl acetate extracts of *Bassia longifolia* (Sapotaceae, *B. longifolia*) and *Gmelina arborea* (Lamiaceae, *G. arborea*) for further investigation.

As a next step, the ability of the promising extracts to intervene in the function of T lymphocytes was investigated as outlined for the TCM project. In cases of injury, DCs secrete IL-8, which in turn stimulates the migration of keratinocytes and, thereby, supports wound closure; hence, the examination of the activation state and the IL-8 secretion of dendritic cells was a further aim of the study.

References

Allison, A.C., 2000. Immunosuppressive drugs: the first 50 years and a glance forward. Immunopharmacology 47, 63–83.

Aslam, B., Wang, W., Arshad, M.I., Khurshid, M., Muzammil, S., Rasool, M.H., Nisar, M.A., Alvi, R.F., Aslam, M.A., Qamar, M.U., Salamat, M.K.F., Baloch, Z., 2018. Antibiotic resistance: a rundown of a global crisis. Infection and Drug Resistance 11, 1645–1658.

Daubert, C., Behar, N., Martins, R.P., Mabo, P., Leclercq, C., 2017. Avoiding non-responders to cardiac resynchronization therapy: a practical guide. European Heart Journal 38, 1463–1472.

Desai, N., 2006. Increased antitumor activity, intratumor Paclitaxel concentrations, and endothelial cell transport of cremophor-free, albumin-bound Paclitaxel, ABI-007, compared with cremophor-based Paclitaxel. Clinical Cancer Research 12, 1317–1324.

Deshpande, A.D., Baheti, K.G., Chatterjee, N.R., 2004. Degradation of β-lactam antibiotics. Current Science 87, 1684–1695.

Hamburger, M., 2019. HPLC-based activity profiling for pharmacologically and toxicologically relevant natural products – principles and recent examples. Pharmaceutical Biology 57, 328–334.

Mathur, S., Hoskins, C., 2017. Drug development: Lessons from nature. Biomedical Reports 6, 612–614.

Newman, D.J., Cragg, G.M., 2016. Natural products as sources of new drugs from 1981 to 2014. Journal of Natural Products 79, 629–661.

Río, J., Comabella, M., Montalban, X., 2009. Predicting responders to therapies for multiple sclerosis. Nature Reviews Neurology 5, 553–560.

Singla, A.K., Garg, A., Aggarwal, D., 2002. Paclitaxel and its formulations. International Journal of Pharmaceutics 235, 179–192.

2. Introduction

2.1. The human immune response

The human immune system fulfills diverse and complex functions, such as the clearance of invading microorganisms, viruses, fungi, parasitic worms, bacteria, and archaea; moreover, it detects tissue damage and triggers repair mechanisms. To perform these complex functions, the immune system employs humoral and cellular defense, as well as regulatory mechanisms (Figure 1).

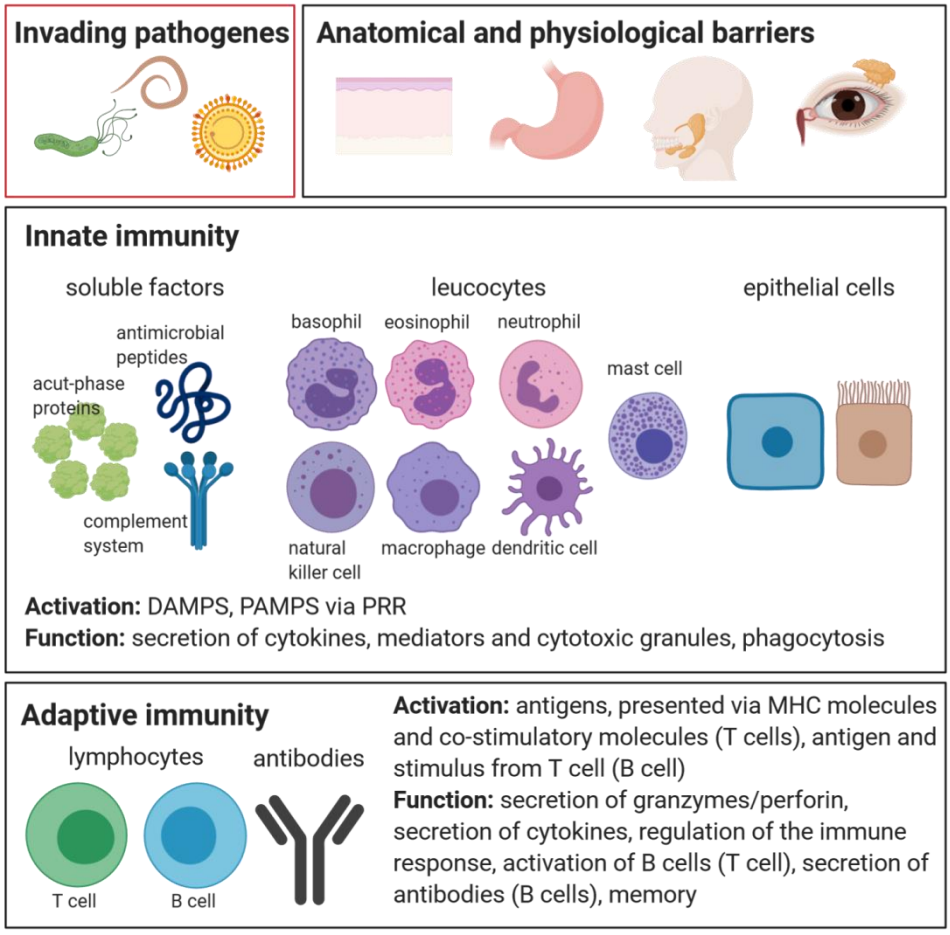

Figure 1: Overview of the human immune system: features and functions

2.1.1. The innate immune response

The first line of defense consists of anatomical and physiological barriers, such as the skin and its acidic environment, mucociliary clearance, antibacterial lysozymes in salivary juice and lachrymal fluid, and gastric pH (Marshall et al., 2018). Additionally, a variety of antimicrobial proteins, acting as natural antibiotics, is produced by mucosal surfaces (Murphy and Weaver, 2016).

If, nevertheless, a pathogen enters the tissue, the innate immunity is activated within minutes (Marshall et al., 2018). Macrophages, natural killer cells (NK cells), neutrophils, basophils, eosinophils, mast cells, and DCs act, in part, to initiate an inflammatory reaction (Stephen and Hajjar, 2018). Additionally, epithelial cells are capable of promoting an immune reaction, mainly by secreting cytokines, chemokines, and antimicrobial molecules (Buckner et al., 2011; Ihara et al., 2017). Furthermore, soluble factors, such as the proteins of the complement system, acute-phase proteins, or antimicrobial peptides complete the innate immunity (Turvey and Broide, 2010). Initially, the innate immune response can be activated by damage-associated molecular patterns (DAMPs)—endogenous biomolecules that are released in response to tissue damage; for example, heat shock proteins or the high-mobility group protein B1 (HMGB1) (Hato and Dagher, 2015; Schaefer, 2014). The innate immune response is also activated by pathogen-associated molecular patterns (PAMPs), which share conserved pathogen-specific surface structures that are not found on host tissue. Common examples of PAMPs are mannans from fungi, hemozoin from parasites, lipopolysaccharides (LPS) from bacteria, and viral double-stranded ribonucleic acid (dsRNA) (Akira et al., 2006). PAMPs are recognized by specific pattern-recognition receptors (PRRs) on and inside innate immune cells, which then initiate an immune reaction. Toll-like receptors (TLRs) and scavenger receptors (SR) are examples of PRRs and can be found on the membranes of specific antigen-presenting cells (APCs) (Abdul Zani et al., 2015; Hato and Dagher, 2015). Aside from the membrane-bound PRR, cytoplasmic PRRs like nucleotide-binding oligomerization domain-like receptors (NOD-like receptors, NLRs), retinoic acid-inducible gene-I-like receptors (RIG-like receptors, RLRs), and other TLRs, complete the innate immunity (Hato and Dagher, 2015). Binding of a PAMP by the PRR of a cell causes phagocytosis of the pathogen and secretion of cytokines (Akira et al., 2006). Cytokines are a key factor during the innate immune response, because they attract and activate further immune cells in order to initiate the cellular immune response. During an early immune reaction, prominent cytokines are tumor necrosis factor α (TNF α), interleukin-1 (IL-1), and interleukin-6 (IL-6) (Marshall et al., 2018). In addition to phagocytosis and cytokine secretion, macrophages are capable of producing cytotoxic mediators, such as reactive oxygen species or degrading enzymes, to defeat pathogens (Murphy and Weaver, 2016). Likewise, the short-lived neutrophils contain cytotoxic granules to support microbial clearance (Marshall et al., 2018). The innate immunity can be maintained for days (Murphy and Weaver, 2016).

2.1.2. The adaptive immune response

Pathogens that are not eliminated by the innate immune system become the target of the adaptive immune response, which starts hours after infection (Murphy and Weaver, 2016). The adaptive immune system features a broad repertoire of highly specific antigen receptors that allow the very efficient clearance of infections. T lymphocytes (T cells) and B lymphocytes (B cells) express epitope-specific antigen receptors and, thus, play a key role in the adaptive immune response (Murphy and Weaver, 2016).

T cell development takes place in the thymus and is hallmarked by the generation of cells with an antigen-specific T cell receptor (TCR) and the ability to distinguish between endogenous and exogenous antigens (Marshall et al., 2018). T cells that react to self-antigens are eliminated during the development process (Marshall et al., 2018). After progression, the naive T cells circulate through the body until they differentiate into functional effector T cells upon contact with their specific antigen. In general, effector T cells are sub-classified into cytotoxic $CD8^+$ T cells and $CD4^+$ T helper cells by their different co-receptors. The main function of the $CD8^+$ T cells is the elimination of the detected pathogen by a process called granulation (Murphy and Weaver, 2016). Exocytosis of cytotoxic granules, which contain granzymes and the pore-forming molecule, perforin (pfn), induces apoptosis of the target cell (Veugelers et al., 2004). The $CD4^+$ T cells are sub-divided into Th_1, Th_2, Th_{17}, Th_9, Th_{22}, follicular T helper cells (Tfh), and regulatory T cells (Tregs) (Ivanova and Orekhov, 2015). The T helper cells secrete a variety of cytokines in order to perform their manifold functions. The pattern of secreted cytokines groups the T helper cells and defines the type of immune reaction that is produced. The Th_1 reaction is characterized by the cytokines IL-2 and IFN-γ and promotes a cell-mediated immune reaction to eliminate virus-infected cells and intracellular pathogens (Bonilla and Oettgen, 2010). The major function of Th_2 cells is the activation of B cells and enhancement of antibody production due to the secretion of interleukin-4 (IL-4), interleukin-5 (IL-5), interleukin-10 (IL-10), and interleukin-13 (IL-13) (Bonilla and Oettgen, 2010). Th_{17} cells are mainly responsible for the clearance of extracellular bacteria and fungi by activating neutrophils (Murphy and Weaver, 2016). Th_9 cells secrete the mast cell factor interleukin-9 (IL-9), which also enhances the immunosuppressive function of Tregs and promotes the cell division of Th_{17} cells (Jia and Wu, 2014a). Th_{22} cells promote immune reactions that are mediated by the epithelial cells of the skin, gut, and respiratory tract (Jia and Wu, 2014b) and Tfh cells promote B cell activation and initiate the germinal center formation (Bonilla and Oettgen, 2010). Tregs are important for the maintenance of self-tolerance, since they secrete the immunosuppressive cytokines IL-10 and transforming growth factor β (TGF-β) (Ivanova and Orekhov, 2015). All T cells express the TCR complex on their surface, which is composed of variable TCRα and TCRβ chains and non-covalently associated CD3γ, CD3δ, CD3ε, and ζ-chain polypeptides (Call and Wucherpfennig, 2007;

Clevers et al., 1988; Ngoenkam et al., 2018). For adequate activation of a T cell, the TCR complex, the CD8 or CD4 co-receptor, and the CD28 co-receptor are essential (Adam et al., 1998; Esensten et al., 2016; Malissen, 2003). Activation occurs via antigen presentation by MHC surface molecules on APCs. MHC molecules are classified as class I or class II. MHC I molecules are found on the surface of all nucleated cells and are responsible for the presentation of intracellular peptides. By contrast, MHCII molecules are only presented by APCs, such as macrophages, DCs, or B lymphocytes. APCs take up and process exogenous antigens and finally present them via MHCII (Rock et al., 2016). Cross-presentation constitutes an optional extracellular antigen presentation, via MHC I molecules, to prime cytotoxic T cells (Kotsias et al., 2019). Cross-presentation proceeds most effectively through DCs, either via the vacuolar or the cytosolic pathway. The vacuolar pathway is initiated by endocytosis of an extracellular antigen by a DC and subsequent phagocytic vesicle formation. Cross-presentation demands decreased levels of antigen degradation inside phagocytic vesicles to preserve epitopes for the presentation on MHC I molecules. After MHC I loading of the extracellular antigen, the complex is transported to the cell membrane for cross-presentation (Kotsias et al., 2019). The cytosolic pathway is also initiated by endocytosis of the extracellular antigen by a DC; thereafter, proteasomal degradation and procession of the antigen takes place in the cytosol and the processed antigen is transported to the endoplasmic reticulum (ER) via a specific peptide transporter (transporter associated with antigen processing, TAP). In the ER, antigen loading to MHC I is realized and, finally, the antigen-MHCI-complex can be cross-presented (Kotsias et al., 2019). Along with the recognition of an MHC presented antigen, the complete activation of a T cell requires the binding of B7 molecules, which are expressed by DCs, to the CD28 co-receptor (Adam et al., 1998). Fully-activated T cells express the α-chain of the IL-2 receptor (CD25) on their surface, which then connects with the β- and γ-chain to build a functional IL-2 receptor (Malek, 2008); the T cells then take up their function.

The major task of B cells is to secrete antibodies, thereby playing a crucial role in the humoral adaptive immune response (Parkin and Cohen, 2001). Both the antibodies and the B cell receptors (BCR) are formed by the protein group of immunoglobulins (Igs) (Yang and Reth, 2016). For a complete activation of B cells, binding of an antigen in combination with a stimulus from a Th_2 cell is necessary (Parkin and Cohen, 2001). Activated B cells differentiate either to antibody secreting plasma cells or memory B cells (Murphy and Weaver, 2016). Antibodies can neutralize pathogens and toxins by activating the complement system and opsonization of pathogens to produce phagocytosis or antibody–dependent cellular cytotoxicity (ADCC) by other immune cells (Forthal, 2014). The function of the memory cells triggers an immune reaction upon renewed infection within hours (Leo et al., 2011; Murphy and Weaver, 2016). This immunological memory is distinguished by its robustness, rapidity, and high level of specificity, which can be lifelong (Inoue et al., 2018). The adaptive immune response can persist for

weeks and is characterized by an ingenious interaction between cell types, components, and accurate regulatory mechanisms (Leo et al., 2011; Murphy and Weaver, 2016).

References

Akira, S., Uematsu, S., Takeuchi, O., 2006. Pathogen recognition and innate immunity. Cell 124, 783–801.

Bonilla, F.A., Oettgen, H.C., 2010. Adaptive immunity. Journal of Allergy and Clinical Immunology 125, S33-40.

Buckner, L.R., Schust, D.J., Ding, J., Nagamatsu, T., Beatty, W., Chang, T.L., Greene, S.J., Lewis, M.E., Ruiz, B., Holman, S.L., Spagnuolo, R.A., Pyles, R.B., Quayle, A.J., 2011. Innate immune mediator profiles and their regulation in a novel polarized immortalized epithelial cell model derived from human endocervix. Journal of Reproductive Immunology 92, 8–20.

Call, M.E., Wucherpfennig, K.W., 2007. Common themes in the assembly and architecture of activating immune receptors. Nature Reviews Immunology 7, 841–850.

Clevers, H., Alarcon, B., Wileman, T., Terhorst, C., 1988. The T cell receptor/CD3 complex: a dynamic protein ensemble. Annual Review of Immunology 6, 629–662.

Esensten, J.H., Helou, Y.A., Chopra, G., Weiss, A., Bluestone, J.A., 2016. CD28 costimulation: From mechanism to therapy. Immunity 44, 973–988.

Hato, T., Dagher, P.C., 2015. How the innate immune system senses trouble and causes trouble. Clinical Journal of the American Society of Nephrology 10, 1459–1469.

Ihara, S., Hirata, Y., Koike, K., 2017. TGF-β in inflammatory bowel disease: a key regulator of immune cells, epithelium, and the intestinal microbiota. Journal of Gastroenterology 52, 777–787.

Inoue, T., Moran, I., Shinnakasu, R., Phan, T.G., Kurosaki, T., 2018. Generation of memory B cells and their reactivation. Immunological Reviews 283, 138–149.

Ivanova, E.A., Orekhov, A.N., 2015. T helper lymphocyte subsets and plasticity in autoimmunity and cancer: An overview. BioMed Research International 2015, 1–9.

Jia, L., Wu, C., 2014a. Differentiation, regulation and function of Th9 Cells, in: Sun, B. (Ed.), T helper cell differentiation and their function. Springer Netherlands, Dordrecht, 181–207.

Jia, L., Wu, C., 2014b. The biology and functions of Th22 Cells, in: Sun, B. (Ed.), T helper cell differentiation and their function. Springer Netherlands, Dordrecht, 209–230.

Kotsias, F., Cebrian, I., Alloatti, A., 2019. Antigen processing and presentation, in: International Review of Cell and Molecular Biology. Elsevier, Amsterdam, 69–121.

Leo, O., Cunningham, A., Stern, P.L., 2011. Vaccine immunology. Perspectives in Vaccinology 1, 25–59.

Malek, T.R., 2008. The Biology of Interleukin-2. Annual Review of Immunology 26, 453–479.

Malissen, B., 2003. An evolutionary and structural perspective on T cell antigen receptor function. Immunological Reviews 191, 7–27.

Marshall, J.S., Warrington, R., Watson, W., Kim, H.L., 2018. An introduction to immunology and immunopathology. Allergy, Asthma & Clinical Immunology 14.

McAdam, A.J., Schweitzer, A.N., Sharpe, A.H., 1998. The role of B7 co-stimulation in activation and differentiation of CD4+ and CD8+ T cells. Immunological Reviews 165, 231–247.

Murphy, K., Weaver, C., 2016. Janeway's Immunobiology, 9th ed. Garland Science, New York, NY.

Ngoenkam, J., Schamel, W.W., Pongcharoen, S., 2018. Selected signalling proteins recruited to the T-cell receptor-CD3 complex. Immunology 153, 42–50.

Parkin, J., Cohen, B., 2001. An overview of the immune system. The Lancet 357, 1777–1789.

Rock, K.L., Reits, E., Neefjes, J., 2016. Present Yourself! By MHC Class I and MHC Class II Molecules. Trends in Immunology 37, 724–737.

Schaefer, L., 2014. Complexity of danger: The diverse nature of damage-associated molecular patterns. Journal of Biological Chemistry 289, 35237–35245.

Stephen, B., Hajjar, J., 2018. Overview of basic immunology and translational relevance for clinical investigators, in: Naing, A., Hajjar, J. (Eds.), Immunotherapy. Springer International Publishing, Cham, 1–41.

Turvey, S.E., Broide, D.H., 2010. Innate immunity. Journal of Allergy and Clinical Immunology 125, 24–32.

Veugelers, K., Motyka, B., Frantz, C., Shostak, I., Sawchuk, T., Bleackley, R.C., 2004. The granzyme B–serglycin complex from cytotoxic granules requires dynamin for endocytosis. Blood 103, 3845–3853.

Yang, J., Reth, M., 2015. Receptor dissociation and B cell activation, in: Kurosaki, T., Wienands, J. (Eds.), B cell receptor signaling. Springer International Publishing, Cham, 27–43.

Zani, I.A., Stephen, S.L., Mughal, N.A., Russell, D., Homer-Vanniasinkam, S., Wheatcroft, S.B., Ponnambalam, S., 2015. Scavenger receptor structure and function in health and disease. Cells 4, 178–201.

2.2. T cell signaling pathways

Antigen recognition by the TCR complex initates several signal transduction cascades (Figure 2). It first leads to clustering of the CD4 or CD8 co-receptor with the lymphocyte-specific protein tyrosine kinase (LCK), which in turn mediates the phosphorylation of the immunoreceptor tyrosine-based activation motifs (ITAMs) of the CD3 chains (Gaud et al., 2018). This phosphorylation causes the recruitment of ζ-chain-associated protein kinase 70 (ZAP70), which is phosphorylated by LCK (Yan et al., 2013). Thereafter, the linker for activation of T cells (LAT)-signalosome is formed. It consists of other adaptor molecules and proteins (GRB2, adhesion- and degranulation-promoting adaptor protein (ADAP), the SH2/SH3 adaptor protein NCK1, the SH2-domain-containing leukocyte protein of 76 kDa (SLP76), phospholipase Cγ1 (PLCγ1), IL-2 inducible T cell kinase (ITK), and VAV1 (Gaud et al., 2018)). PLCγ1 catalyzes the hydrolysis of phosphatidylinositol 4,5-bisphosphate (PIP2) into inositol trisphosphate (IP3) and diacylglycerol (DAG). DAG is membranous, whereas IP3 binds to the IP3 receptor in the membrane of the ER to allow calcium ER store depletion. This, in turn, causes clustering of stromal interaction molecule 1 (STIM1) and calcium release-activated calcium channel protein 1 (ORAI1) to form the calcium release-activated channel (CRAC) and allow a strong store-operated calcium entry (SOCE) from the outer cell compartment to refill the exhausted ER calcium store (Hogan et al., 2010). The elevated calcium concentration in the cytosol enables calmodulin and the phosphatase calcineurin to bind calcium ions and become partially activated. Complex formation of calcineurin and calmodulin leads to a full activation of calcineurin and facilitates dephosphorylation and, thus, unmasking of the nuclear localization sequence of the transcription factor NFAT (Srikanth et al., 2017); consequently, NFAT can translocate to the nucleus to activate target genes, such as IL-2. Further, PLCγ1 promotes the mitogen-activated protein kinase (MAPK) pathway by activating Ras via RasGRP. Ras, in turn, activates the MAPK signaling cascade that includes RAF (MAP3K), Mek1 (MAP2K), and the extracellular signal-regulated kinase (Erk). Erk activates Elk, which stimulates the serum response factor to transcribe the Fos genes (Myers et al., 2019); thereby, Elk is responsible for the formation of AP-1, consisting of Fos and Jun. For a full activation of AP-1, phosphorylation of Jun by Jun kinase (JNK) is required (Murphy and Weaver, 2016). JNK is activated by protein kinase C-θ (PKC-θ), a further key player of T cell signaling that is recruited by the second messenger DAG. Aside from the activation of JNK, PKC-θ triggers the pathway, resulting in the activation of NF-κB. The first step in this signaling axis is the phosphorylation of CARD-containing MAGUK protein 1 (CARMA1) by PKC-θ to induce BCM complex formation (Smith-Garvin et al., 2009). The BCM complex comprises B-cell lymphoma/leukemia 10 (Bcl-10), CARMA1, and mucosa-associated lymphoid tissue lymphoma translocation protein 1 (MALT1), and it enables the degradation of the inhibitor of κB (IκB) by IκB kinase (IKK) via a phosphorylation cascade of TRAF-6 and TAK1 (Smith-Garvin et al., 2009). IκB degradation

results in the release of NF-κB and its translocation to the nucleus (Sun, 2012). For the transcription of the *iL-2* gene NFAT, AP-1, and NF-κB are required to bind the respond elements, respectively. IL-2 is an autocrine growth factor of T lymphocytes and plays a major role in the function and regulation of the immune response, stimulating the proliferation and differentiation of T cells (Ross and Cantrell, 2018). Contrary to expectations, genetic deletion of *iL-2* or its receptor causes autoimmunity, rather than immune deficiency (Abbas et al., 2018), which can be explained by the role of IL-2 for the development and function of Tregs, emphasizing the importance of IL-2 for the regulation of the immune system (Abbas et al., 2018; Zhang and Tang, 2015).

Figure 2: Overview of T cell signaling pathways

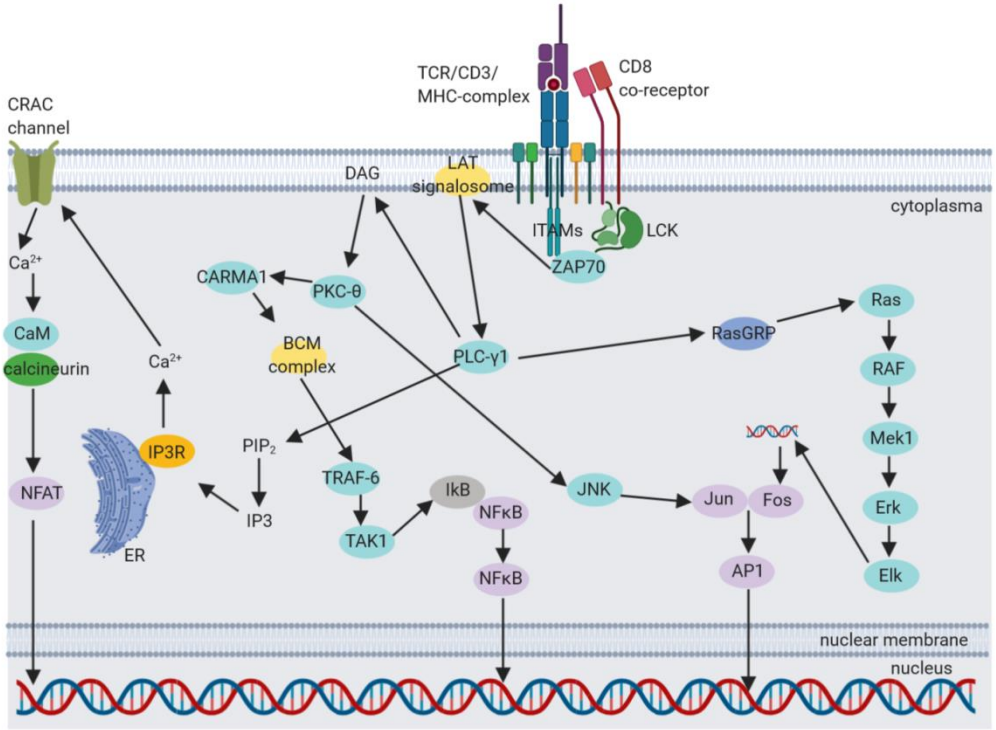

References

Abbas, A.K., Trotta, E., R Simeonov, D., Marson, A., Bluestone, J.A., 2018. Revisiting IL-2: Biology and therapeutic prospects. Science Immunology 3.

Gaud, G., Lesourne, R., Love, P.E., 2018. Regulatory mechanisms in T cell receptor signaling. Nature Reviews Immunology 18, 485–497.

Hogan, P.G., Lewis, R.S., Rao, A., 2010. Molecular basis of calcium signaling in lymphocytes: STIM and ORAI. Annual Review of Immunology 28, 491–533.

Murphy, K., Weaver, C., 2016. Janeway's Immunobiology, 9th ed. Garland Science, New York, NY.

Myers, D.R., Wheeler, B., Roose, J.P., 2019. mTOR and other effector kinase signals that impact T cell function and activity. Immunological Reviews 291, 134–153.

Ross, S.H., Cantrell, D.A., 2018. Signaling and function of interleukin-2 in T lymphocytes. Annual Review of Immunology 36, 411–433.

Smith-Garvin, J.E., Koretzky, G.A., Jordan, M.S., 2009. T cell activation. Annual Review of Immunology 27, 591–619.

Srikanth, S., Woo, J.S., Sun, Z., Gwack, Y., 2017. Immunological disorders: Regulation of Ca^{2+} signaling in T lymphocytes, in: Groschner, K., Graier, W.F., Romanin, C. (Eds.), Store-operated Ca^{2+} Entry (SOCE) Pathways. Springer International Publishing, Cham, 397–424.

Sun, Z., 2012. Intervention of PKC-θ as an immunosuppressive regimen. Frontiers in Immunology 3.

Yan, Q., Barros, T., Visperas, P.R., Deindl, S., Kadlecek, T.A., Weiss, A., Kuriyan, J., 2013. Structural basis for activation of ZAP-70 by phosphorylation of the SH_2-kinase linker. Molecular and Cellular Biology 33, 2188–2201.

Zhang, M., Tang, Q., 2015. Manipulating IL-2 and IL-2R in autoimmune diseases and transplantation. Immunotherapy 7, 1231–1234.

2.3. Autoimmune diseases

An autoimmune disease is defined as a breakdown of immune tolerance, leading to an immune reaction to endogenous cells or tissue (Khan and Ghazanfar, 2018). Approximately 5% of the population suffer from an autoimmune disease with a rising incidence (Khan and Ghazanfar, 2018), emphasizing the importance of understanding this disease pattern (Murphy and Weaver, 2016); however, due to several immune system mechanisms (Figure 3) autoimmune diseases are usually prevented.

The first important mechanism for ensuring self-tolerance is known as central tolerance and takes place during lymphocyte development in the bone marrow (B cells) and the thymus (T cells)

(Romagnani, 2006; Theofilopoulos et al., 2017). A strong recognition of the self-antigens that circulate in the blood plasma, or are presented in the bone marrow by stromal cells or hematopoietic cells, causes rearrangement of the B cell immunoglobulin genes (receptor editing), apoptosis, or functional unresponsiveness (anergy) (Romagnani, 2006). For T lymphocytes, central tolerance is more complex. In the thymus, medullary thymic epithelial cells (mTECs) and thymic dendritic cells (TDCs) present tissue-specific antigens, under the control of the transcription factor autoimmune regulator (AIRE) and FEZ family zinc finger 2 (FEZF2) (Passos et al., 2018; Takaba and Takayanagi, 2017; Theofilopoulos et al., 2017); hence, central tolerance can be generated for a broad repertoire of self-antigens. Despite the fact that these mechanisms being well-orchestrated, some self-reactive lymphocytes evade the system and leave the primary lymphoid organs (Khan and Ghazanfar, 2018); a number of self-reactive lymphocytes is important, since they contribute, for example, to the renewal of tissue (Murphy and Weaver, 2016).

To ensure tolerance with regard to mature self-reactive lymphocytes, the immune system has several other safety mechanisms available; thus, only if the concentration of antigens rises exponentially and rapidly, as is the case during infections, lymphocytes become activated. By contrast, self-antigens with an abundant, but constant, concentration can provide tolerance (Murphy and Weaver, 2016). Moreover, low antigen concentrations, as well as physical barriers (e.g., the blood–brain barrier), induce ignorance of self-antigens by T cells (Khan and Ghazanfar, 2018). These phenomena are collectively referred to as clonal ignorance (Khan and Ghazanfar, 2018).

The concept of peripheral tolerance involves numerous mechanisms that occur in secondary lymphoid tissues or at the site of inflammation. An effective mechanism for preventing autoimmunity is activation-induced cell death (AICD), which is triggered by iterated TCR activation and mediated by interaction of the Fas death receptor and its ligand (Walker and Abbas, 2002). During infection, pro-inflammatory cytokines and co-stimulatory molecules produce an appropriate immune reaction. An absence of cytokines and co-stimulatory molecules induces negative signals, leading to functional unresponsiveness (anergy) or the development of Tregs in place of effector cells (Khan and Ghazanfar, 2018). Additionally, T cells and other immune cells (NK, natural killer T (NKT) cells, B cells, macrophages, and some DCs) express the inhibitory programmed cell death protein 1 (PD-1) receptor transiently upon TCR engagement. Antigen clearance causes the disappearance of PD-1 whereas, in the case of a continuous stimulus, PD-1 expression remains high and leads to T cell “exhaustion” (Schildberg et al., 2016). The ligand PD-ligand 1 (PD-L1) is expressed on hematopoietic and non-hematopoietic cells whereas the PD-ligand 2 (PD-L2) can be found on the surface of dendritic cells, macrophages, and non-hematopoietic lung cells. The interaction of PD-L1 or PD-L2 with PD1 downregulates TCR signaling via dephosphorylation of signaling molecules, as a negative feedback

loop, to prevent immunity-related tissue damage (Schildberg et al., 2016). Tregs suppress a variety of autoreactive lymphocytes, either by expressing cytotoxic T-lymphocyte-associated protein 4 (CTLA-4), which binds to the B7 molecules present on DCs, or by the secretion of IL-10 and TGF-β, which directly interfere with the signaling of the effector cells (Göschl et al., 2019). Finally, the predefined limitation of the proliferation and survival of lymphocytes can terminate immune responses to foreign and self-antigens.

The peripheral tolerance of B cells is based on the dependence of B cell activation on a T cell stimulus; hence, activation of an autoreactive B cell would only be possible in response to stimulation of an autoreactive T cell.

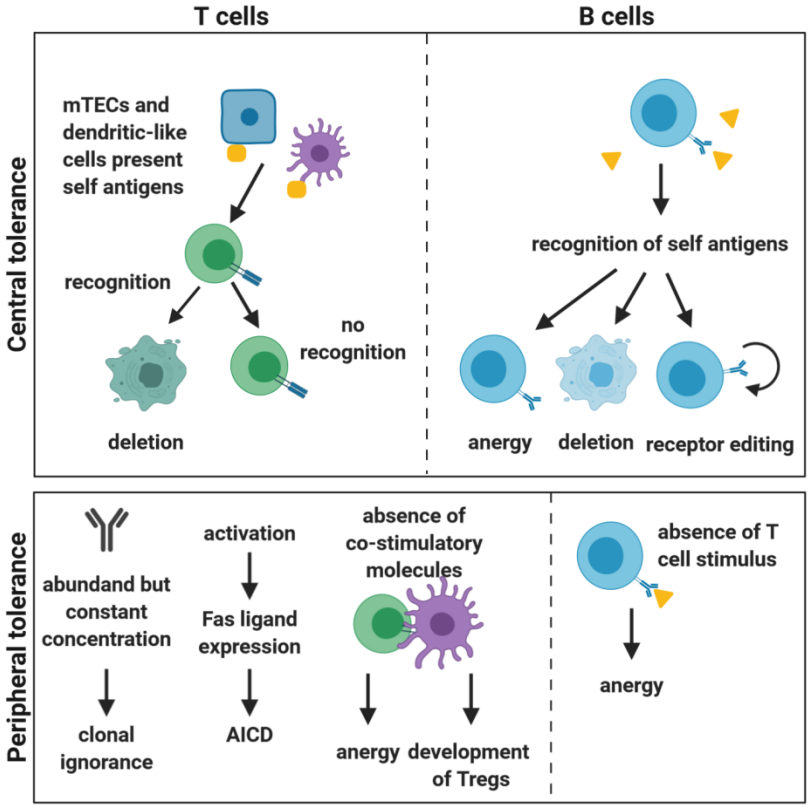

Figure 3: Overview of the tolerance mechanisms in T and B cells

Despite the fact that these mechanisms preventing autoimmunity are fine-tuned and well-organized, autoimmune diseases may occur. The mechanisms underlying the development of autoimmune diseases are not completely clear, but genetic predisposition, in combination with environmental triggers, seems to contribute to their emergence (Zhang and Lu, 2018).

Autoimmunity can be classified according to organ-specific or systemic autoimmune diseases (Amaya-Uribe et al., 2019). Organ-specific autoimmune diseases, such as multiple sclerosis, lead to a destruction of a specific tissue, whereas in the case of systemic autoimmune diseases, such as rheumatoid arthritis, the immune cells react to antigens, which are spread through different parts of the body (Theofilopoulos et al., 2017).

2.3.1. Treatment of autoimmune diseases

Since a causal therapy for autoimmune diseases is currently unavailable, the prevention of tissue damage is achieved by symptomatic treatment with immune suppressive drugs. These drugs include derivatives of the glucocorticoid family, called corticosteroids. One of the most commonly applied corticosteroid drugs is prednisone, a prodrug actively metabolized to prednisolone (Becker, 2013). Steroid hormones pass through the cell membrane to bind and activate their intracellular receptor. Activation of the receptor causes its transport to the nucleus and enables DNA binding; thus, corticosteroids can regulate many genes expressed in lymphocytes, such as NF-κB, AP-1, or the signal transducer and activator of transcription (STAT), and thereby suppress the function of lymphocytes (Frenkel et al., 2015; Oakley and Cidlowski, 2013). Moreover, they can induce apoptosis or decrease the expression of adhesion molecules, which are important for the migration of lymphocytes (Ramamoorthy and Cidlowski, 2016). Although quite effective, corticosteroids cause a range of side effects, such as diabetes or osteoporosis (Ramamoorthy and Cidlowski, 2016).

Drugs like cyclophosphamide or mycophenolate cause even more side effects. They act through the inhibition of DNA synthesis and, thus, by inhibiting the proliferation of lymphocytes, as well as cells in the skin, the gut lining, and the bone marrow. The side effects range from leukopenia, damage of the epithelium, cardiotoxicity, and hemorrhagic cystitis to hair loss and fetal death (Allison, 2000; Murphy and Weaver, 2016).

A further option is offered by a group of drugs that interfere with the T cell signaling. This group includes some natural-product-derived drugs, such as cyclosporin A, tacrolimus, rapamycin, and fingolimod, and synthetic Janus kinase inhibitors (Jakinhibs), such as tofacitinib (Wiseman, 2016). The mode of action of these drugs is versatile, since the T cell signaling is complex and affords many target locations. Cyclosporin A and tacrolimus both prevent T cell proliferation by inhibition of the phosphatase calcineurin, but chronic nephrotoxicity is a side effect (Allison, 2000; Tedesco and Haragsim, 2012; Wiseman, 2016). Rapamycin inhibits T lymphocyte proliferation via blockage of the mammalian target of rapamycin (mTor) activation, but thereby induces hyperlipidemia, leukopenia,

and thrombocytopenia (Allison, 2000; Pallet et al., 2018). Fingolimod impedes the migration of lymphocytes, because it interferes with the lipid sphingosine 1-phosphate receptor on lymphocytes; the compound is specifically used to treat multiple sclerosis. (Buc, 2018).

Nowadays, a group of biotechnically manufactured, most of all protein-based, drugs are increasingly the focus of research and clinical application (Chan and Chan, 2017). These so-called biologics comprise a high level of specificity and a low level of toxicity (AlDeghaither et al., 2015). A major group of biologics are immune therapy releated antibodies (AlDeghaither et al., 2015; Murphy and Weaver, 2016). Antibodies against cytokines, or their receptors, are popular (Moroncini et al., 2017; Wagner, 2019). In addition, antibodies that inhibit the lymphocyte survival and antibody production of pathogenic B cells by neutralizing the B cell activating factor (BAFF) are promising (Wagner, 2019). Moreover, interference with co-stimulatory pathways can be achieved with CTLA-4 Igs, which compete with the T cell co-receptor for B7 molecules (Wagner, 2019). Last but not least, biologics can achieve an unspecific removal of lymphocytes. In autoimmune diseases, which are mediated by autoantibodies, recovery may come with antibodies against CD20 (retuximab), which induce apoptosis in B cell precursor cells (Moroncini et al., 2017; Wagner, 2019). The side effects of these biologics are not wide-ranging, yet an increased risk of developing serious infections must be considered (Moroncini et al., 2017).

References

Al Deghaither, D., Smaglo, B.G., Weiner, L.M., 2015. Beyond peptides and mAbs-current status and future perspectives for biotherapeutics with novel constructs. Journal of Clinical Pharmacology 55 Suppl 3, S4-20.

Allison, A.C., 2000. Immunosuppressive drugs: the first 50 years and a glance forward. Immunopharmacology 47, 63–83.

Amaya-Uribe, L., Rojas, M., Azizi, G., Anaya, J.-M., Gershwin, M.E., 2019. Primary immunodeficiency and autoimmunity: A comprehensive review. Journal of Autoimmunity 99, 52–72.

Becker, D.E., 2013. Basic and clinical pharmacology of glucocorticosteroids. Anesthesia Progress 60, 25–32.

Buc, M., 2018. New biological agents in the treatment of multiple sclerosis. Bratisl Lek Listy 119, 191–197.

Chan, J.C., Chan, A.T., 2017. Biologics and biosimilars: what, why and how? ESMO Open 2.

Frenkel, B., White, W., Tuckermann, J., 2015. Glucocorticoid-induced osteoporosis, in: Wang, J.-C., Harris, C. (Eds.), Glucocorticoid Signaling. Springer New York, New York, NY, 179–215.

Göschl, L., Scheinecker, C., Bonelli, M., 2019. Treg cells in autoimmunity: from identification to Treg-based therapies. Seminars in Immunopathology 41, 301–314.

Khan, U., Ghazanfar, H., 2018. T lymphocytes and autoimmunity, in: International Review of Cell and Molecular Biology. Elsevier, pp. 125–168.

Moroncini, G., Calogera, G., Benfaremo, D., Gabrielli, A., 2018. Biologics in inflammatory immune-mediated systemic diseases. Current Pharmaceutical Biotechnology 18, 1008–1016.

Murphy, K., Weaver, C., 2016. Janeway's immunobiology, 9th ed. Garland Science, New York, NY.

Oakley, R.H., Cidlowski, J.A., 2013. The biology of the glucocorticoid receptor: New signaling mechanisms in health and disease. Journal of Allergy and Clinical Immunology 132, 1033–1044.

Pallet, N., Fernández-Ramos, A.A., Loriot, M.-A., 2018. Impact of immunosuppressive drugs on the metabolism of T Cells, in: International review of cell and molecular biology. Elsevier, Amsterdam, 169–200.

Passos, G.A., Speck-Hernandez, C.A., Assis, A.F., Mendes-da-Cruz, D.A., 2018. Update on Aire and thymic negative selection. Immunology 153, 10–20.

Ramamoorthy, S., Cidlowski, J.A., 2016. Corticosteroids. Rheumatic Disease Clinics of North America 42, 15–31.

Romagnani, S., 2006. Immunological tolerance and autoimmunity. Internal and Emergency Medicine 1, 187–196.

Schildberg, F.A., Klein, S.R., Freeman, G.J., Sharpe, A.H., 2016. Coinhibitory pathways in the B7-CD28 ligand-receptor family. Immunity 44, 955–972.

Takaba, H., Takayanagi, H., 2017. The mechanisms of T cell selection in the thymus. Trends in Immunology 38, 805–816.

Tedesco, D., Haragsim, L., 2012. Cyclosporine: A review. Journal of Transplantation 2012, 1–7.

Theofilopoulos, A.N., Kono, D.H., Baccala, R., 2017. The multiple pathways to autoimmunity. Nature Immunology 18, 716–724.

Wagner, U., 2019. Biologika in der Rheumatologie. Der Internist 60, 1036–1042.

Walker, L.S.K., Abbas, A.K., 2002. The enemy within: keeping self-reactive T cells at bay in the periphery. Nature Reviews Immunology 2, 11–19.

Wiseman, A.C., 2016. Immunosuppressive medications. Clinical Journal of the American Society of Nephrology 11, 332–343.

Zhang, P., Lu, Q., 2018. Genetic and epigenetic influences on the loss of tolerance in autoimmunity. Cellular & Molecular Immunology 15, 575–585.

2.4. Natural product-based drug discovery

Despite the achievements of modern medicine in developing innovative medications, continuous research on novel drugs is crucial for overcoming current and future limitations. The problems of current therapies include various side effects, nonresponding, the development of bacterial or viral resistance, or the high cost of available pharmaceuticals (Allison, 2000; Aslam et al., 2018; Daubert et al., 2017; Mathur and Hoskins, 2017; Río et al., 2009). Natural-product-based drug discovery has played a substantial role in the field of drug development since the isolation of morphine, in 1804, established rational drug discovery from plants (Atanasov et al., 2015; Pollastro et al., 2009). The discovery of penicillin in 1928 extended the field of natural products for pharmaceutical purposes to microbial sources (David et al., 2014); furthermore, the pharmaceutical industry moved from crude extracts and partially-purified natural products to pure compounds during these times (David et al., 2014). The rapid progress in the field of chemistry in the twentieth and twenty-first centuries has promoted high-throughput screenings (HTS) of synthetic compound libraries for drug development (Atanasov et al., 2015), resulting in natural products taking a backseat (Bäumler, 2007). The important advantages of plant-based molecules, compared to synthetic compounds, however, are mainly related to structural differences: a lower flexibility and a higher size and number of chiral centers, resulting in stronger and more specific activity (Atanasov et al., 2015). The restricted chemical diversity within the synthetic compound libraries was reflected in a declining number of drug approvals, and this development finally led to a return to natural-product-based drug discovery (Kingston, 2010). This progression was exemplified by the analysis of Newman and Cragg, postulating that 1/3 of the drugs approved by the Food and Drug Administration (FDA) between 1981 and 2014 were based on natural products (Newman and Cragg, 2016). 2018 was a very successful year with respect to both the number of FDA-approved drugs based on natural products and the overall FDA-approved drugs (Figure 4) (de la Torre and Albericio, 2019). In this year, 10 of 59 (16%) of all approved drugs were of natural origin. The majority of these drugs were bacteria-inspired (de la Torre and Albericio, 2019); they included three tetracycline antibiotics, originating from *Streptomyces*; two carbohydrate-inspired drugs, which were derived from a combination of nojirimycin, originally produced from *Streptomyces* (Argoudelis et al., 1976), and gentamicin from *Micromonospora purpurea* (Wei et al., 2019); and two macrocycles—one a semi-synthetic derivate of nemadectin, a fermented product of *Streptomyces cyaneogriseus* ssp. *Noncyanogenus* (Song et al., 2018), and rifamycin, which is isolated semi-synthetically from *Amycolatopsis rifamycinica sp. nov.*(Bala et al., 2004). Furthermore, one combination of the steroid estrogen ethinylestradiol and progestin segestrone acetate, as well as a fish oil-derived fatty acid emulsion, called Omegaven™, were successfully approved. Finally, cannabidiol, which is derived from the marijuana plant, was licensed by the FDA in 2018 (de la Torre and Albericio, 2019). There are

several more prominent examples of new chemical entities that were discovered in the world of higher plants in the past 40 years: paclitaxel (from the bark of the Pacific yew, *Taxus brevifolia*), vinblastine (from the Madagascar periwinkle, *Catharanthus roseus*), and camptothecin (from the bark and stem of a Chinese tree, *Camptotheca acuminata*) exemplify the importance of plant-based natural products as a drug discovery source (Atanasov et al., 2015; Kinghorn et al., 2011).

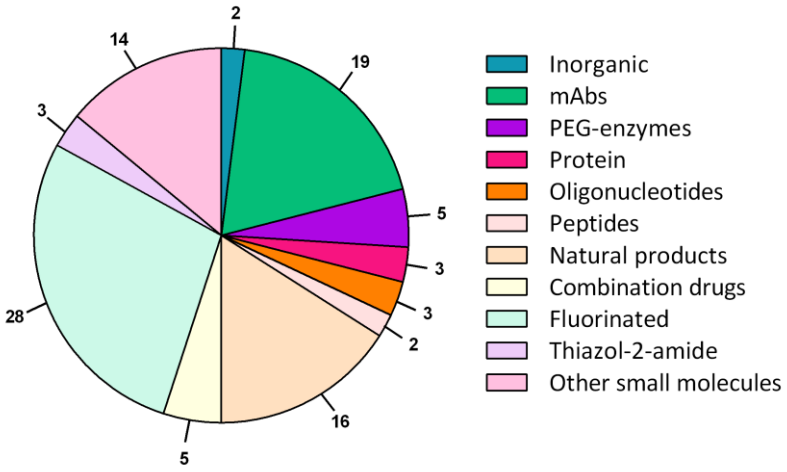

Figure 4: Drugs approved by the FDA in 2018 and classified on the basis of their chemical structure (adapted from de la Torre and Albericio, 2019). Numbers indicate the percentages for the groups.

Plant-based drug discovery is bedeviled with intricacies and challenges (Figure 5). The first step involves the identification of plants by reference to morphological, anatomical, genetic, and chemical classifications, which can be challenging in respect of nomenclatural synonyms and changes in the plant taxonomy (Atanasov et al., 2015). A further problem is the availability of plant material, as well as the accessibility of remotely-existing plants, reductions due to natural catastrophes, local wars, or legal regulations (Atanasov et al., 2015). Furthermore, guaranteeing a steady quality supply of the crude plant material is crucial. Climatic conditions, light availability, soil conditions (including fertilization), and the harvest season affect active ingredients and, thus, the quality of the plant material (Bäumler, 2007). To compensate for this natural variability of the plants, the pharmaceutical industry is nowadays switching from wild harvesting to controlled biological cultivation or to the use of composites from different crop years and locations (Bäumler, 2007). The processing of plant material is essential for the standardization of a plant extract, which requires unification and comprehensive documentation at all levels of manufacturing (Bäumler, 2007). Total synthesis of bioactive compounds from natural sources represents an alternative to standardized plant extracts; the challenge, however, is that natural products are often characterized by the high complexity of their chemical structures, demanding specialized synthesis methods (Atanasov et al., 2015; Calixto, 2019).

Despite the challenges of natural product drug discovery, the heavy financial burden attending the common and popular big molecules (biologicals) has renewed interest in small molecules from natural products (Pollastro et al., 2009). Such research requires interdisciplinary experimental approaches with a fine-tuned choice of biological assays and chemical methods for fractionation, compound isolation, and structure elucidation.

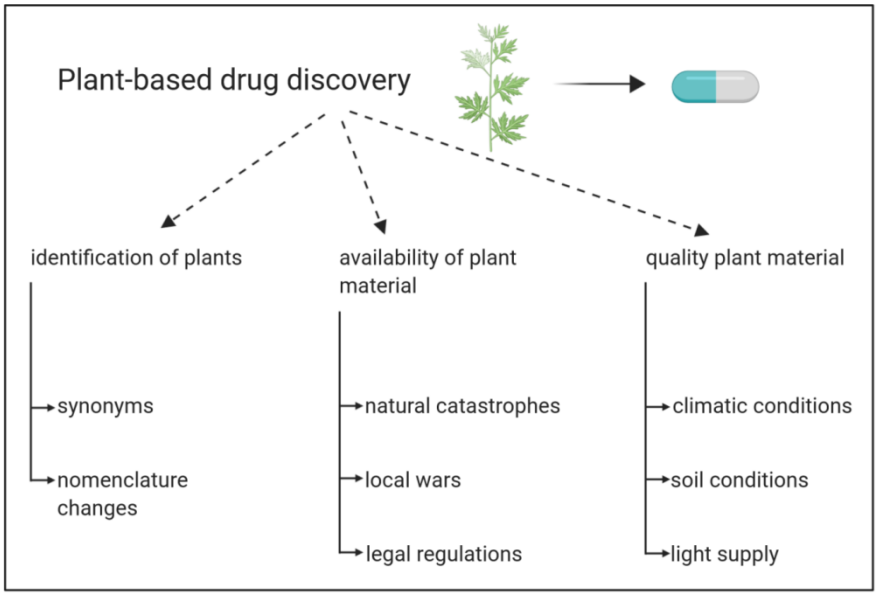

Figure 5: Basic considerations and challenges regarding plant-based-drug discovery

References

Allison, A.C., 2000. Immunosuppressive drugs: the first 50 years and a glance forward. Immunopharmacology 47, 63–83.

Argoudelis, A.D., Reusser, F., Mizsak, S.A., Baczynskyj, L., 1976. Antibiotics produced by *Streptomyces ficellus II*. Feldamycin and nojirimycin. Journal of Antibiotics 29, 1007–1014.

Aslam, B., Wang, W., Arshad, M.I., Khurshid, M., Muzammil, S., Rasool, M.H., Nisar, M.A., Alvi, R.F., Aslam, M.A., Qamar, M.U., Salamat, M.K.F., Baloch, Z., 2018. Antibiotic resistance: a rundown of a global crisis. Infection and Drug Resistance 11, 1645–1658.

Atanasov, A.G., Waltenberger, B., Pferschy-Wenzig, E.-M., Linder, T., Wawrosch, C., Uhrin, P., Temml, V., Wang, L., Schwaiger, S., Heiss, E.H., Rollinger, J.M., Schuster, D., Breuss, J.M., Bochkov, V., Mihovilovic, M.D., Kopp, B., Bauer, R., Dirsch, V.M., Stuppner, H., 2015. Discovery and resupply of pharmacologically active plant-derived natural products: A review. Biotechnology Advances 33, 1582–1614.

Bala, S., Khanna, R., Dadhwal, M., Prabagaran, S.R., Shivaji, S., Cullum, J., Lal, R., 2004. Reclassification of *Amycolatopsis mediterranei* DSM 46095 as *Amycolatopsis rifamycinica sp. nov.* International Journal of Systematic and Evolutionary Microbiology 54, 1145–1149.

Bäumler, S., 2006. Heilpflanzenpraxis Heute: Porträts - Rezepturen - Anwendung. Urban & Fischer bei Elsevier, München.

Calixto, J.B., 2019. The role of natural products in modern drug discovery. Anais da Academia Brasileira de Ciências 91 Suppl 3.

Daubert, C., Behar, N., Martins, R.P., Mabo, P., Leclercq, C., 2017. Avoiding non-responders to cardiac resynchronization therapy: a practical guide. European Heart Journal 38, 1463–1472.

David, B., Wolfender, J.-L., Dias, D.A., 2015. The pharmaceutical industry and natural products: historical status and new trends. Phytochemistry Reviews 14, 299–315.

de la Torre, B.G., Albericio, F., 2019. The Pharmaceutical Industry in 2018. An analysis of FDA drug approvals from the perspective of molecules. Molecules 24, 809.

Kinghorn, A.D., Pan, L., Fletcher, J.N., Chai, H., 2011. The relevance of higher plants in lead compound discovery programs. Journal of Natural Products 74, 1539–1555.

Kingston, D.G.I., 2011. Modern natural products drug discovery and its relevance to biodiversity conservation. Journal of Natural Products 74, 496–511.

Mathur, S., Hoskins, C., 2017. Drug development: Lessons from nature. Biomedical Reports 6, 612–614.

Newman, D.J., Cragg, G.M., 2016. Natural products as sources of new drugs from 1981 to 2014. Journal of Natural Products 79, 629–661.

Pollastro, F., Fontana, G., Appendino, G., 2009. In comprehensive natural products II chemistry and biology. 205–236.

Río, J., Comabella, M., Montalban, X., 2009. Predicting responders to therapies for multiple sclerosis. Nature Reviews Neurology 5, 553–560.

Song, X., Zhang, Y., Xue, J., Li, C., Wang, Z., Wang, Y., 2018. Enhancing nemadectin production by Streptomyces cyaneogriseus ssp. noncyanogenus through quantitative evaluation and optimization of dissolved oxygen and shear force. Bioresource Technology. 255, 180–188.

Wei, Z., Shi, X., Lian, R., Wang, W., Hong, W., Guo, S., 2019. Exclusive production of Gentamicin C1a from *Micromonospora purpurea* by metabolic engineering. Antibiotics (Basel) 8, 267.

2.5. Reverse pharmacology approach

In this study, screening of plant extract libraries was performed with a "reverse pharmacology" phenotypic approach, using a cell-based test system (Figure 6). The "reverse pharmacology" phenotypic approach begins with the selection of a model for *in vitro* testing, which can be target-oriented (e.g. function of a specific protein) or phenotypic (e.g. cell proliferation or wound healing) (Atanasov et al., 2015). Thereafter, promising hits must be validated with appropriate *in vivo* models. This approach allows minimal animal testing, since *in vitro* non-active substances are excluded from *in vivo* assays (Atanasov et al., 2015). The great demand for novel and innovative drugs, as well as the number and diversity of candidates that are relevant for testing, has led to the establishment of HTS assays in the field of natural product drug discovery. HTS assays are classified as biochemical assays and cell-based assays. Biochemical assays mainly involve enzyme inhibition and receptor-ligand binding assays (Zang et al., 2012), which allow downscaling to a test model with low variation, but the disadvantages are the limited availability of targets. Also, possible effects may not occur in a cellular context. By contrast, cell-based assays can provide considerable information about the concentration–response relationship of a test substance with respect to diverse cellular functions in a biologically-relevant micro-environment (Butterweck and Nahrstedt, 2012; Nierode et al., 2016; Zang et al., 2012).

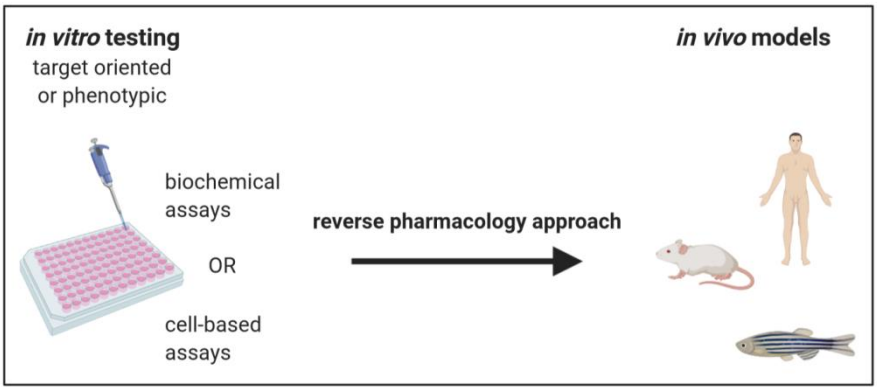

Figure 6: Reverse pharmacology approach for HTS based drug discovery

References

Atanasov, A.G., Waltenberger, B., Pferschy-Wenzig, E.-M., Linder, T., Wawrosch, C., Uhrin, P., Temml, V., Wang, L., Schwaiger, S., Heiss, E.H., Rollinger, J.M., Schuster, D., Breuss, J.M., Bochkov, V., Mihovilovic, M.D., Kopp, B., Bauer, R., Dirsch, V.M., Stuppner, H., 2015. Discovery and resupply of pharmacologically active plant-derived natural products: A review. Biotechnology Advances 33, 1582–1614.

Butterweck, V., Nahrstedt, A., 2012. What is the best strategy for preclinical testing of botanicals? A critical perspective. Planta Medica 78, 747–754.

Nierode, G., Kwon, P.S., Dordick, J.S., Kwon, S.-J., 2016. Cell-based assay design for high-content screening of drug candidates. Journal of Microbiology and Biotechnology 26, 213–225.

Zang, R., Li, D., Tang, I.-C., Wang, J.-F., Yang, S.-T., 2012. Cell-based assays in high-throughput screening for drug discovery. International Journal of Biotechnology for Wellness Industries 1, 31-51.

2.6. Cell-based *in vitro* test systems

This study applies phenotypic model assays using either primary human cells or immortalized human cell lines. Immortalized cell lines support a cheap and reproducible test system (Atanasov et al., 2015). They are easy to cultivate because they are homogenous cell populations, highly proliferative, and adapted to the cell culture environment (Atanasov et al., 2015; Zang et al., 2012); however, they often accumulate mutations and show aberrant phenotypes (Atanasov et al., 2015; Zang et al., 2012). Overall, immortalized cell lines reflect the *in vivo* situation in an inferior way to primary cells (Atanasov et al., 2015; Zang et al., 2012). Primary cells represent an alternative, but they are laborious to cultivate, since they need to be freshly prepared. Moreover, their lifespan in a culture is limited and the experimental reproducibility is sometimes challenging (Atanasov et al., 2015; Zang et al., 2012). Altogether, cell-based assays are a reasonable and simple option for evaluating pharmacological activity and elucidating the underlying molecular mechanism. Furthermore, cell-based assays can be applied in bioactivity-guided fractionations to identify and isolate active compounds from natural products, but some pitfalls need to be considered during the planning and performance of cell-based *in vitro* experiments (Figure 7) (Atanasov et al., 2015). When planning cell-based experiments, it is mandatory to ensure a reliable and robust test system, so suitable controls and an appropriate sample size for adequate statistical analysis are obligatory. A further important issue is the choice of test concentrations that are realistic for further drug development. In this regard, Butterweck and Nahrstedt recommended IC_{50} values below 100 µg/mL for extracts and 25 µM for pure compounds (Butterweck and Nahrstedt, 2012). Also, care must taken, since the solvent, such as dimethyl sulfoxide (DMSO), can itself affect the cells (Butterweck and Nahrstedt, 2012). Moreover, the increased solubility might yield compounds that would never be dissolved under normal physiological conditions. These compounds might influence test results although they might be irrelevant for the therapeutic effect. Furthermore, plant extracts may contain solid constituents that can cause oxidative stress or toxic effects when they come into contact with cells during the experimental procedure; therefore, it is recommended to use only clear supernatants obtained by centrifugation prior to experimental use (Butterweck and Nahrstedt, 2012).

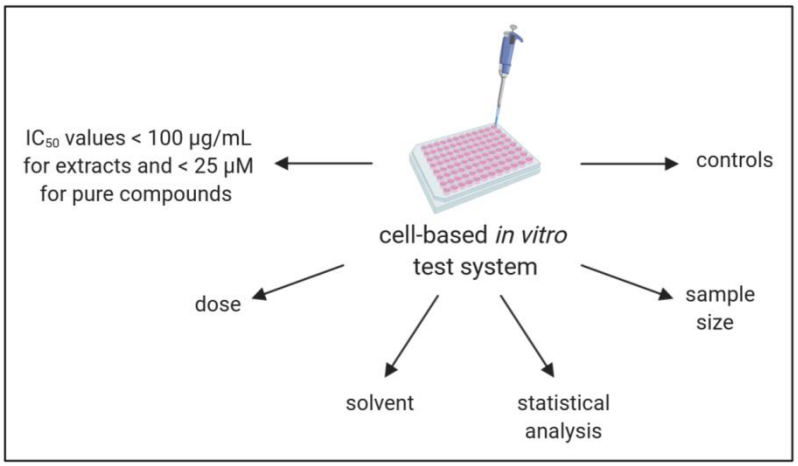

Figure 7: Considerations for *in vitro* cell-based test systems (adapted from Butterweck and Nahrstedt, 2012).

References

Atanasov, A.G., Waltenberger, B., Pferschy-Wenzig, E.-M., Linder, T., Wawrosch, C., Uhrin, P., Temml, V., Wang, L., Schwaiger, S., Heiss, E.H., Rollinger, J.M., Schuster, D., Breuss, J.M., Bochkov, V., Mihovilovic, M.D., Kopp, B., Bauer, R., Dirsch, V.M., Stuppner, H., 2015. Discovery and resupply of pharmacologically active plant-derived natural products: A review. Biotechnology Advances 33, 1582–1614.

Butterweck, V., Nahrstedt, A., 2012. What is the best strategy for preclinical testing of botanicals? A critical perspective. Planta Medica 78, 747–754.

Zang, R., Li, D., Tang, I.-C., Wang, J.-F., Yang, S.-T., 2012. Cell-based assays in high-throughput screening for drug discovery. International Journal of Biotechnology for Wellness Industries 1, 31-51.

2.7. Flow cytometry-based analysis

Flow cytometry (FCM) is currently state-of-the art in the field of immunology. A flow cytometer includes three interacting systems: fluidic, optic, and electronic (Figure 8) (McKinnon, 2018). A sheath fluid (mostly PBS) (fluidic) transports and presents the sample for analysis by the laser system. The optical system consists of lasers (excitation optics), photomultiplier tubes (PMTs), and photodiodes (collection optics). It is responsible for the detection of visible and fluorescent light, which is then converted into digital signals by the electronic system (McKinnon, 2018). This complex interaction of systems allows the detection of light scattered by a particle in the forward direction (forward scatter; Fsc) and in the sideways direction (side scatter; Ssc); thereby, the Fsc indirectly gives information about

the size of the particle, whereas the Ssc shows its granularity (McKinnon, 2018). A flow cytometer is capable of detecting fluorescence signals that can be generated by either staining with fluorescence dyes (e.g., PI) or fluorescence marked antibodies (e.g., CD4-APC). Furthermore, analysis of fluorescence proteins (e.g., green fluorescent protein) produced by transfected cells is possible (Cossarizza et al., 2019; McKinnon, 2018).

Overall, this technology can be used to analyze complex cell phenotypes, the molecules produced after stimulation by a specific cell population, signaling processes, proliferation, differentiation, cell–cell interactions, cytotoxicity, and cell death (Figure 8) (Cossarizza et al., 2019). Specific surface markers allow the characterization of lymphocyte subsets or activation stages, while the production of cytokines is linked to the functional stages. In addition, differentiation stages and homing capacities can be analyzed (Cossarizza et al., 2019; McKinnon, 2018).

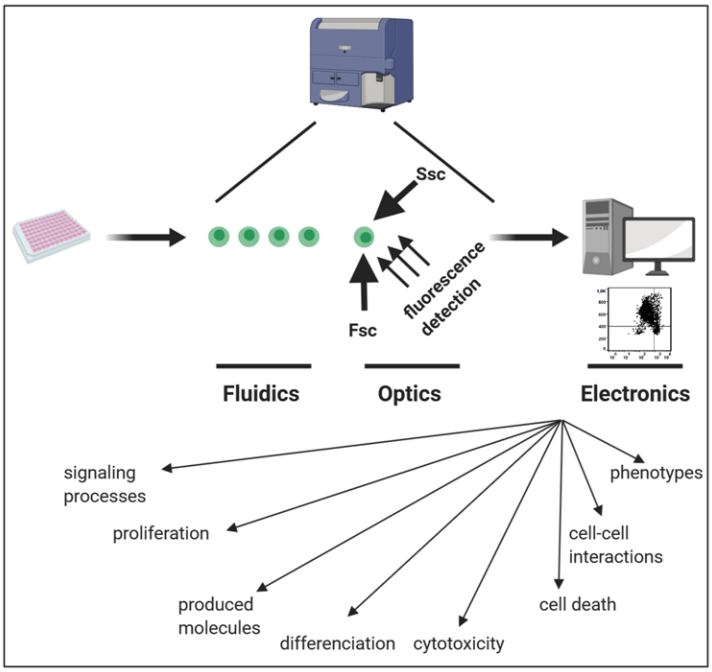

Figure 8: Overview of the flow cytometry process

References

Cossarizza, A., Chang, H.-D., Radbruch, A., Acs, A., Adam, D., Adam-Klages, S., et al., 2019. Guidelines for the use of flow cytometry and cell sorting in immunological studies (second edition). European Journal of Immunology 49, 1457–1973.

McKinnon, K.M., 2018. Flow Cytometry: An Overview. Current Protocols in Immunology 120, 5.1.1-5.1.11.

2.8. High-performance liquid chromatography (HPLC)-based activity profiling

Depending on a comprehensive characterization of crude plant extracts and further mode of action tests, this study addressed the identification and isolation of the compounds responsible for the activity of the extract guided by HPLC-based activity profiling. The classical bioactivity-guided isolation approach includes repetitive fractionation cycles, combined with biological tests, whereby inactive fractions are dropped and active fractions are further separated to identify bioactive compounds (Atanasov et al., 2015). This arduous approach is incompatible with the rapid development of modern medicine (Hamburger, 2019). By contrast, HPLC-based activity profiling offers an accelerated approach for tracking the bioactivity of active compounds (Figure 9). HPLC can be performed analytically and fractions are collected as microfractions, either by time windows or based on specific peaks (Potterat and Hamburger, 2014a). The microfractions are tested with the biological assay of interest, allowing the activity to be correlated with specific peaks or regions of the chromatogram (Hamburger, 2019). This is then followed by the targeted isolation of compounds found in this region, which can be tested by a simple run on the HPLC, instead of by time-consuming biological testing (Hamburger, 2019; Potterat and Hamburger, 2014a). In parallel to the fractionation process, structural information is obtained on-line by ultraviolet (UV) light, evaporative light scattering (ELS), or mass spectrometry (MS) detection (Hamburger, 2019; Potterat and Hamburger, 2014a). Another means of shedding light on chemical structures is an off-line approach using microprobe nuclear magnetic resonance (NMR) on fractions obtained from a semi-preparative fractionation, since a larger sample is required in this case. NMR is required for a full elucidation of the structure (relative configuration) of a purified compound. It is a highly robust method and does not involve delicate adjustments (Potterat and Hamburger, 2014a). Recurring difficulties of this approach can result from the complexity of the plant extract, whereby compounds can act together additively or synergistically. In this case, the fractionation process would prevent the compound interactions and consequently result in lower activity. In addition, promising bioactive compounds may have low concentrations in the crude extract or be masked by other abundant compounds (Atanasov et al., 2015), and some compounds (e.g. tannins) may interfere with the bioassay readout (Hamburger, 2019).

Nevertheless, HPLC-based activity profiling can be applied to a variety of bioassays with little adaption. An early prioritization of samples for further investigation facilitates and accelerates the process of compound discovery, showing that HPLC-based activity profiling is a powerful tool for identifying and characterizing the potential and novel immunosuppressive leads from natural products (Potterat and Hamburger, 2014a).

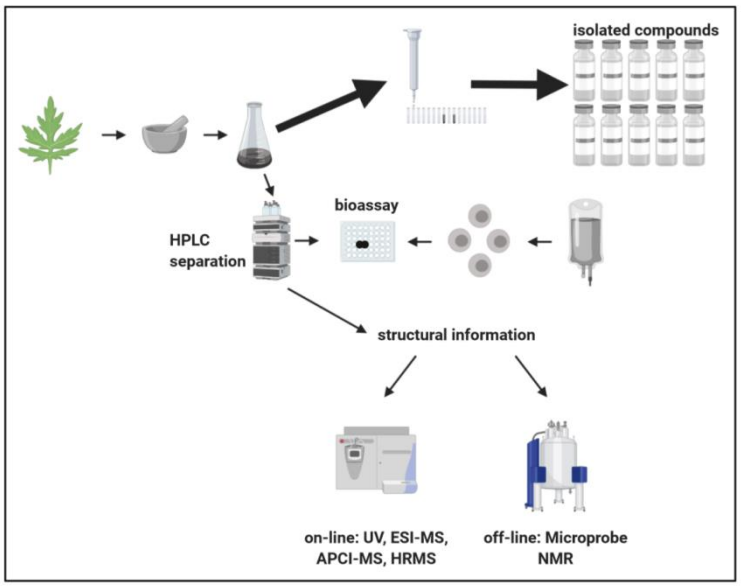

Figure 9: Principle of HPLC-based activity profiling

References

Atanasov, A.G., Waltenberger, B., Pferschy-Wenzig, E.-M., Linder, T., Wawrosch, C., Uhrin, P., Temml, V., Wang, L., Schwaiger, S., Heiss, E.H., Rollinger, J.M., Schuster, D., Breuss, J.M., Bochkov, V., Mihovilovic, M.D., Kopp, B., Bauer, R., Dirsch, V.M., Stuppner, H., 2015. Discovery and resupply of pharmacologically active plant-derived natural products: A review. Biotechnology Advances 33, 1582–1614.

Hamburger, M., 2019. HPLC-based activity profiling for pharmacologically and toxicologically relevant natural products – principles and recent examples. Pharmaceutical Biology 57, 328–334.

Potterat, O., Hamburger, M., 2014. Combined use of extract libraries and HPLC-based activity profiling for lead discovery: Potential, challenges, and practical considerations. Planta Medica 80, 1171–1181.

3. Results and discussion

3.1. Sesquiterpene lactones from Artemisia argyi: absolute configuration and immunosuppressant activity

Reinhardt, J.K., **Klemd, A.M.**, Danton, O., De Mieri, M., Smieško, M., Huber, R., Bürgi, T., Gründemann, C., Hamburger, M., 2019. Sesquiterpene Lactones from Artemisia argyi: Absolute Configuration and Immunosuppressant Activity. Journal of Natural Products 82, 1424–1433.

A library of 435 extracts from plants used in traditional Chinese medicine was screened for a T cell proliferation inhibitory potential. An ethyl acetate extract of *Artemisia argyi* suppressed the cell division of activated human T cells independently of apoptosis and necrosis induction. HPLC-based activity profiling was performed to track the active compounds. Thereby, guaianolides, seco-tanapartholides, flavonoids, and sesquiterpene lactones were identified. Comparison of experimental spectra with calculated electronic circular dichroism (ECD) spectra or experimental and calculated vibrational circular dichroism (VCD) spectra, yielded the absolute configurations. A T cell proliferation assay discovered the immunosuppressive potential of guaianolides and seco-tanapartholides, reflected by IC_{50} values between between 1.0 and 3.7 µM. Apoptosis and necrosis induction was excluded to be responsible for these effects.

My contribution: I performed the T cell proliferation and T cell viability experiments, analyzed the data, calculated the statistics, prepared the figures and wrote the draft manuscript of the corresponding parts.

Amy Marisa Zimmermann-Klemd

JOURNAL OF NATURAL PRODUCTS

Article

Cite This: J. Nat. Prod. XXXX, XXX, XXX−XXX

pubs.acs.org/jnp

Sesquiterpene Lactones from *Artemisia argyi*: Absolute Configuration and Immunosuppressant Activity

Jakob K. Reinhardt,[†,#] Amy M. Klemd,[‡,#] Ombeline Danton,[†] Maria De Mieri,[†] Martin Smieško,[§] Roman Huber,[‡] Thomas Bürgi,[⊥] Carsten Gründemann,[‡] and Matthias Hamburger*[,†]

[†]Pharmaceutical Biology, Pharmacenter, University of Basel, Klingelbergstrasse 50, 4056 Basel, Switzerland

[‡]Center for Complementary Medicine, Institute for Infection Prevention and Hospital Epidemiology, Faculty of Medicine, University of Freiburg, Breisacher Straße 115 B, 79106 Freiburg, Germany

[§]Department of Molecular Modeling, University of Basel, Klingelbergstrasse 50, 4056 Basel, Switzerland

[⊥]Department of Physical Chemistry, University of Geneva, 30 Quai Ernest Ansermet, 1211 Geneva, Switzerland

Supporting Information

ABSTRACT: A library of extracts from plants used in Chinese Traditional Medicine was screened for inhibition of T lymphocyte proliferation. An ethyl acetate extract from aerial parts of *Artemisia argyi* showed promising activity and was submitted to HPLC-based activity profiling to track the active compounds. From the most active time window, three guaianolides (**1**, **2**, and **5**) and two *seco*-tanapartholides (**3** and **4**) were identified and, in a less active time window, five new sesquiterpene lactones (**8**−**11**, **17**), along with six known sesquiterpene lactones and two known flavonoids. The absolute configurations of compounds **1**, **2**, **5**−**10**, **13**−**15**, **17**, and **18** were established by comparison of experimental with calculated electronic circular dichroism (ECD) spectra. For *seco*-tanapartholides B (**3**) and A (**4**), ECD yielded ambiguous results, and their absolute configurations were determined by comparing experimental and calculated vibrational circular dichroism (VCD) spectra. Compounds **1**−**5** showed significant, noncytotoxic inhibition of T lymphocyte proliferation, with IC_{50} values between 1.0 and 3.7 μM.

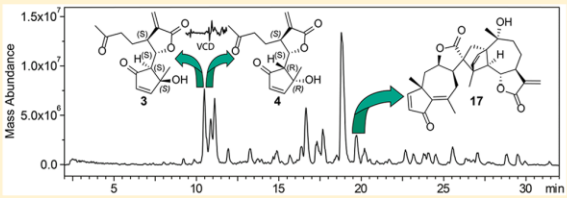

Immune malfunction is characterized by the body's inability to adequately differentiate between non-self and self-antigen structures. In immune deficiencies, the immune system fails to identify and eliminate pathogens, while in autoimmune diseases it fails to recognize endogenous cells from one's self.[1] Autoimmune diseases such as type I diabetes, rheumatoid arthritis, or multiple sclerosis are characterized by an increased T cell proliferation.[2] Presently, no causal therapies are available, and autoimmune diseases are typically treated symptomatically with immunosuppressive drugs.[3] As these substances often show severe side effects, the search for compounds with new modes of action and fewer adverse effects is warranted. Natural products have a successful track record for providing immunosuppressive compounds with unique modes of action, such as cyclosporine A, tacrolimus, rapamycin, mycophenolic acid, and myriocin.[4] Compared to actinomycetes and fungi, higher plants have been much less investigated as a source for immunosuppressive lead compounds. In an effort to explore the potential of plant secondary metabolites, a focused library of extracts from plants used in Traditional Chinese Medicine (TCM) was screened for their ability to inhibit T cell proliferation in vitro.

RESULTS AND DISCUSSION

Compound Isolation and Structure Elucidation. A library of 435 extracts was screened at a single concentration of 20 μg/mL for the ability to inhibit T lymphocyte proliferation.[5] A total of 40 extracts inhibited proliferation by ≥70% without exhibiting cytotoxicity at this concentration. This was verified by annexin V and propidium iodide (PI) double staining. These extracts were then tested at four concentrations ranging from 3 to 100 μg/mL. The ethyl acetate extract from aerial parts of *Artemisia argyi* Levl. et Vant. (Asteraceae) exhibited significant activity (IC_{50} 16.2 μg/mL) and was submitted to HPLC-based activity profiling.[6,7] Microfractions were collected and tested at four different dilutions, and a theoretical IC_{50} value was calculated and normalized to 100% (residual proliferation) as a measure of activity.

Pronounced inhibition of T cell proliferation was found in the time window of 10−12 min, and moderate activity in the window of 16−20 min (Figure 1). Preparative isolation of compounds **1**−**18** for structure elucidation and biological testing was achieved by a combination of open column chromatography on silica gel and semipreparative and preparative HPLC on C_{18} and cyano columns.

The UV spectra of compounds **1**−**11**, **13**−**15**, and **18** showed absorption maxima between 200 and 220 nm, while compounds

Received: September 17, 2018

DOI: 10.1021/acs.jnatprod.8b00791
J. Nat. Prod. XXXX, XXX, XXX−XXX

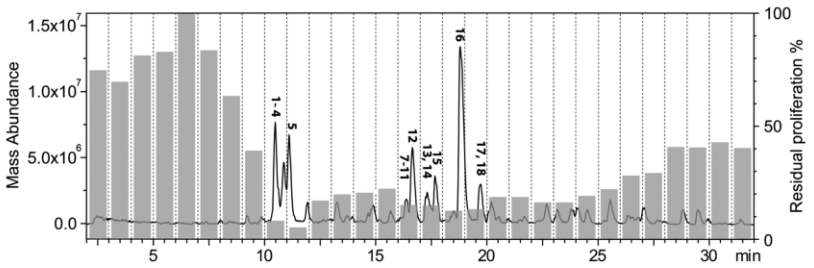

Figure 1. HPLC-ESIMS (base peak chromatogram) and activity profile (gray bars) of a EtOAc extract of *A. argyi*. Residual proliferation levels of T lymphocytes are expressed in % on inoculation with 1 min HPLC microfractions. Bold numbers in the chromatogram refer to compounds **1**–**18**.

Chart 1

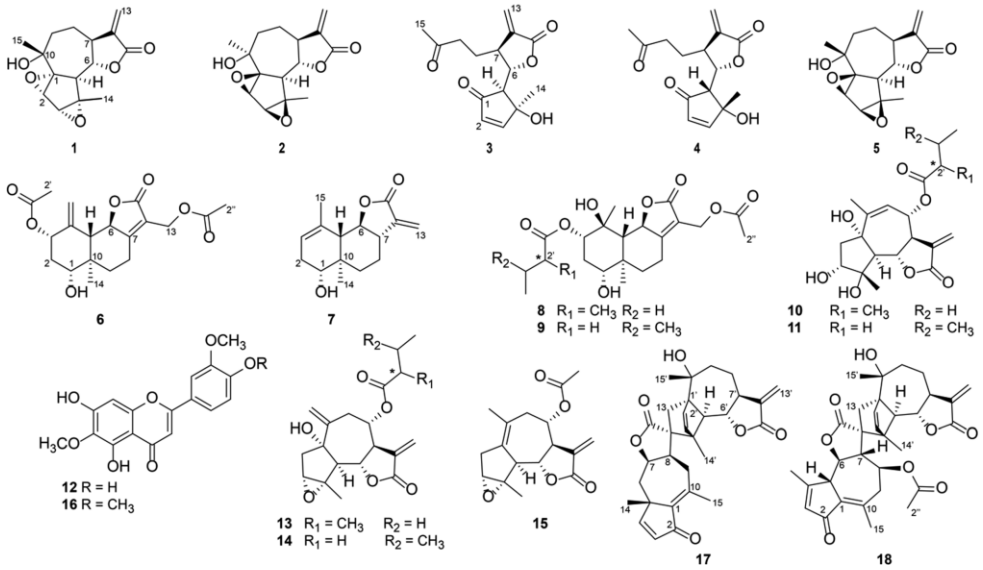

12 and **16** exhibited two UV maxima between 270 and 275 nm and 340−345 nm indicative of flavones.[8]

Compounds **6** and **7** were identified as the known eudesmanolide sesquiterpene lactones eudesmaafraglaucolide (**6**)[9] and santamarin (**7**).[10] The absolute configuration of **6** has not been established up to now and was determined by electronic circular dichroism (ECD) in comparison to the calculated spectrum as (1*R*,3*S*,5*S*,6*R*,10*R*) (Figure S42, Supporting Information).

3*α*,4*α*-Epoxyrupicoline D (**13**) and E (**14**) were isolated as a mixture and identified by comparison of their NMR spectra with published data (Table S5, ORTEP diagram in Figure S68, Supporting Information).[11] Compound **14** crystallized from the mixture, but the X-ray diffraction data were not of sufficient quality (Flack parameter (0.10(19)) to determine the absolute configuration. An ECD spectrum was recorded for the mixture and compared with the corresponding calculated spectra (Figure S67, Supporting Information). Thus, the absolute configuration of the scaffold in **13** and **14** was established as (1*S*,3*R*,4*S*,5*R*,6*S*,7*R*,8*S*). Given the lack of a suitable chromophore in the vicinity of C-2′, the absolute configuration of this stereocenter in **13** could not be determined by ECD.

Arteglasin A (**15**) was isolated as white crystals and identified by X-ray diffraction analysis (Table S7, ORTEP diagram in Figure S70, Supporting Information). NMR data were in good agreement with literature values.[12] The absolute configuration of **15** was determined as (3*R*,4*S*,5*S*,6*S*,7*R*,8*S*) (Flack parameter = 0.06 (15)) and confirmed by comparison of experimental and calculated ECD spectra (Figure S69, Supporting Information).

The flavones jaceosidin (**12**) and eupatilin (**16**) had been previously reported from *Artemisia argyi*.[13]

The NMR data of **1**, **2**, and **5** indicated that they are stereoisomers possessing a planar structure corresponding to that of canin (**1**).[14] Two of them were identified as canin (**1**) and artecanin (**5**) (Figure 2).[15]

The ECD spectrum of **1** exhibited a strong positive Cotton effect (CE) at 200 nm and a broad negative CE at 250 nm (Figure 3). The calculated spectrum for (1*R*)-canin was in good agreement with the experimental data obtained. An independent confirmation of the absolute configuration was obtained from the vibrational circular dichroism (VCD) spectrum that was compared to the calculated spectra of **1**, **2**, and **5** (at the B3LYP/6-31+G(d,p) level of theory) (Figure 4). For an unbiased comparison of VCD spectra, similarity indices *Sim*VA (for vibrational absorption) and *Sim*VCD were calculated with VCD SpecTech.[16] Similarity indices calculated for scaling factors between 0.939 and 1.009 are shown in Figure 4. The maximal value of *Sim*VCD was determined for (1*R*)-canin (**1**) at a wavenumber scale factor of 0.9865, which was used to plot the calculated spectra. A visual inspection of the main bands at 1772

DOI: 10.1021/acs.jnatprod.8b00791
J. Nat. Prod. XXXX, XXX, XXX−XXX

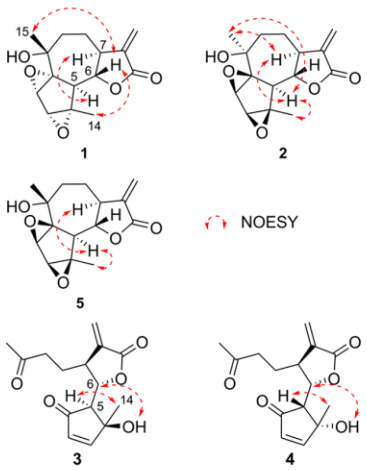

Figure 2. Selected NOESY correlations for compounds **1**–**5**.

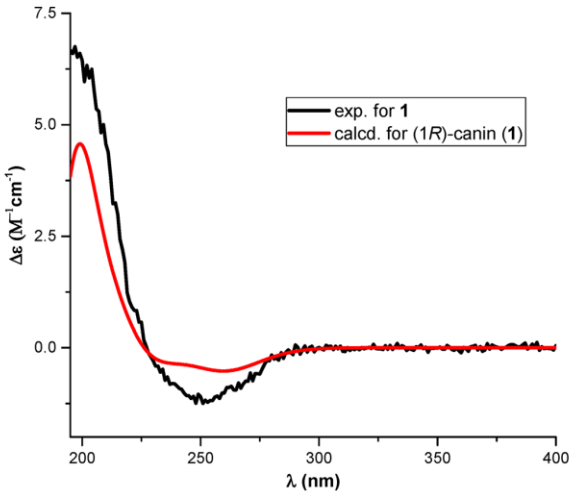

Figure 3. Comparison of experimental and calculated ECD spectra for compound **1** in MeOH.

(−), 1260 (+), 1205 (−), and 1150 (−) cm^{-1} in the VCD confirmed the assignment of the absolute configuration as (1*R*)-canin (**1**).

The absolute configuration of **5** was determined as (1*S*,2*R*,3*S*,4*R*,5*S*,6*S*,7*S*,10*R*), corresponding to (1*S*)-artecanin, by comparison of the experimental and calculated ECD spectra (Figure S38, Supporting Information). Additionally, the VCD spectrum of **5** was measured in DMSO-d_6 and compared to the computed spectra of compounds **1**, **2**, and **5** (Figure S40, Supporting Information). Although the relative configuration of **5** was clearly established from the NOESY correlations, the experimental VCD spectrum showed the best fit with the calculated spectrum of **1** when an automated comparison was used. Visual comparison of the experimental and the calculated spectra of **1** and **5** showed that they were all very similar with respect to the major CEs (e.g., 1277 (+), 1257 (+), 1215 (−), 1154 (−), and 1133 (+) cm^{-1}). However, a positive CE at 1385 cm^{-1} was seen in the experimental and calculated spectra of **5**, whereas a negative CE was present at this wavenumber in the calculated spectrum of **1**.

In contrast to **1** and **5**, compound **2** exhibited NOESY correlations between Me-15 (δ_H 1.41), H-5 (δ_H 2.26), and H-7 (δ_H 2.57), placing them in an α-orientation opposite H-6 (δ_H 4.12). A NOESY correlation between H-5 and Me-14 indicated a β-orientation of the two epoxy groups as in **5**. Therefore, compound **2** was the 10-epimer of artecanin. A compound with this structure was previously published as 10-*epi*-canin.[17] The structural assignment was at that time solely based on ^{1}H NMR data, but some of the published chemical shifts differed significantly from those measured for **2** (e.g., H-5 and H-7 reported: δ_H 2.62 and 3.40; measured for **2**: δ_H 2.26 and 2.57 ppm, Table S1, Supporting Information). Thus, the structural assignment for the previously published 10-*epi*-canin is likely incorrect. The absolute configuration of **2** was determined as (1*S*,2*R*,3*S*,4*R*,5*S*,6*S*,7*S*,10*S*) by comparison of experimental and calculated ECD spectra (Figure S17, Supporting Information).

Compounds **3** and **4** were obtained as stereoisomers with the planar structure of *seco*-tanapartholides.[17,18] The ^{1}H and ^{13}C NMR chemical shifts of **3** and **4** differed slightly, but the compounds exhibited the same correlations in their COSY, HMBC, and NOESY spectra (Table S2 and Figures S18–S29, Supporting Information). For both compounds, a NOESY correlation between H-5 (**3** δ_H 2.23, **4** δ_H 2.50) and Me-14 (**3** δ_H 1.41, **4** δ_H 1.45) was used to establish their orientations as *cis*-α or *cis*-β. The scalar coupling between H-6 and H-7 (**3** $J_{6,7}$ 3.1, **4** $J_{6,7}$ 5.8) indicated a *trans* orientation of H-6 (**3** δ_H 4.45, **4** δ_H 4.52) and H-7 (**3** δ_H 3.27, **4** δ_H 3.50). The dihedral angles between these two protons in the two most populated conformers in chloroform were determined as −115° and 132° for compound **3** and as 132° and 120° for compound **4**. Both the relative configurations of (4*S**,5*S**,6*S**,7*S**)-*seco*-tanapartholide B (**3**) and (4*R**,5*R**,6*S**,7*S**)-*seco*-tanapartholide A (**4**) were in accord with the NMR data, and only the *J* values between geminal H-5 and H-6 differed (**3** $J_{5,6}$ 7.3, **4** $J_{5,6}$ 2.1). On the basis of this difference, Kawazoe et al. previously postulated **3** as (4*S**,5*S**,6*S**,7*S**) and **4** as (4*R**,5*R**,6*S**,7*S**).[19] However, the two most populated conformers of compound **3** showed dihedral angles of 172° and 77° between H-5 and H-6, while angles of 72° and 173° were obtained for compound **4**. Thus, an assignment based on geminal *J* values was ambiguous.

Compounds **3** and **4** had enantiomer-like ECD spectra (Figure 5) but, given that the compounds had been separated on nonchiral stationary phases, could not be enantiomers. Calculated ECD spectra of **3** and **4** (absolute configuration as drawn) reproduced these CEs, although the experimental spectrum of **3** could also be explained by the computed enantiomeric spectrum of **4** and vice versa. Thus, the absolute configuration of **3** was either (4*S*,5*S*,6*S*,7*S*) or (4*S*,5*S*,6*R*,7*R*), and that of **4** was (4*R*,5*R*,6*S*,7*S*) or (4*R*,5*R*,6*R*,7*R*).

The experimental VCD spectrum of **3** in chloroform (Figure 6) was compared to calculated spectra of the (4*S*,5*S*,6*S*,7*S*) (**3**) and the (4*R*,5*R*,6*S*,7*S*) (**4**) stereoisomer. A good fit between the experimental and calculated spectra of **3** was obtained with a scaling factor of 0.9815 and confirmed by a visual comparison of major CEs at 1271 (+), 1323 (+), 1365 (−), 1380 (+), 1711 (+), and 1718 (+) cm^{-1} in the measured and calculated IR and VCD spectra. Hence, the absolute configuration of **3** was established as (4*S*,5*S*,6*S*,7*S*). In the same manner (Figure S31, Supporting Information) the absolute configuration of **4** was determined as (4*R*,5*R*,6*S*,7*S*).

Argyinolides K (**8**) and L (**9**) were obtained as an inseparable mixture. In the HRESIMS, the sodium adduct ion (*m*/*z* =

DOI: 10.1021/acs.jnatprod.8b00791
J. Nat. Prod. XXXX, XXX, XXX−XXX

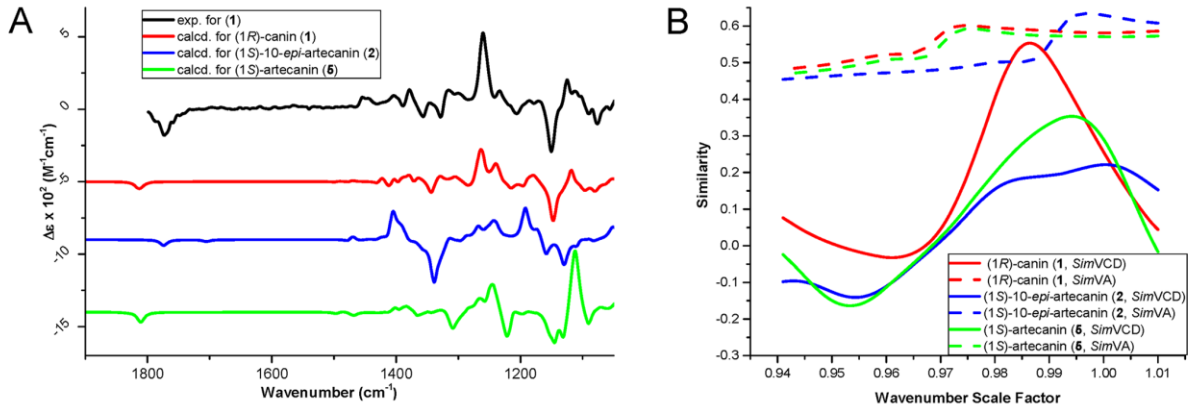

Figure 4. Comparison of experimental and computed VCD spectra in chloroform for compound **1**. The region of 1900−1050 cm^{-1} is shown (A). Similarities (*Sim*VA and *Sim*VCD) of the experimental VA and VCD spectra of **1** to the calculated spectra of possible stereoisomers were plotted as functions of wavenumber scale factor (B). The wavenumber scale factor corresponding to the maximal *Sim*VCD value in B (0.9865) was used to scale the computed spectra in A.

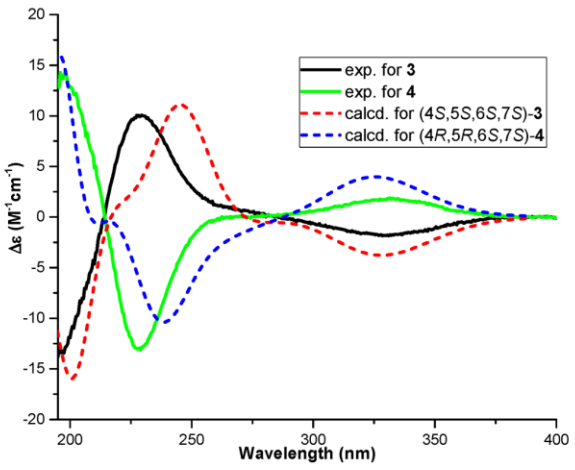

Figure 5. Comparison of experimental and calculated ECD spectra of **3** and **4** in MeOH.

447.2018 $[M + Na]^+$, calcd for $C_{22}H_{32}O_8Na$ 447.1989) indicated a molecular formula of $C_{22}H_{32}O_8$ for both compounds. Analysis of ^1H NMR and ^{13}C NMR data (Table 1) pointed to a eudesmanolide scaffold similar to that in **6**, but with the methylene group replaced by an sp^3-hybridized carbon (C-4, δ_C = 72.8) connected to a methyl group (Me-15 δ_H = 1.29, δ_C = 17.7) and a hydroxy group. Additional methyl signals were assigned to a 2-methylbutyryl moiety in **8** (Me-4′, δ_H 0.87, dd, J = 7.5, 7.5; Me-5′, δ_H 1.07, d, J = 7.0), a 3-methylbutyryl moiety in **9** (Me-4′/5′ δ_H 0.92, d, J = 6.7), and an acetyl group (Me-2″, δ_H 2.01, δ_C 20.6) in both compounds. Me-2″ showed HMBC correlations to C-13 (δ_H 4.72, δ_C 54.6). HMBC correlations between H-3 (δ_H = 4.60) and both butyryl carbonyl carbons (**8** δ_C = 175.0; **9** δ_C = 171.6) led to the identification of two regioisomers. The ratio between **8** and **9** was estimated as 2:1, based on the integrals of the Me-4′ (**8** δ_H = 0.87; **9** δ_H = 0.92) and Me-5′ (**8** δ_H = 1.07; **9** δ_H = 0.92) resonances in the ^1H NMR spectrum. This ratio was confirmed by the integration of the Me-15 resonances (**8** δ_H = 1.29; **9** δ_H = 1.28). The relative configurations of **8** and **9** were determined from the NOESY

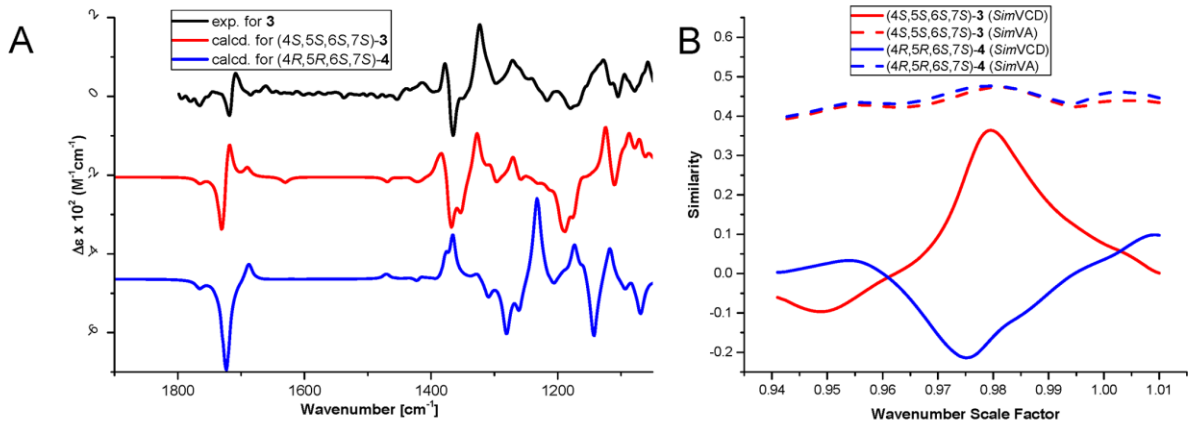

Figure 6. Comparison of experimental and computed VCD spectra in $CDCl_3$ for compound **3**. The region of 1900−1050 cm^{-1} is shown (A). Similarities (*Sim*VA and *Sim*VCD) of the experimental VA and VCD spectra of **3** to the calculated spectra of possible stereoisomers were plotted as functions of wavenumber scale factor (B). The wavenumber scale factor corresponding to the maximal *Sim*VCD value in B (0.9810) was used to scale the computed spectra in A.

DOI: 10.1021/acs.jnatprod.8b00791
J. Nat. Prod. XXXX, XXX, XXX−XXX

spectrum. Only the configuration at C-2′ in **8** could not be determined (Figure 7).

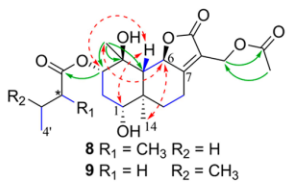

Figure 7. Selected COSY (blue bonds), HMBC (green arrows), and NOESY correlations (red arrows) for compounds **8** and **9**.

The ECD spectrum of the mixture (Figure S51, Supporting Information) showed maxima at 200 and 252 nm together with a minimum at 228 nm. Spectra were calculated for **9** and for both possible stereoisomers of **8**. The three spectra showed a positive CE at 200 nm and negative CEs between 215 and 235 nm. Only the maximum at 252 nm in the experimental spectrum was not reproduced in the calculations. Therefore, the absolute configurations of the rings in compounds **8** and **9** were established as (1*R*,4*S*,5*S*,6*R*,10*R*). Due to the limited amount available, it was not possible to measure the VCD spectrum of the mixture as an attempt to establish the absolute configuration of C-2′ in **8**.

Argyinolide M (**10**) gave a molecular formula of $C_{20}H_{28}O_7$ (HRESIMS data *m*/*z* 403.1750 [M + Na]$^+$, calcd for $C_{20}H_{28}O_7Na$, 403.1727), which suggested seven degrees of unsaturation. NMR data (Table 2, Figures S52−57, Supporting Information) indicated a guaianolide scaffold similar to that in a previously published compound.[20] In compound **10**, a 2-methylbutyryl group was attached at C-8, as indicated by the HMBC correlations between H-8 (δ_H 5.24) and C-1′ (δ_C 175.2). The relative configuration of **10** was established through NOESY correlations (Figure 8), and the absolute configuration

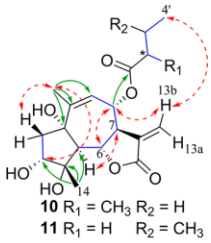

Figure 8. Selected COSY (blue bonds), HMBC (green arrows), and NOESY correlations (red arrows) for compounds **10** and **11**.

of the scaffold of **10** was determined via comparison of experimental and computed ECD spectra (Figure S58, Supporting Information) as (1*S*,3*R*,4*S*,5*R*,6*S*,7*R*,8*S*). As in the case of **8**, the absolute configuration at C-2′ could not be established.

Argyinolide N (**11**) was determined as being a regioisomer of **10** containing a 3-methylbutyryl unit instead of a 2-methylbutyryl group at C-8. Apart from the resonances attributed to the side chain, correlations in COSY, HMBC, and NOESY spectra were similar to those of **10**. The UV and ECD spectra were measured (Figures S65 and S66, Supporting Information). A strong positive CE at 195 nm in the calculated ECD spectrum was in agreement with the experimental data. However, the strong negative CE at 220 nm and a weak positive CE at 250 nm were not present in the experimental spectrum, and an unambiguous assignment of the absolute configuration was thus not possible for compound **11**.

Compound **18** was identified as 8-acetylarteminolide.[21] Its relative, but not its absolute configuration, has been reported previously. The absolute configuration was established as (5*S*,6*R*,7*R*,8*S*,12*S*,1′*R*,4′*R*,5′*S*,6′*S*,7′*S*,10′*R*) by comparison of measured and calculated ECD and VCD spectra (Figures S77, S78, and S79, Supporting Information).

Argyinolide O (**17**) gave a molecular formula of $C_{30}H_{34}O_6$ (HRESIMS *m*/*z* 513.2261 [M + Na]$^+$, calcd for $C_{30}H_{34}O_6Na$, 513.2248), corresponding to 14 degrees of unsaturation. Inspection of the NMR data (Table 3, Figures S71−76, Supporting Information) indicated that the molecule **17** consists of two distinct portions, each containing a γ-lactone ring. Thus, the structure of **17** resembled that of **18**, with one sesquiterpene portion being identical in these compounds.[21] In the other portion of **17**, a contiguous spin system between C-6 and C-9 was determined from the COSY spectrum (Figure 9).

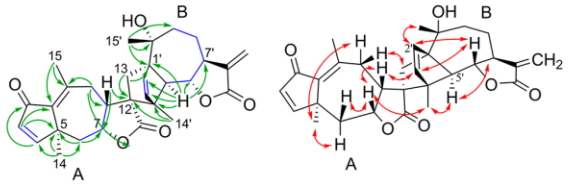

Figure 9. Selected COSY (blue bonds), HMBC (green arrows), and ROESY for compound **17**. For better visibility, ROESY correlations (red arrows) are shown in a spatial representation (right). A and B refer to the two sesquiterpene lactone portions.

Substituents at the bridgehead C-5 were characterized by HMBC correlations from Me-14 (δ_H 1.27) to C-4 (δ_C 155.3), C-5 (δ_C 38.4), and C-6 (δ_C 39.5). The orientation of the cyclopentenone ring was established by diagnostic HMBC correlations from the olefinic protons H-3 and H-4 to C-1, C-2, and C-5. A γ-lactone moiety was attached to the seven-membered ring at C-8 (δ_C 43.7) and C-7 (δ_C 75.4). The linkage of the two sesquiterpene portions A and B was established by HMBC correlations. Me-14′ (δ_C 16.1) and the diastereotopic protons at C-13 (δ_H 1.62, 2.50) of portion B, and H-8 (δ_H 2.32) of portion A, exhibited HMBC cross-peaks with C-12 (δ_C 61.3), and H_2-13 also with C-1′. The relative configuration of **17** was established via a series of diagnostic ROESY correlations (Figure 9). Correlations between H-5′ (δ_H 2.96), H-7′ (δ_H 3.39), and H_α-13 (δ_H 2.50, correlations not drawn in Figure 9) and between H-6′ (δ_H 4.00), H-2′ (δ_H 6.17), H_β-13 (δ_H 5.35), and H_β-9 (δ_H 6.17) indicated their respective cofacial orientation and thus helped determine the linkage of the lactone ring at C-6′ (δ_C 79.6) and C-7′ (δ_C 43.0) as *trans*. The β-orientation of Me-15′ (δ_H 1.38) was indicated by a ROESY cross-peak with H-2′. The configuration of C-12 was established through correlations between Me-14′ (δ_H 1.54) and H-7 (δ_H 4.77) and between H-3′ (δ_H 5.90) and H-8 (δ_H 2.32). The UV and ECD spectra of **17** were measured and compared to calculated data (Figures S74 and S75, Supporting Information). A strong negative CE in the ECD spectrum at 210 nm was present in the calculated spectrum, but not the broad negative CE occurring in the experimental spectrum between 230 and 290 nm. Considering the relative magnitudes of the absorption maxima in the UV

DOI: 10.1021/acs.jnatprod.8b00791
J. Nat. Prod. XXXX, XXX, XXX−XXX

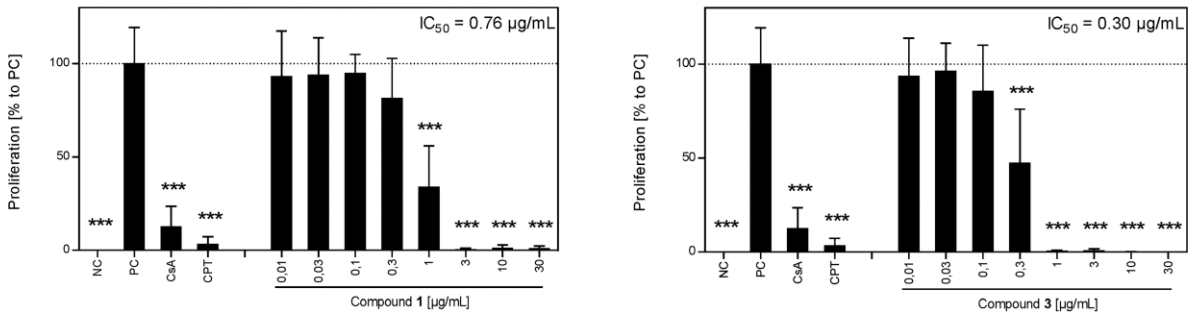

Figure 10. Inhibitory effects of compounds **1** and **3** on the proliferation of T lymphocytes. Data of three independent experiments were summarized and depicted as means ± standard deviation in relation to the untreated, stimulated control (PC; = 100% ± SD). Nonstimulated cells were used as the negative control (NC), cyclosporin A (CsA) was used as a known inhibitor of T cell proliferation, and camptothecin (CPT) was used as a known inducer of apoptosis. $*p < 0.05$, $**p < 0.01$, $***p < 0.001$.

spectrum, the negative CE at 210 nm was considered as being more relevant, and the absolute configuration assigned tentatively as (5*S*,7*R*,8*R*,12*S*,1′*R*,4′*R*,5′*S*,6′*S*,7′*S*,10′*R*). This is also in accord with the absolute configuration of compound **18**.

The absolute configurations of canin (**1**) and its stereoisomers **2** and **5** had not been previously determined, and the representation of their structures since their first description in 1969 followed a previous convention.[15] We determined the absolute configurations of canin (**1**) and artecanin (**5**) using ECD and VCD in combination with ab initio calculations. In addition, the absolute configurations of other sesquiterpene lactones were determined if a reliable assignment of such information was lacking. However, this was not established for the 2-methylbutyryl side chain in compounds **8**, **10**, and **14**, due to the lack of a suitable chromophore in proximity, and the limited amounts of pure compounds precluded the measurement of VCD spectra. In the case of *seco*-tanapartholides B (**3**) and A (**4**), the rotatable bond between the two chromophores impeded an assignment of the absolute configuration via ECD. However, analysis of the VCD spectra proved to be successful. For compounds **1**, **5**, and **18**, a comparison of experimental and computed VCD spectra confirmed the absolute configuration determined by ECD, and for arteglasin A (**15**) the X-ray crystallographic data supported the assigned absolute configuration. Automated comparison of VCD spectra using *Sim*VCD and *Sim*VA proved to be helpful in the case of **1**, **3**, **4**, and **18**. However, a visual examination of spectra is warranted to avoid false attributions, as would have been the case with compound **5**.

Immunosuppressant Activity. Compounds were tested for their ability to inhibit proliferation of stimulated T lymphocytes at a concentration range of 0.01−30 µg/mL. FACS analyses of the forward and side scatters in the proliferation experiments were used to simultaneously assess immunosuppressive activity and cytotoxicity. The results for compounds **1** and **3** are shown in Figure 10, and IC_{50} values for all compounds tested were determined (Table 4, Figure S2, Supporting Information).

Compounds **3**, **4**, and **15** and the mixture of **13** and **14** significantly inhibited T lymphocyte proliferation, having IC_{50} values of <2 µM. For **3** and **4**, beginning cytotoxicity was seen at a concentration that was 10-fold higher than the IC_{50} value in the T-cell proliferation assay. For compound **15**, signs of cytotoxicity were observed at a concentration that was 3-fold higher than the IC_{50} value. Compounds **1**, **5**, and **18** were less active ($IC_{50} \leq 4$ µM), and compounds **6**−**9**, **12**−**14**, and **16** had no significant activity in the T-cell proliferation assay. When comparing the activity profile (Figure 1) with the IC_{50} values of pure compounds, it appeared that sesquiterpenes **1** and **3**−**5** contribute to a large extent to the activity of the extract.

Table 1. ^{1}H and ^{13}C NMR Spectroscopic Data (500 MHz, $CDCl_3$) for Compounds 8 and 9

	8		9		
position	δ_C, type	δ_H (J in Hz)	δ_C, type	δ_H (J in Hz)	HMBC[b]
1	73.3, CH	3.29, dd (11.9, 3.7)	73.3, CH	3.29, dd (11.9, 3.7)	9, 10, 14
2α	33.3, CH_2	1.59[a]		1.59[a]	1, 3, 4, 10
2β		1.76, m	33.3, CH_2	1.76, m	1, 4, 10
3	76.6, CH	4.60, dd (12.5, 4.6)	76.6, CH	4.60, dd (12.5, 4.6)	1′, 4, 15
4	72.8, C		72.8, C		
5	56.0, CH	1.41, d (11.3)	56.0, CH	1.41, d (11.3)	4, 6, 9, 10, 14, 15
6	79.2, CH	5.32, d (11.3)	79.2, CH	5.32, d (11.3)	4, 5, 7, 11, 12
7	171.8, C		171.8, C		
8a	22.3, CH_2	2.92, dd (13.3, 2.3)	22.3, CH_2	2.92, dd (13.3, 2.3)	
8b		2.39[a]		2.39[a]	9, 11
9a	39.6, CH_2	2.06, dd (13.3, 5.0)[a]	39.6, CH_2	2.06, dd (13.3, 5.0)[a]	
9b		1.12, m		1.12, m	
10	40.6, C		40.6, C		
11	117.8, C		117.8, C		
12	171.0, C		171.0, C		
13	54.6, CH_2	4.72, s	54.6, CH_2	4.72, s	1″, 7, 11, 12
14	13.0, CH_3	0.98, s	13.0, CH_3	0.98, s	1, 5, 9, 10
15	17.8, CH_3	1.29, s	17.8, CH_3	1.28, s	3, 4, 5
1′	175.0, C		171.6, C		
2′	40.5, CH	2.37[a]	43.1, CH_2	2.17, dd (7.0, 4.9)	1′, 3′, 4′, 5′
3′a	26.4, CH_2	1.58[a]	25.6, CH	2.00[a]	1′,[c] 4′, 5′
3′b		1.46, ddq (13.9, 7.5, 6.9)			1′,[c] 4′,[c] 5′[c]
4′	11.2, CH_3	0.87, dd (7.5, 7.5)	22.2, CH_3	0.92, d (6.7)	2′, 3′
5′	16.4, CH_3	1.07, d (7.0)	22.2, CH_3	0.92, d (6.7)	1′,[c] 2′, 3′
1″	170.1, C		170.1, C		
2″	20.6, CH_3	2.01, s[a]	20.6, CH_3	2.01, s[a]	1′, 13

[a]Overlapped signals. [b]HMBC spectrum for compounds **8** and **9** as observed in the mixture. [c]Observed solely for compound **8**. [d]Observed solely for compound **9**.

DOI: 10.1021/acs.jnatprod.8b00791
J. Nat. Prod. XXXX, XXX, XXX−XXX

Table 2. ^{1}H and ^{13}C NMR Spectroscopic Data (500 MHz, DMSO-d_6) for 10 and 11

	10			11[b]	
position	δ_C, type	δ_H (J in Hz)	HMBC	δ_C, type	δ_H (J in Hz)
1	78.4, C			78.4, C	
2α	46.8, CH_2	1.61, dd (14.2, 4.3)[a]	1, 3, 4, 10	46.8, CH_2	1.61, dd (14.2, 3.8)
2β		2.62, dd (14.2, 6.0)	1, 3, 4, 5, 10		2.61, dd (14.2, 6.0)
3	77.6, CH	3.55, dd (6.0, 4.7)	1, 4, 5	77.5, CH	3.55, dd (6.0, 4.0)
4	79.2, C			79.2, C	
5	60.6, CH	2.28, d (9.8)	1, 4, 6, 7, 10, 14,	60.7, CH	2.28, d (9.8)[a]
6	75.4, CH	4.38, dd (9.8, 9.8)	4, 5, 7, 8	75.4, CH	4.38, dd (9.6, 9.6)
7	41.2, CH	4.15, dddd (9.8, 9.8, 3.4, 3.2)	5, 6, 11, 12	41.1, CH	4.14, dddd (9._, 9.5, 3.1, 2.4)
8	72.5, CH	5.24, dd (9.8, 4.9)	1′, 9, 10, 11	72.5, CH	5.24, dd (9.8, 4.3)
9	121.4, CH	5.33, brd (4.9)	1, 7, 10, 15	121.6, CH	5.34, d (4.3)
10	143.9, C			143.7, C	
11	138.7, C			138.5, C	
12	169.4, C			169.4, C	
13a	120.9, CH_2	6.06, d (3.4)	7, 8, 11, 12	121.0, CH_2	6.05, d (3.1)
13b		5.54, d (3.0)	7, 8, 12		5.57, d (2.4)
14	23.1, CH_3	1.24, s	3, 4, 5	23.1, CH_3	1.24, s
15	24.9, CH_3	1.81, s	1, 9, 10	24.9, CH_3	1.81, s
1′	175.2, C			171.9, C	
2′	40.3, CH	2.41, ddq (13.7, 13.7, 7.0)	1′, 3′, 4′, 5′	42.4, CH_2	2.26, d (7.0)
3′a	26.0, CH_2	1.65, m[a]	1′, 2′, 4′, 5′	25.1, CH	2.02, m
3′b		1.44, ddq (13.7, 13.7, 7)	1′, 2′, 4′, 5′		
4′	11.5, CH_3	0.88, dd (7.2, 7.2)	2′, 3′	22.1, CH_3	0.93, d (6.4)[a]
5′	16.4, CH_3	1.10, d (7.0)	1′, 2′, 3′	22.1, CH_3	0.93, d (6.4)[a]

[a]Overlapping signals. [b]HMBC data for the core structure were identical to those of **10**.

Table 3. ^{1}H and ^{13}C NMR Spectroscopic Data (500 MHz, $CDCl_3$) for 17

position	δ_C, type	δ_H (J in Hz)	HMBC
1	130.7, C		
2	185.5, C		
3	126.1, CH	6.21, d (9.8)	1, 5
4	155.3, CH	6.78, d (9.8)	2, 6, 10, 14
5	38.4, C		
6α	39.5, CH_2	2.45, dd (15.3, 2.1)	4, 5, 7, 8, 14
6β		1.57, dd (15.3, 4.9)	4, 5, 14
7	75.4, CH	4.77, ddd (4.9, 4.9, 2.1)	6, 9
8	43.7, CH	2.32[a]	9, 11, 12
9α	28.3, CH_2	2.04, m	1, 8, 10, 12
9β		2.67, dd (13.7, 6.7)	1, 7, 8, 10
10	155.4, C		
11	180.1, C		
12	61.3, C		
13α	37.6, CH_2	2.50, d (11.9)	1′, 2′, 8, 10, 11, 12
13β		1.62, d (11.9)	2′, 5′, 8, 11, 12
14	24.9, CH_3	1.27, s	4, 5, 6
15	10.8, CH_3	1.90, s[a]	1, 10
1′	63.2, C		
2′	139.0, CH	6.17, d (5.8)	1′, 3′, 4′, 5′
3′	137.1, CH	5.90, d (5.8)	1′, 2′, 4′, 5′, 14′
4′	61.4, C		
5′	65.2, CH	2.96, d (10.0)	1′, 2′, 3′, 4′, 6′, 7′, 13
6′	79.6, CH	4.00, dd (9.8, 9.8)	5′, 8′
7′	43.0, CH	3.39, m	
8′α	23.6, CH_2	2.28[a]	6′, 7′, 9′
8′β		1.45, m	10′
9′a	34.8, CH_2	1.89, m;[a] 1.83[a]	1′, 7′, 10′
9′b		1.83, m[a]	1′, 8′, 10′
10′	72.4, C		
11′	170.3, C		
12′	140.5, C		
13′a	118.7, CH_2	6.07, d (3.7)	7′, 11′, 12′
13′b		5.35, d (3.4)	7′, 11′
14′	16.1, CH_3	1.54, s	3′, 4′, 5′, 12
15′	29.9, CH_3	1.38, s	1′, 9′, 10

[a]Overlapping signals.

EXPERIMENTAL SECTION

General Experimental Procedures. Optical rotations were measured at a concentration of 1 mg/mL in chloroform utilizing a PerkinElmer 341 polarimeter with a 10 cm microcell. UV and ECD spectra were recorded in methanol (66−400 μg/mL) on a Chirascan CD spectrometer using 1 mm path precision cells (110 QS, Hellma Analytics). IR and VCD spectra were recorded on a Bruker PMA 50 accessory coupled to a Tensor 27 Fourier transform infrared spectrometer. A photoelastic modulator (Hinds PEM 90) set at 1/4 retardation was used to modulate the handedness of the circular-polarized light. Demodulation was performed by a lock-in amplifier (SR830 DSP). An optical low-pass filter (<1800 cm^{-1}) in front of the photoelastic modulator was used to enhance the signal/noise ratio. Solutions of 3−8 mg in 130−400 μL of deuterated solvent ($CDCl_3$ or DMSO-d_6) were prepared and measured in a transmission cell equipped with CaF_2 windows and a 200 μm spacer. The VCD spectrum of the pure solvent served as the reference and was subtracted from the VCD spectrum of the compound in order to eliminate artifacts. For both the sample and the reference, ca. 24 000 scans at 4 cm^{-1} resolution were averaged. NMR data were recorded on a Bruker Avance III NMR spectrometer operating at 500.13 MHz for ^{1}H and 125.77 MHz for ^{13}C nuclei. ^{1}H NMR data and COSY, HSQC, HMBC, and NOESY spectra were measured at 18 °C in a 1 mm TXI probe with a z-gradient. ^{13}C NMR/DEPTQ spectra were recorded at 23 °C in 3 mm tubes with a 5 mm BBI probe. Spectra were analyzed by Bruker TopSpin 3.0 and ACDLabs Spectrus Processor. Either a Bruker Kappa Apex 2 diffractometer or a Stoe StadiVari diffractometer equipped with a Pilatus 300 K detector was used to collect X-ray diffraction data. The structure was solved with Superflip[22] and refined using Crystals.[23] HPLC-PDA-ELSD-ESIMS data were recorded in the positive mode on a Shimadzu LC-MS/MS 8030 triple quadrupole MS connected via a T-splitter (1:10) to a Shimadzu HPLC system consisting of degasser, binary high-pressure mixing pump, autosampler, column oven, and diode array detector, and via a T-splitter to an Alltech 3300 ELSD detector. Data acquisition and processing was performed with LabSolution software. Semipreparative HPLC separations were carried out with an Agilent HP 1100 Series system consisting of a quaternary pump, autosampler, column oven, and a diode array detector (G1315B). Chemstation software was used for data acquisition and processing. Waters SunFire C_{18} (3.5 μm, 3.0 × 150 mm i.d., equipped with a guard column 10 × 3.0 mm i.d.), SunFire Prep C_{18} (5 μm, 10 × 150 mm i.d., equipped with a guard column 10 × 10 mm i.d.), and SunFire Prep C_{18} OBD (5 μm, 30 × 150 mm i.d., equipped with a guard column 10 × 20 mm i.d.) columns were used for analytical, semipreparative, and preparative separations, respectively. HPLC-grade methanol, acetonitrile (Scharlau Chemie), and water from a Milli-Q water purification system (Merck Millipore) were used for

DOI: 10.1021/acs.jnatprod.8b00791
J. Nat. Prod. XXXX, XXX, XXX−XXX

Table 4. In Vitro Inhibitory Concentrations of *Artemisia argyi* Extract and Selected Constituents Leading to Inhibition of T-Cell Proliferation by 50% (IC_{50}) in [μg/mL] (Middle Column) and [μM] (Right Column)

compound[a]	IC_{50} [μg/mL] ± SD	IC_{50} [μM] ± SD
1	0.8 ± 0.3	2.7 ± 0.9
3	0.3 ± 0.1	1.0 ± 0.4
4	0.3 ± 0.1	1.2 ± 0.3
5	1.0 ± 0.3	3.7 ± 1.1
6	5.0 ± 2.2	13.8 ± 5.9
7	4.9 ± 1.3	19.6 ± 5.3
8 + **9** (ratio 2:1)	7.1 ± 3.9	16.8 ± 9.2
12	1.9 ± 0.6	5.8 ± 1.7
13 + **14** (ratio 1:1)	0.7 ± 0.2	1.8 ± 0.4
15	0.6 ± 0.2	1.9 ± 0.7
16	4.0 ± 0.5	11.7 ± 1.4
18	1.7 ± 0.7	3.2 ± 1.3
CsA	0.3 ± 0.2	0.2 ± 0.2
extract	16.1 ± 3.6	

[a]Compounds **2**, **10**, **11**, and **17** were not tested due to the limited amounts available.

HPLC separations. The mobile phase used for analytical HPLC contained 0.1% formic acid. An analytical Nucleodur 100-5 CN column (5.0 μm, 4.0 × 125 mm i.d.) and a semipreparative Nucleodur 100-5 CN column (5.0 μm, 10.0 × 150 mm i.d.) (both Macherey-Nagel) were used for normal-phase HPLC separations. NMR spectra were recorded in $CDCl_3$ (Sigma-Aldrich) or DMSO-d_6 (Armar Chemicals). Technical-grade solvents purified by distillation were used for extraction and open column chromatography. Silica gel (63−200 μm and 15−40 μm, Merck) was used for open column chromatography. HRESIMS data were measured on a LQT XL Orbitrap mass spectrometer (Thermo Scientific) via direct injection.

Plant Material. *Artemisia argyi* whole plants, batch number 150788859, were purchased from Peter Weinfurth, Bochum, Germany, in March 2016. A voucher specimen (number 00 979) has been deposited at the Division of Pharmaceutical Biology, University of Basel, Switzerland.

Microfractionation. Microfractionation of *A. argyi* EtOAc extract was carried out by analytical RP-HPLC on an LC-MS 8030 system (Shimadzu) connected with an FC 204 fraction collector (Gilson). A solution of 10 mg/mL extract in DMSO was prepared. In total, three injections were performed: 2 × 30 μL using only DAD for detection for collection (0.6 mg of extract in total) and 1 × 10 μL with UV-ELSD-ESIMS detection without collection. Water with 0.1% formic acid (A) and acetonitrile with 0.1% formic acid (B) were used as mobile phase. The gradient was 5% to 100% B in 30 min followed by 5 min at 100% B. Fractions of 1 min each were collected from minute 2 to minute 32, resulting in 30 microfractions in total. Microfractions of two successive injections of the extract were collected into the corresponding wells of a 96-deep-well plate. The plate was dried in a Genevac EZ-2 evaporator.

Extraction and Isolation. A 400 g aliquot of plant material was ground using a M20 universal mill (IKA). The powdered material was mixed with 400 g of sea sand and percolated with EtOAc (ca. 12 L) to afford 42 g of crude extract. A portion (20 g) of the extract was fractionated by column chromatography (CC) on silica gel (80 × 5 cm, 63−200 μm) using a gradient of *n*-hexane−EtOAc−MeOH (95:5:0 to 0:100:0 to 0:50:50) as mobile phase. Fractions A−R were combined based on TLC patterns (silica gel, *n*-hexane−EtOAc, 70:30, 50:50, and 35:65, respectively; detection with 1% ethanolic vanillin and 10% sulfuric acid, followed by heating). Fraction M (80 mg) was submitted to preparative RP-HPLC [H_2O (A), MeCN (B); 15 → 100% B (0−30 min), 100% B (30−35 min), flow rate 25 mL/min; sample concentration 100 mg/mL in DMSO; injection volume 700 μL], yielding jaceosidin (**12**, 8.7 mg, t_R 15.1 min), santamarin (**7**, 3.9 mg, t_R 16.0 min), and eupatilin (**16**, 21.8 mg, t_R 17.4 min). Fraction P (769 mg) was submitted to preparative RP-HPLC [H_2O (A), MeCN (B); 25 → 60% B (0−30 min), 60 → 100% B (30−32 min), 100% B (32−37 min), flow rate 20 mL/min; sample concentration 100 mg/mL in DMSO; injection volume 1000 μL], yielding fractions P_1−P_{26}. Fraction P_5 afforded crystals of artecanin (**5**, 18.5 mg). P_{14} consisted of eudesmaafraglaucolide (**6**, 15.9 mg, t_R 15.6 min), and P_{17} was found to be a mixture of **8** and **9** (2.0 mg, t_R 18.8 min). P_{26} consisted of 8-acetylarteminolide (**18**, 7 mg, t_R 28.0 min). P_3 was purified by semipreparative HPLC on a Nucleodur 100-5 CN column [*n*-heptane (A), isopropanol (B); 5% B (0−3 min), 5 → 15% B (3−6 min), 15% (6−16 min), flow rate 3 mL/min; sample concentration 20 mg/mL in 2:1 isopropanol−*n*-heptane; injection volume 75 μL] to afford canin (**1**, 2.9 mg, t_R 16.2 min), *seco*-tanapartholides B (**3**, 8.1 mg, t_R 16.9 min) and A (**4**, 4.8 mg, t_R 17.9 min), and 10-*epi*-artecanin (**2**, 0.8 mg, t_R 18.8 min). Fraction K (452 mg) was separated by preparative RP-HPLC [H_2O (A), MeCN (B); 45% (0−2 min), 45 → 70% B (2−30 min), 60 → 100% B (30−31 min), 100% B (31−40 min), flow rate 20 mL/min; sample concentration 75 mg/mL in DMSO; injection volume 100−900 μL]. K_{11} consisted of a mixture of 3α,4α-epoxyrupicolines E and D (**13** and **14**, 2.3 mg, t_R 21.3 min). Crystals formed in the vial were identified by X-ray crystallography as 3α,4α-epoxyrupicolin E (**14**). K_5 consisted of arteglasin A (**15**, 3.0 mg, t_R 14.7 min). From a second portion of extract (20 g) a targeted isolation of compounds **8** and **9** was performed. For this, the extract was fractionated on an MPLC glass column (Büchi) packed with silica gel (40 × 7 cm, 15−40 μm) utilizing an Interchim Puriflash 4100 system [*n*-hexane (A), EtOAc (B); 20% B (0−15 min) 20 → 30% B (15−20 min), 30% B (15−50 min), 30 → 80% (50−80 min), 80% (80−130 min), 80 → 95% (130−160 min), 95% (160−215 min), flow rate 30 mL/min; sample introduction via dry load, with 20 g of extract adsorbed on 40 g silica gel 15−40 μm]. Separation was monitored by HPLC-ESIMS, and fractions containing the target molecules were combined, dried, and submitted to preparative RP-HPLC [H_2O (A), MeCN (B); 25% B (0−3 min), 25 → 30% B (3−10 min), 30% B (10−40 min); flow rate 20 mL/min; sample concentration 130 mg/mL in DMSO; injection volume 900 μL]. This separation yielded compounds **10** (1.9 mg, t_R 27.3 min) and **11** (1.7 mg, t_R 29.8 min) and a peak (5.4 mg, t_R 36.1 min), which was further purified by semipreparative HPLC (Nucleodur 100-5 CN) [H_2O (A), MeCN (B); 17 → 20% B (0−27 min), 20 → 100% B (27−29 min), 100% B (29−40 min); flow rate 4 mL/min; sample concentration 20 mg/mL in DMSO; injection volume 100 μL] to afford a mixture of **8** and **9** (1.4 mg, t_R 20.3 min).

*Canin (**1**):* white solid; $[\alpha]_D^{25}$ +7 (*c* 0.1 g/100 mL, CH_2Cl_2); UV λ_{max} (MeOH) (log ε) 209 (4.0) nm; ECD (MeOH, *c* 0.96 mM, 0.1 cm); $\Delta\varepsilon$ +4.0 (202 nm) −0.9 (252 nm); ^{1}H and ^{13}C NMR, see Table S1, Supporting Information; HRESIMS *m*/*z* 301.1054 [M + Na]$^+$ (calcd for $C_{15}H_{18}O_5Na$, 301.1052).

*10-epi-Canin (**2**):* UV λ_{max} (MeOH) (log ε) 207 (3.9) nm; ECD (MeOH, *c* 0.54 mM, 0.1 cm); $\Delta\varepsilon$ +4.9 (195 nm) −0.8 (257 nm); ^{1}H and ^{13}C NMR, see Table S1, Supporting Information; HRESIMS *m*/*z* 301.1057 [M + Na]$^+$ (calcd for $C_{15}H_{18}O_5Na$, 301.1052).

*(−)-seco-Tanapartholide B (**3**):* colorless gum; $[\alpha]_D^{25}$ −62 (*c* 0.1 g/100 mL, CHCl3); UV λ_{max} (MeOH) (log ε) 213 (4.2) nm; ECD (MeOH, *c* 0.60 mM, 0.1 cm); $\Delta\varepsilon$ +10.0 (228 nm) −1.8 (330 nm); ^{1}H and ^{13}C NMR see Table S2, Supporting Information; HRESIMS *m*/*z* 301.1055 [M + Na]$^+$ (calcd for $C_{15}H_{18}O_5Na$, 301.1052).

*(+)-seco-Tanapartholide A (**4**):* colorless gum; $[\alpha]_D^{25}$ +79 (*c* 0.1 g/100 mL, $CHCl_3$); UV λ_{max} (MeOH) (log ε) 209 (4.2) nm; ECD (MeOH, *c* 0.60 mM, 0.1 cm); $\Delta\varepsilon$ −13.1 (228 nm) +1.8 (330 nm); ^{1}H and ^{13}C NMR, see Table S2, Supporting Information; HRESIMS *m*/*z* 301.1057 [M + Na]$^+$ (calcd for $C_{15}H_{18}O_5Na$, 301.1052).

*Artecanin (**5**):* UV λ_{max} (MeOH) (log ε) 211 (4.2), 208 (3.7) nm; ECD (MeOH, *c* 1.44 mM, 0.1 cm); $\Delta\varepsilon$ +2.7 (202 nm), −0,5 (251 nm); ^{1}H and ^{13}C NMR, see Table S1, Supporting Information; HRESIMS *m*/*z* 301.1054 [M + Na]$^+$ (calcd for $C_{15}H_{18}O_5Na$, 301.1052).

*Eudesmaafraglaucolide (**6**):* white solid; UV λ_{max} (MeOH) (log ε) 215 (4.0), 288 (2.7) nm; ECD (MeOH, *c* 1.1 mM, 0.1 cm); $\Delta\varepsilon$ +3.2 (217 nm), −0.8 (243 nm); ^{1}H and ^{13}C NMR, see Table S3, Supporting Information; HRESIMS *m*/*z* 387.1431 [M + Na]$^+$ (calcd for $C_{19}H_{24}O_7Na$, 387.1414).

DOI: 10.1021/acs.jnatprod.8b00791
J. Nat. Prod. XXXX, XXX, XXX−XXX

Santamarin (7): white solid; UV λ_{max} (MeOH) (log ε) 211 (4.2), 273 (3.8), 334 (3.9) nm; ECD (MeOH, *c* 0.26 mM, 0.1 cm); $\Delta\varepsilon$ +2.4 (202 nm); ^{1}H and ^{13}C NMR, see Table S3, Supporting Information; HRESIMS *m/z* 271.1317 $[M + Na]^+$ (calcd for $C_{15}H_{20}O_3Na$, 271.1305).

Argyinolides K (8) and L (9): white solid; UV λ_{max} (MeOH) (log ε) 210 (3.7) nm; ECD (MeOH, *c* 0.85 mM, 0.1 cm); $\Delta\varepsilon$ −2.4 (225 nm); ^{1}H and ^{13}C NMR see Table 1; HRESIMS *m/z* 447.2018 $[M + Na]^+$ (calcd for $C_{24}H_{31}O_8Na$, 447.1989).

Argyinolide M (10): yellow solid; UV λ_{max} (MeOH) (log ε) 200 (4.0) nm; ECD (MeOH, *c* 0.79 mM, 0.1 cm); $\Delta\varepsilon$ +8.5 (195 nm) −0.4 (255 nm); ^{1}H and ^{13}C NMR see Table 2; HRESIMS *m/z* 403.1750 $[M + Na]^+$ (calcd for $C_{20}H_{28}O_7Na$, 403.1727).

(+)-Argyinolide N (11): yellow solid; $[\alpha]_D^{25}$ +20 (*c* 0.15 g/100 mL, $CHCl_3$); UV λ_{max} (MeOH) (log ε) 200 (4.1) nm; ECD (MeOH, *c* 0.79 mM, 0.1 cm); $\Delta\varepsilon$ +9.0 (195 nm) −0.5 (256 nm); ^{1}H and ^{13}C NMR see Table 2; HRESIMS *m/z* 403.1748 $[M + Na]^+$ (calcd for $C_{20}H_{28}O_7Na$, 403.1727).

Jaceosidin (12): yellow solid; ^{1}H and ^{13}C NMR, see Table S4, Supporting Information; HRESIMS *m/z* 353.0649 $[M + Na]^+$ (calcd for $C_{17}H_{14}O_7Na$, 353.0656).

3α,4α-Epoxyrupicolines D and E (13 and 14): UV λ_{max} (MeOH) (log ε) 285 (2.8) nm; ratio 1:1; identification by ^{1}H and ^{13}C NMR, see Table S5, Supporting Information; HRESIMS *m/z* 385.1634 $[M + Na]^+$ (calcd for $C_{20}H_{26}O_6Na$, 385.1622).

(+)-Arteglasin A (15): $[\alpha]_D^{25}$ +86 (*c* 0.07 g/100 mL, $CHCl_3$); UV λ_{max} (MeOH) (log ε) 195 (4.2) nm; ECD (MeOH, *c* 0,65 mM, 0.1 cm); $\Delta\varepsilon$ +7.4 (209 nm) −1.0 (231 nm); ^{1}H and ^{13}C NMR, see Table S5, Supporting Information; HRESIMS *m/z* 327.1220 $[M + Na]^+$ (calcd for $C_{17}H_{20}O_5Na$, 327.1203).

Eupatilin (16): yellow solid; identification by ^{1}H and ^{13}C NMR see Table S4, Supporting Information; HRESIMS *m/z* 367.0808 $[M + Na]^+$ (calcd for $C_{18}H_{16}O_7Na$, 367.0788).

(−)-Argyinolide N (17): white solid; $[\alpha]_D^{25}$ −120 (*c* 0.08 g/100 mL, $CHCl_3$); UV λ_{max} (MeOH) (log ε) 205 (4.2) nm; ECD (MeOH, *c* 0.31 mM, 0.1 cm); $\Delta\varepsilon$ +12.3 (195 nm), +27.5 (207 nm); ^{1}H and ^{13}C NMR see Table 3; HRESIMS *m/z* 513.2261 $[M + Na]^+$ (calcd for $C_{30}H_{34}O_6Na$, 513.2248).

(+)-8-Acetylarteminolide (18): white solid; $[\alpha]_D^{25}$ +27 (*c* 0,1 g/100 mL, $CHCl_3$); UV λ_{max} (MeOH) (log ε) 253 (3.8) nm; ECD (MeOH, *c* 0.73 mM, 0.1 cm); $\Delta\varepsilon$ −8.4 (210 nm), +0.7 (240 nm), −1.2 (269 nm); ^{1}H and ^{13}C NMR, see Table S6, Supporting Information; HRESIMS *m/z* 571.2313 $[M + Na]^+$ (calcd for $C_{32}H_{36}O_8Na$, 571.2308).

X-ray Analysis of 3α,4α-Epoxyrupicolin E (14). A crystal of **14** with the dimensions 0.11 × 0.13 × 0.21 mm, obtained as a colorless block from $CHCl_3$, was mounted on a Bruker Kappa Apex 2 diffractometer and was kept at 123 K during data collection (CCDC 1862952). The orthorhombic space group $P2_12_12_1$ was observed using Cu Kα radiation ($\hat{L}$ = 1.541 78 Å, *a* = 9.1487(7) Å, *b* = 10.3308(7) Å, *c* = 20.0261(14) Å, $\alpha = \beta = \gamma = 90°$, *V* = 1892.7(2) Å^3), giving 3419 independent reflections. The structure was solved with Superflip[22] and refined using Crystals.[23] Non-hydrogen atoms were refined anisotropically, and hydrogen atoms were fixed at the calculated positions. The final indices were *R* = 0.0473, R_w = 0.0496 and goodness of fit = 1.0832.

X-ray Analysis of Arteglasin A (15). A crystal of **15** with the dimensions 0.05 × 0.09 × 0.14 mm, obtained as a colorless block from $CHCl_3$, was mounted on a Stoe StadiVari diffractometer equipped with a Pilatus 300 K detector and was kept at 123 K during data collection (CCDC 1862953). The orthorhombic space group $P2_12_12_1$ was observed using Ga Kα radiation ($\hat{L}$ = 1.341 43 Å, *a* = 19.8206(4) Å, *b* = 9.5646(2) Å, *c* = 8.4390(2) Å, $\alpha = \beta = \gamma = 90°$, *V* = 1599.83(6) Å^3), giving 3101 independent reflections. Non-hydrogen atoms were refined anisotropically, and hydrogen atoms were fixed at the calculated positions. The final indices were *R* = 0.0265, R_w = 0.0294 and goodness of fit = 1.1151.

Computational Methods. Conformational analysis was performed with Schrödinger MacroModel 9.8 (Schrödinger, LLC, New York, USA) employing the OPLS2005 (optimized potential for liquid simulations) force field in H_2O or chloroform for ECD or VCD calculations, respectively. Selected conformers within a 8 kcal/mol energy window from the global minimum were submitted to geometrical optimization and energy calculation applying density functional theory (DFT) with the Beck's nonlocal three-parameter exchange and correlation functional and the Lee−Yang−Parr correlation functional level (B3LYP), using the B3LYP/6-31G** basis set, the SCRF method, and the CPMC model for solvation (MeOH for ECD calculations) with the Gaussian 09 program package.[24] Vibrational analysis was done at the same level to confirm minima. Excitation energy (denoted by wavelength in nm), rotator strength (R_{str}), dipole velocity (R_{vel}), and dipole length (R_{len}) were calculated in MeOH by TD-DFT/B3LYP/6-31G(d,p). ECD curves were obtained on the basis of rotator strengths with a half-band of 0.3 eV using SpecDis v1.64.[25] Vibrational frequencies (given as wavenumbers in cm^{-1}), rotator strength (R_{str}), IR intensity (IR_{inten}), and dipole strength (R_{str}) were calculated in chloroform or dimethyl sulfoxide with B3LYP/6-31+G(d,p). While the conformational search for compounds measured in chloroform was also performed in chloroform, it was carried out in water for samples measured in methanol or DMSO-d_6. VCD curves were obtained on the basis of rotator strengths with a bandwidth of 10 cm^{-1} using VCDspecTech v22.0.[26,27] ECD and VCD spectra were calculated from the spectra of individual conformers according to their contribution calculated by Boltzmann weighting. Comparison was done visually and by calculation of similarity indices (*Sim*VA, *Sim*VCD) which were generated by VCDspecTech v22.0.[18] The SimVCD values were plotted against the scaling factors of the *x* axis, and graphs compared between the different stereoisomers.

Ethics Statement. Patients gave their written consent to donate blood for scientific research. All experiments conducted on human material were approved by the Ethics Committee of the University of Freiburg (55/14).

Preparation and Cultivation of Human Peripheral Lymphocytes. Peripheral blood mononuclear cells (PBMCs) were isolated from the blood of healthy adult donors obtained from the Blood Transfusion Centre (University Medical Center, Freiburg, Germany). Venous blood was centrifuged on a LymphoPrep gradient (density: 1.077 g/cm^3, 20 min, 500*g*, 20 °C; Progen). After centrifugation, cells were washed twice with phosphate-buffered saline (PBS) and subsequently cultured in RPMI 1640 medium supplemented with 10% heat-inactivated fetal calf serum (GE Healthcare Life Sciences), 2 mM L-glutamine, 100 U/mL penicillin, and 100 U/mL streptomycin (all from Life Technologies). The cells were cultured at 37 °C in a humidified incubator with a 5% CO_2/95% air atmosphere.

T Cell Proliferation Assay. Lymphocytes were isolated, washed twice in cold PBS, and resuspended in PBS at a concentration of 5 × 10^6 cells/mL. Cells were stained for 10 min at 37 °C with carboxyfluorescein diacetate succinimidyl ester (CFSE; 5 μM: Sigma-Aldrich, St. Louis, MO, USA). The staining was stopped by washing twice with complete medium. Stained lymphocytes (2 × 10^6 cells/mL) were stimulated with anti-human CD3 (clone HIT3a) and anti-human CD28 (clone 28.2) mAbs (each 100 ng/mL; eBioscience) in the presence of either medium, cyclosporin A (CsA; 4.16 μM; Novartis Pharma), camptothecin (CPT; 300 μM; Tocris), or plant extracts/single compounds (concentration range 0.01−100 μg/mL) and incubated for 72 h. The negative control remained unstimulated. Flow cytometric analysis of the cell division was performed using a FACSCalibur instrument (BD Biosciences).

Determination of Apoptosis and Necrosis of T Cells. Lymphocytes were isolated, washed twice in cold PBS, and resuspended in medium at a concentration of 2 × 10^6 cells/mL. Cells were stimulated with anti-human CD3 (clone HIT3a) and anti-human CD28 (clone 28.2) mAbs (each 100 ng/mL; eBioscience) in the presence of either medium, camptothecin (CPT; 300 μM; Tocris), 0.5% Triton-X 100, or plant extracts/single compounds (concentration range 0.01−100 μg/mL) and cultivated for 48 h. The negative control remained unstimulated. Cultured cells were washed with PBS and stained with annexin V-FITC using the apoptosis-detection kit (eBioscience) according to the manufacturer's instructions. Propidium iodide (eBioscience) was added, and cells were stained for 15 min at room temperature in the dark. Apoptosis and necrosis rates were determined

DOI: 10.1021/acs.jnatprod.8b00791
J. Nat. Prod. XXXX, XXX, XXX−XXX

by flow cytometric analysis using a FACSCalibur instrument (BD Biosciences).

Testing of Microfractions. The dried microfractions in 96-deep-well plates were dissolved in 25 μL of DMSO by sonication and mixing with a pipet. Of these stock solutions, dilutions of 1:1, 1:3, 1:10, and 1:30 were prepared and tested in duplicates for T lymphocyte proliferation inhibition as described above. Assuming an equal distribution of 200 ng substance in each of the microfractions, theoretical IC_{50} values were calculated to be used as a relative measure of activity. They were normalized to 100% with the highest value representing 100%.

■ ASSOCIATED CONTENT

Supporting Information

The Supporting Information is available free of charge on the ACS Publications website at DOI: 10.1021/acs.jnatprod.8b00791.

T lymphocyte proliferation inhibition data for compounds **1**, **3**−**5**, **15**, and **18**; ^{1}H and ^{13}C NMR data for compounds **1**−**7**, **12**−**16**, and **18**; experimental and computed ECD spectra of compounds **2**, **5**−**11**, **13**−**15**, **17**, and **18**; experimental and computed VCD spectra of compounds **4** and **18**; 1D and 2D NMR spectra of compounds **1**−**5**, **8**−**11**, and **17**; table of crystallographic data and ORTEP diagrams for compounds **14** and **15** (PDF)

Crystallographic data for **14** (CIF)

Crystallographic data for **15** (CIF)

■ AUTHOR INFORMATION

Corresponding Author

*Tel: +41 61 267 14 25. Fax: +41 61 267 14 74. E-mail: matthias.hamburger@unibas.ch.

ORCID

Maria De Mieri: 0000-0001-5567-2072

Martin Smieško: 0000-0003-2758-2680

Thomas Bürgi: 0000-0003-0906-082X

Matthias Hamburger: 0000-0001-9331-273X

Author Contributions

#J. K. Reinhardt and A. M. Klemd contributed equally to this work.

Notes

The authors declare no competing financial interest.

■ ACKNOWLEDGMENTS

ECD spectra were measured at the Biophysics Facility, Biozentrum, University of Basel. X-ray diffraction was measured by Dr. Markus Neuburger at the Laboratory for Chemical Crystallography, University of Basel.

■ REFERENCES

(1) Lleo, A.; Invernizzi, P.; Gao, B.; Podda, M.; Gershwin, M. E. *Autoimmun. Rev.* **2010**, *9*, A259−A266.

(2) Chaplin, D. D. *J. Allergy Clin. Immunol.* **2010**, *125*, S3−23.

(3) Her, M.; Kavanaugh, A. *J. Allergy Clin. Immunol.* **2016**, *137*, 19−27.

(4) Taylor, A. L.; Watson, C. J.; Bradley, J. A. *Crit. Rev. Oncol./Hematol.* **2005**, *56*, 23−46.

(5) Quah, B. J.; Parish, C. R. *J. Visualized Exp.* **2010**, *44*, No. e2259.

(6) Potterat, O.; Hamburger, M. *Nat. Prod. Rep.* **2013**, *30*, 546−64.

(7) Potterat, O.; Hamburger, M. *Planta Med.* **2014**, *80*, 1171−81.

(8) Harborne, J. B.; Mabry, T. J.; Mabry, H. *The Flavonoids*; Academic Press: New York, 1975.

(9) Jakupovic, J.; Klemeyer, H.; Bohlmann, F.; Graven, E. H. *Phytochemistry* **1988**, *27*, 1129−1133.

(10) Romo de Vivar, A.; Jimenez, H. *Tetrahedron* **1965**, *21*, 1741−1745.

(11) Jin, H. Z.; Lee, J. H.; Lee, D.; Hong, Y. S.; Kim, Y. H.; Lee, J. J. *Phytochemistry* **2004**, *65*, 2247−2253.

(12) Lee, K. H.; Matsueda, S.; Geissman, T. A. *Phytochemistry* **1971**, *10*, 405−410.

(13) Nakasugi, T.; Nakashima, M.; Komai, K. *J. Agric. Food Chem.* **2000**, *48*, 3256−3266.

(14) Lee, K. H.; Simpson, R. F.; Geissman, T. A. *Phytochemistry* **1969**, *8*, 1515−1521.

(15) Hewlett, M. J.; Begley, t. l. M. J.; Groenewegen, W. A.; Heptinstall, S.; Knight, D. W.; May, J.; Salan, U.; Toplis, D. *J. Chem. Soc., Perkin Trans. 1* **1996**, *1*, 1979−1986.

(16) Polavarapu, P. L.; Covington, C. L. *Chirality* **2014**, *26*, 539−52.

(17) Bohlmann, F.; Zdero, C. *Phytochemistry* **1982**, *21*, 2543−2549.

(18) Tan, R. X.; Jakupovic, J.; Bohlmann, F.; Jia, Z. J.; Huneck, S. *Phytochemistry* **1991**, *30*, 583−587.

(19) Kawazoe, K.; Tsibouchi, Y.; Abdullah, N.; Takaishi, Y.; Shibata, H.; Higuti, T.; Hori, H.; Ogawa, M. *J. Nat. Prod.* **2003**, *66*, 538−539.

(20) Ahmed, A. A.; El-Moghazy, S. A.; El-Shanawany, M. A.; Abdel-Hani, H. F.; Karchedy, J.; Sturtz, G.; Dalley, K.; Paré, P. W. *J. Nat. Prod.* **2004**, *67*, 1705−1710.

(21) Lee, S.-H.; Kang, H.-M.; Song, H.-C.; Lee, H.; Lee, U. C.; Son, K.-H.; Kim, S.-H.; Kwona, B.-M. *Tetrahedron* **2000**, *56*, 4711−4715.

(22) Palatinus, L.; Chapuis, G. *J. Appl. Crystallogr.* **2007**, *40*, 786−790.

(23) Betteridge, P. W.; Carruthers, J. R.; Cooper, R. I.; Prout, K.; Watkin, D. J. *J. Appl. Crystallogr.* **2003**, *36*, 1487−1487.

(24) Frisch, M. J.; Trucks, G. W.; Schlegel, H. B.; Scuseria, G. E.; Robb, M. A.; Cheeseman, J. R.; Scalmani, G.; Barone, V.; Mennucci, B.; Petersson, G. A.; Nakatsuji, H.; Caricato, M.; Li, X. H. H. P.; Izmaylov, A. F.; Bloino, J. Z. G.; Sonnenberg, J. L.; Hada, M.; Ehara, M.; Toyota, K.; Fukuda, R.; Hasegawa, J.; Ishida, M.; Nakajima, T.; Honda, Y.; Kitao, O.; Nakai, H.; Vreven, T.; Montgomery, J. A., Jr.; Peralta, J. E.; Ogliaro, F.; Bearpark, M. J.; Heyd, J.; Brothers, E. N.; Kudin, K. N.; Staroverov, V. N.; Kobayashi, R.; Normand, J.; Raghavachari, K.; Rendell, A. P.; Burant, J. C.; Iyengar, S. S.; Tomasi, J.; Cossi, M.; Rega, N.; Millam, N. J.; Klene, M.; Knox, J. E.; Cross, J. B.; Bakken, V.; Adamo, C.; Jaramillo, J.; Gomperts, R.; Stratmann, R. E.; Yazyev, O.; Austin, A. J.; Cammi, R.; Pomelli, C.; Ochterski, J. W.; Martin, R. L.; Morokuma, K.; Zakrzewski, V. G.; Voth, G. A.; Salvador, P.; Dannenberg, J. J.; Dapprich, S.; Daniels, A. D.; Farkas, O.; Foresman, J. B.; Ortiz, J. V.; Cioslowski, J.; Fox, D. J. *Gaussian 09*; Gaussian, Inc.: Wallingford, CT, USA, 2009.

(25) Bruhn, T.; Schaumlöffel, A.; Hemberger, Y. *SpecDis* v1.64; University of Würzburg: Germany, 2015.

(26) Covington, C. L.; Polavarapu, P. L. *VCDspecTech* v22.0; https://sites.google.com/site/cdspechtech1/, 2017.

(27) Covington, C. L.; Polavarapu, P. L. *Chirality* **2017**, *29*, 178−192.

DOI: 10.1021/acs.jnatprod.8b00791
J. Nat. Prod. XXXX, XXX, XXX−XXX

3.2. Immunosuppressive activity of *Artemisia argyi* extract and isolated compounds

Zimmermann-Klemd, A.M., **Reinhardt, J.K.**, Morath, A., Schamel, W.W., Steinberger, P., Leitner, J., Huber, R., Hamburger, M., Gründemann, C., 2020. Immunosuppressive Activity of Artemisia argyi Extract and Isolated Compounds. Frontiers in Pharmacology 11.

Previous investigations identified an ethyl acetate extract of *Artemisia argyi* to suppress the proliferation of stimulated human T lymphocytes *in vitro* and yielded active compounds, linked to anti-proliferative effects (Reinhardt et al., 2019a). In this work the immunosuppressive effect of *A. argyi* on human T cells could be extended to suppression of activation and an inhibition of the IL-2 and IFN-γ production. In order to determine the target of *A. argyi* extract and isolated bioactive compounds, the activity of the *il-2* transcription factors AP-1, NF-κB, and NFAT was analyzed, within the frame of a T cell signal transduction monitoring. Thereby, the IL-2 conditioned T cell proliferation inhibition could be linked to a suppression of NF-κB and NFAT. Moreover, the T cell signal transduction monitoring revealed an inhibitory impact of the *A. argyi* extract on the calcium flux of activated Jurkat T cells. However, the isolated compounds had no on the calcium flux, pointing towards a different mode-of-action.

My contribution: I collected all data, except the data for figure 6. I analyzed all data, calculated the statistics and prepared the figures, except Figure 5. I wrote the draft manuscript together with Jakob K. Reinhardt. This work also yielded my master thesis.

Amy Marisa Zimmermann-Klemd

frontiers in Pharmacology

ORIGINAL RESEARCH
published: 08 April 2020
doi: 10.3389/fphar.2020.00402

Immunosuppressive Activity of *Artemisia argyi* Extract and Isolated Compounds

Amy M. Zimmermann-Klemd[1†], *Jakob K. Reinhardt*[2†], *Anna Morath*[3,4,5], *Wolfgang W. Schamel*[3,4,6], *Peter Steinberger*[7], *Judith Leitner*[7], *Roman Huber*[1], *Matthias Hamburger*[2] *and Carsten Gründemann*[8*]

[1] Center for Complementary Medicine, Institute for Infection Prevention and Hospital Epidemiology, Faculty of Medicine, University of Freiburg, Freiburg, Germany, [2] Pharmaceutical Biology, Pharmacenter, University of Basel, Basel, Switzerland, [3] Signalling Research Centres BIOSS and CIBSS, University of Freiburg, Freiburg, Germany, [4] Faculty of Biology, University of Freiburg, Freiburg, Germany, [5] Spemann Graduate School of Biology and Medicine, University of Freiburg, Freiburg, Germany, [6] Center for Chronic Immunodeficiency, Medical Center Freiburg and Faculty of Medicine, University of Freiburg, Freiburg, Germany, [7] Center for Pathophysiology, Infectiology, and Immunology, Institute of Immunology, Medical University of Vienna, Vienna, Austria, [8] Translational Complementary Medicine, Department of Pharmaceutical Sciences, University of Basel, Basel, Switzerland

OPEN ACCESS

Edited by:
Judit Hohmann,
University of Szeged, Hungary

Reviewed by:
Edgar Serfling,
Julius Maximilian University of Würzburg, Germany
Orazio Taglialatela-Scafati,
University of Naples Federico II, Italy

***Correspondence:**
Carsten Gründemann
carsten.gruendemann@unibas.ch

[†]*These authors have contributed equally to this work*

Specialty section:
This article was submitted to Ethnopharmacology, a section of the journal Frontiers in Pharmacology

Received: *17 December 2019*
Accepted: *17 March 2020*
Published: *08 April 2020*

Citation:
Zimmermann-Klemd AM, Reinhardt JK, Morath A, Schamel WW, Steinberger P, Leitner J, Huber R, Hamburger M and Gründemann C (2020) Immunosuppressive Activity of Artemisia argyi Extract and Isolated Compounds. Front. Pharmacol. 11:402. doi: 10.3389/fphar.2020.00402

The need for novel drugs for the treatment of autoimmune diseases is high, since available pharmaceuticals often have substantial side effects and limited efficacy. Natural products are a good starting point in the development of immunosuppressive leads. Since enhanced T cell proliferation is a common feature of autoimmune diseases, we investigated the T cell proliferation inhibitory potential of an extract library of plants used in traditional Chinese medicine. Using a newly established cell-based screening platform, an ethyl acetate extract of *Artemisia argyi* H.Lév. & Vaniot (Asteraceae, *A. argyi*) was found to suppress the proliferation of human primary T lymphocytes *in vitro* in an IL-2-dependent manner. Flow cytometry- and ELISA-based techniques further demonstrated that the *A. argyi* extract reduced the activation and function of T cells. Transcription factor analysis and flow cytometric calcium influx investigations indicated that the immunomodulatory effect was based on specific modification of T cell signaling in a non-cytotoxic manner which is mediated *via* the NFAT pathway and a non-sequestrant inhibition of the calcium influx. A series of guaianolide and *seco*-guaianolide sesquiterpene lactones, as well as a flavonoid, were identified in a previous study as the bioactive compounds in the *A. argyi* extract. The effects of these bioactive compounds were compared to those of the crude extract. The tested sesquiterpene lactones act *via* the transcription factor NFAT and NF-κB, thereby exhibiting their immunosuppressive potential, but have an overall effect on T cell biology on a more-downstream level than the crude *A. argyi* extract.

Keywords: Artemisia, immunosuppression, interleukin-2, T cell signalling, sesquiterpene lactones

INTRODUCTION

T cells play a major role in the immune system. A complex mechanism of antigen recognition and signal transduction ensures a highly specific and highly efficient clearance of pathogens.

Upon T cell activation, several adaptor molecules and signaling proteins are phosphorylated to initiate three main axis of signal transduction in T cells. In this process, phosphatidylinositol-4,5-bisphosphate (PIP_2) is hydrolyzed to generate inositol-1,4,5-trisphosphate (IP_3) and diacylglycerol (DAG). While DAG is membrane associated, IP_3 binds to the IP_3 receptor in the membrane of the endoplasmic reticulum (ER) leading to calcium ER store depletion. Upon calcium ER store depletion, release-activated channels (CRAC channels) mediate a strong store-operated calcium entry (SOCE) (Hogan et al., 2010). The rising calcium concentration in the cytosol causes dephosphorylation and thereby unmasking of the nuclear location sequence of the nuclear factor of activated T cells (NFAT) *via* second messenger and phosphatase activation (Srikanth et al., 2017). On a further axis the mitogen-activated protein kinase (MAPK) pathway is triggered, resulting the formation of activator protein 1 (AP-1) and its nuclear transport (Myers et al., 2019). The third axis induces phosphorylation of nuclear factor of the kappa-light-polypeptide-gene enhancer in B cells inhibitor (IκB), leading to its degradation. Subsequently, the nuclear factor kappa-light-chain enhancer of activated B cells (NF-κB) is released for nuclear transport (Sun, 2012). The transcription factors NFAT, NF-κB, and AP-1 all bind to the *interleukin-2* (*il-2*) gene to allow transcription and secretion of interleukin-2 (IL-2) (Myers et al., 2019). IL-2 autocrinally stimulates T cell proliferation, and thus, is crucial for a proper immune response. Consequently, IL-2 can be linked to immune overreactions.

Overreaction of the immune system can be linked to autoimmune diseases such as rheumatoid arthritis or multiple sclerosis (Chaplin, 2010; Wang et al., 2015). The treatment of autoimmune diseases usually involves different classes of immunosuppressive drugs (Her and Kavanaugh, 2016). Glucocorticoids inhibit the function of immune cells as the activated glucocorticoid receptor directly interferes with the transcription factors NF-κB and AP-1 (van der Laan and Meijer, 2008; Frenkel et al., 2015; Wang et al., 2017). Glucocorticoids are quite effective, but this potency is accompanied by a range of side effects (Ramamoorthy and Cidlowski, 2016). Drugs such as cyclophosphamide or mycophenolate interfere with the cell cycle and, thereby, inhibit lymphocyte proliferation (Allison, 2000; Wang et al., 2015). Despite their clinical efficacy, these drugs also show severe side effects (Allison, 2000; Wang et al., 2015). Biopharmaceuticals, also called biologics, are widely used due to minor toxicity and high levels of specificity. They intervene strongly in the immune system and, therefore, lead to an increased susceptibility to infections and paradoxical inflammation (Her and Kavanaugh, 2016; Moroncini et al., 2017; Wagner, 2019). Small-molecule drugs (e.g., cyclosporine A, tacrolimus, or tofacitinib) interfering in T cell signaling lead to a suppression of T cell proliferation by addressing different molecular targets (Allison, 2000; Tedesco and Haragsim, 2012; Wiseman, 2016), and they all show adverse effects, such as nephrotoxicity and an increased susceptibility to infections (Allison, 2000).

Hence, compounds with novel modes of action and fewer side effects are needed. Natural products remain a promising source for the discovery and development of new drugs. A recent analysis emphasized their relevance by demonstrating that one third of new chemical entities (NCEs) approved by the Food and Drug Administration (FDA) between 1981 and 2014 were based on natural products (Newman and Cragg, 2016). Plant secondary metabolites possess high structural diversity which has likely evolved for serving different biological functions (Atanasov et al., 2015).

Aiming the discovery of new plant derived drugs, we recently tested a library of 435 extracts from plants used in traditional Chinese medicine (TCM), whereby immunosuppressive activity and inhibition of T lymphocyte proliferation *in vitro*, without apparent cytotoxicity, was targeted. One of the best hits in this library was an ethyl acetate extract of *Artemisia argyi* H. Lév. & Vaniot (Asteraceae). *A. argyi* (also called "Chinese mugwort") grows in China, Japan, and Korea and is traditionally used for the treatment of abdominal pain, dysmenorrhea, uterine hemorrhage, and inflammation (Yun et al., 2016). In previous studies, fatty acids, essential amino acids, sesquiterpene lactones, coumarins, sterols, terpenes, and polyphenols were the main compound classes isolated from *A. argyi* (Bao et al., 2013; Kim et al., 2015). *A. argyi* was recently shown to have anti-inflammatory properties (Yun et al., 2016). The anti-inflammatory effects were supported by *in vivo* experiments that showed reduced cytokine levels and immune infiltration in mouse models for contact dermatitis (Yun et al., 2016) and allergic asthma (Shin et al., 2017). The anti-inflammatory properties of *A. argyi* were linked to some compounds in the extracts, such as the flavonoids jaceosidin, eupatilin, and luteolin, and to a sesquiterpene dimer. These compounds were recently shown to decrease the production of inflammatory mediators and cytokines (Zeng et al., 2014; Li et al., 2018).

We previously showed that the *A. argyi* extract inhibited the proliferation of stimulated human T lymphocytes *in vitro*, and a series of related guaianolides and *seco*-guaianolides was found to be responsible for most of the inhibitory effects of the extract (Reinhardt et al., 2019). In the present study, we aimed to further

Abbreviations: AP-1, activator protein 1; APC, allophycocyanin; CD, cluster of differentiation; CFSE, carboxyfluorescein succinimidyl ester; CPT, camptothecin; CsA, cyclosporine A; CRAC channel, calcium release activated channel; DAG, diacylglycerine; DMSO, dimethyl sulfoxide; EDTA, ethylenediaminetetraacetic acid; ELISA, enzyme-linked immunosorbent assay; ER, endoplasmic reticulum; FACS, fluorescence-activated cell sorting; FCS, fetal bovine serum; FDA, Food and Drug Administration; FITC, Fluorescein isothiocyanate; GFP, green fluorescent protein; HPLC, High-performance liquid chromatography; IFN-, interferon-; IκB, nuclear factor of kappa light polypeptide gene enhancer in B-cells inhibitor; IL-, interleukin; IC_{50}, half maximal inhibitory concentration; IP3, inositol 1,4,5-trisphosphate; mAb, monoclonal antibody; MAPK, mitogen-activated protein kinase; NCEs, new chemical entities; NFAT, Nuclear factor of activated T-cells; NF-κB, nuclear factor kappa-light-chain-enhancer of activated B cells; p, p-value; Par, parthenolide; PIP_2, phosphatidylinositol 4,5-bisphosphate; PBMC, peripheral blood mononuclear cell; PBS, phosphate buffered saline; PE, phycoerythrin; PI, propidium iodide; PMA, phorbol-12-myristat-13-acetate; RPMI, Roswell Park Memorial Institute medium; SD, standard deviation; SOCE, store-operated calcium entry; TNF-α, tumor necrosis factor alpha; TCM, traditional Chinese medicine; TCR, T cell receptor.

substantiate the rationale for the use of *A. argyi* as an anti-inflammatory herbal drug. We here address the effects of *A. argyi* extract and selected compounds on the activation and function of T cells *in vitro*, as well as the effects of these compounds on relevant signaling pathways.

MATERIALS AND METHODS

Ethics Approval Statement

Written informed consent was obtained from patients prior to blood donation for research purposes. All experiments conducted on human material were approved by the Ethics Committee of the University of Freiburg (55/14; 11.02.2014). All performed methods are compliant with the regulations of the Ethics Committee of the University of Freiburg.

Preparation and Cultivation of Human Peripheral Lymphocytes

Preparation and cultivation of human peripheral lymphocytes were performed as indicated (Zimmermann-Klemd et al., 2019). Briefly, peripheral blood mononuclear cells (PBMCs) were isolated from the blood of healthy adult donors, which was obtained from a blood transfusion center (University Medical Center, Freiburg, Germany). Venous blood was centrifuged on a LymphoPrep™ gradient (1.077 g/cm^3, 20 min, 500 × g, 20°C; Progen, Heidelberg, Germany). After centrifugation cells were washed twice with phosphate buffered saline (PBS) and subsequently cultured in Roswell Park Memorial Institute medium (RPMI) 1640 medium supplemented with 10% heat-inactivated fetal calf serum, 2 mM L-glutamine, 100 U/ml penicillin, and 100 U/ml streptomycin (all from Life Technologies, Paisley, UK). Cells were cultured at 37°C in a humidified incubator with a 5% CO_2/95% air atmosphere.

Activation and Treatment of Lymphocytes

Lymphocytes were activated with anti-CD3 (clone OKT3) and anti-CD28 (clone 28.2) mAbs (each 100 ng/ml; both from eBioscience, Frankfurt, Germany) in the presence of medium; cyclosporine A (CsA; 4.16 μM; Sandimmun 50 mg/ml, Novartis Pharma, Basel, Switzerland); camptothecin (CPT; 300 μM: Tocris, Bristol, UK); 0.5% Triton-X 100; plant extract; or isolated compounds from *A. argyi*, as described previously (Zimmermann-Klemd et al., 2019). After cultivation, the cells were used in biological tests.

Determination of Apoptosis and Necrosis of T Cells

Determination of apoptosis and necrosis of T cells was performed as described previously (Zimmermann-Klemd et al., 2019). Cells were treated for 48 h. Cultured cells were washed with PBS and stained with Annexin V-FITC using the apoptosis detection kit (eBioscience, Frankfurt, Germany) according to instructions of the manufacturer. Propidium iodide (PI; eBioscience, Frankfurt, Germany) was added, and cells were stained for 15 min at room temperature in the dark. The proportion of apoptotic/necrotic lymphocytes was determined by flow cytometric analysis (FACSCalibur instrument; BD Biosciences, Franklin Lakes, NJ).

Determination of T Cell Proliferation

The proliferation of T lymphocytes was determined using carboxyfluorescein diacetate succinimidyl ester (CFSE) staining, as described previously (Parish et al., 2009; Gründemann et al., 2012). Lymphocytes were isolated, washed twice in cold PBS, and resuspended in PBS at a concentration of 5 × 10^6 cells/ml. Cells were stained for 10 min at 37°C with CFSE (5 μM; Sigma-Aldrich, St. Louis, MO). The staining reaction was stopped by washing twice with a complete medium. Stained cells were treated for 72 h. The progress of cell division was determined by flow cytometric analysis (FACSCalibur instrument; BD Biosciences, Franklin Lakes, NJ).

Analysis of Activation Marker of T Cells

The activation state of T lymphocytes was determined *via* cell-surface analysis of CD25 and CD69, as previously reported (Gründemann et al., 2014). Briefly, cells were treated for 24 h. Then, cells were washed with PBS and stained with PE-labeled, anti-CD25 mAbs; FITC-labeled, anti-CD69; and, for the differentiation of CD4$^+$ and CD4 T cells, with APC-labeled, anti-CD4 mAbs (all from eBioscience, Frankfurt, Germany) for 20 min at 4°C. Afterward, cells were washed twice with PBS, resuspended, and transferred into FACS vials. The expression of CD25 and CD69 was measured for CD4$^+$ and CD4 T cells, respectively, by flow cytometric analysis (FACSCalibur instrument; BD Biosciences, Franklin Lakes, NJ).

Determination of Cytokine Secretion

After 20 h of treatment, cells were restimulated with PMA (50 ng/ml; Sigma-Aldrich, Taufkirchen, Deutschland) and ionomycin (500 ng/ml; Sigma-Aldrich, Taufkirchen, Deutschland) for 4 h. Supernatants were stored at −20°C. The amount of cytokines was quantified using ELISA technique according to manufacturer's instructions (Affymetrix, Frankfurt, Germany).

Determination of Cytokine-Producing Cells

Cells were treated for 20 h, as described in section 2.3, and restimulated with PMA (50 ng/ml; Sigma-Aldrich, Taufkirchen, Deutschland) and ionomycin (500 ng/ml; Sigma-Aldrich, Taufkirchen, Germany) for an additional 4 h at 37°C. During this time, they were additionally treated with GolgiPlug (0.5 μl; BD Biosciences, Heidelberg, Germany). After incubation, cells of each sample were divided into three approaches: one for the determination of IL-2, one for the determination of TNFα, one for the determination of IFN-γ. The cells were fixed with 100 μl of 4% PFA (Morphisto, Frankfurt, Germany) for 10 min at room temperature and washed with PBS. Afterward, permeabilization was performed using 100 μl of 1× BD Perm/Wash Puffer (BD Biosciences, Heidelberg, Germany) per sample for 15 min at 4°C. Finally, cells were stained with 1 μl anti-IL-2 or anti-IFN-γ (both Affymetrix, Frankfurt, Germany) for 30 min at 4°C. After two washing steps samples were analyzed by flow cytometric analysis (FACS LSR Fortessa Instrument; BD Biosciences, Franklin Lakes, NJ).

Analysis of T Cell Degranulation

A CD107a surface staining was performed, as described previously (Gründemann et al., 2013), to determine the T cell degranulation capacity. Cells were treated for 20 h and then restimulated for 4 h with PMA (50 ng/ml; Sigma-Aldrich, Taufkirchen, Deutschland) and ionomycin (500 ng/ml; Sigma-Aldrich, Taufkirchen, Deutschland). To each well containing 200 µl of cell suspension, 2.5 µl (~0.25 µg) of PE-conjugated, anti-CD107a mAbs (eBioscience, Frankfurt, Germany) was added. After incubation at 37°C for 1 h, 2 µl of 1/10 diluted GolgiStop (Becton Dickinson, Franklin Lakes, NJ) was added per well, and the cells were incubated for another 3 h. Samples were analyzed by flow cytometric analysis (FACSCalibur instrument; BD Biosciences, Franklin Lakes, NJ).

Reporter Cell Experiments for the Determination of NFAT-, NF-κB-, and AP-1 Activity

A 96 well F-bottom cell culture plate was coated with anti-human CD3 mAb (clone OKT3, 1 µg/ml, 50 µl/well) or PBS (unstim. control) at 4°C over-night. Reporter cells (Jutz et al., 2016) were harvested, washed twice with PBS, and seeded in a 5% FCS RPMI cell culture medium (0.15×10^6 cells in 200 µl/well). Cells were treated with inhibitors (1 nM SP100030 for AP-1, 5 µg/ml cyclosporine A for NFAT, and 20 µM parthenolide for NF-κB), plant extract or isolated compounds from *A. argyi* or remained untreated (unstim. control, stim. control). Cells were incubated at 37°C for 8 h (AP-1) or 24 h (NFAT and NF-κB). Cells were washed twice with PBS and the expression of eGFP was determined by flow cytometric analysis (FACSCalibur instrument; BD Biosciences, Franklin Lakes, NJ).

Determination of Intracellular Calcium

Jurkat cells (0.5×10^6) were stained in 200 µl RPMI medium, containing 1% FCS, 2.6 µM Fluo3 AM (Life Technologies, Carlsbad, California), 5.5 µM FuraRed AM (Invitrogen, Carlsbad, California), and 0.1% (w/v) Pluronic F-127 (Invitrogen, Carlsbad, California) in the presence of test substances (30 µg/ml *A. argyi* extract or 10 µg/ml compound/compound mix; merely for the determination of the calcium ER store depletion) for 45 min at 37°C. For differentiation of calcium ER store depletion and SOCE, the staining solution was further supplemented with 0.6 mM ethylenediaminetetraacetic acid (EDTA). Cell suspensions were gently mixed every 10 min. After staining cells were resuspended in 100 µl of 1% FCS RPMI medium containing the test substance (30 µg/ml *A. argyi* extract or 10 µg/ml compound/compound mix; merely for the determination of the calcium ER store depletion). For the measurement of calcium influx, 50 µl of cell suspension were prewarmed (37°C, 5 min) in 700 µl of 1% FCS RPMI medium supplemented with 0.6 mM EDTA (for differentiation of ER store depletion and SOCE) and the test substance (30 µg/ml *A. argyi* extract or 10 µg/ml compound/compound mix; merely for the determination of the calcium ER store depletion). Baseline calcium levels were determined by flow cytometric measurement (FACS CyAn ADP; Beckman Coulter, Brea, California) for 1 min. Afterward, calcium influx was induced *via* stimulation with anti-CD3 mAbs (clone OKT3, 1 µg/ml). After 2 min, the test substance (30 µg/ml *A. argyi* extract or 10 µg/ml compound/compound mix) was added, followed, 30 s later, by the addition of calcium dichloride (1 mM). Calcium influx was measured for 5 min.

Analysis of Data

For statistical analysis, data were processed with Microsoft Excel and SPSS software (Version 22.0, IBM, Armonk, USA). Statistical significance was determined with the SPSS software by a one-way ANOVA followed by Dunnett's *post hoc* pairwise comparisons. Values are presented as mean ± standard deviation (SD) for the indicated number of independent experiments. The asterisks represent significant differences from controls (*$p < .05$).

Tested Compounds

The compounds used in this work were isolated from *A. argyi* ethyl acetate extract in a previous study (Reinhardt et al., 2019).

RESULTS

Anti-Proliferative Effects of the *A. argyi* Extract on T Lymphocytes

Previously, we evaluated the effect of 435 plant extracts from a focused extract library of TCM plants on the proliferative capacity of primary expanded human T lymphocytes *in vitro*. The ethyl acetate extract of *A. argyi* inhibited the proliferation of human T lymphocytes in a concentration-dependent manner, with a half maximal inhibitory concentration (IC_{50}) of 16.2 µg/ml (Reinhardt et al., 2019) (**Figure 1A**). The focused library also comprised extracts from other plants of the Asteraceae family (**Supplement 2**), but none of these exhibited notable activity in the assay.

To verify that the observed immunosuppressive activity was not due to cytotoxicity of the extract, flow cytometry analysis was performed to analyze the apoptosis and necrosis events of the cells. Using Annexin V/PI double staining, we found that the *A. argyi* extract had no toxic effects in the concentration range that was used for the mechanistic studies (**Figures 1B, C**).

Effects of the *A. argyi* Extract on T Lymphocyte Function

Next, the effect of the *A. argyi* extract on the effector function of human T cells was examined. Stimulation of T lymphocytes *via* the T cell receptor (TCR) leads to the expression of the activation markers CD25 and CD69. We found that after TCR stimulation the treatment of T cells with the *A. argyi* extract significantly and concentration-dependently lowered CD25 and CD69 expressions (**Figures 2A, B**). This was the case in both the $CD4^+$ and CD4 T cells. In addition, we observed a significantly reduced CD25 expression of CD4 T cells after treatments with low concentrations (3 and 10 µg/ml) of the *A. argyi* extract (**Figure 2A**).

Upon activation, T cells secrete IL-2, which is important for proliferation, and interferon-γ (IFN-γ), which defines T cell function. The *A. argyi* extract significantly suppressed IL-2 as well as the IFN-γ secretion capacity of activated T lymphocytes (**Figures 2C, D**).

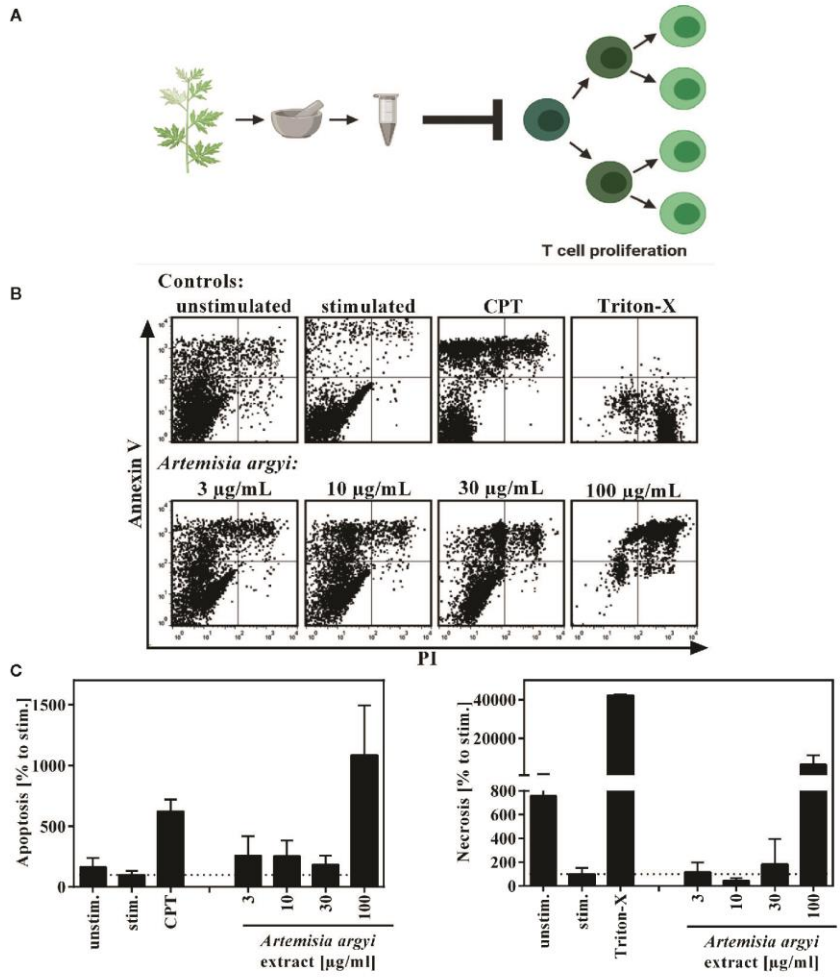

FIGURE 1 | Overview of recently published results **(A)** and effect of the *A. argyi* extract on the viability of T lymphocytes **(B, C)**. Expanded human lymphocytes (2×10^5) were left unstimulated (unstim.) or were stimulated (stim.) with anti-CD3 and anti-CD28 mAbs (100 ng each) and incubated for 48 h with medium (unstim., stim.), camptothecin (CPT; 300 µM), Triton-X 100 (0.5%) or the *A. argyi* extract. Annexin V-FITC and PI double stainings were performed after incubation. The proportions of viable, necrotic, and apoptotic cells were determined by flow cytometry. Data are depicted as dot plots **(B)**, and the proportion of apoptotic/necrotic lymphocytes in relation to the stimulated control was determined from two independent experiments. Data are depicted as mean ± SD **(C)**.

Influence of the *A. argyi* Extract on the Transcription Factors AP-1, NFAT, and NF-κB

To understand how the activation and proliferation of human T cells is inhibited by the *A. argyi* extract, we analyzed the effect of the *A. argyi* extract on the transcription factors AP-1, NFAT, and NF-κB. All three transcription factors regulate the transcription of the *il-2* gene, which is a key regulator in these processes. Jurkat T cell reporter lines (Ratzinger et al., 2014; Jutz et al., 2016), in which eGFP is fused to the response elements of these transcription factors, were used for this purpose. After stimulation with anti-CD3 mAbs, activity of the transcription factors was quantified *via* flow cytometry. The treatment with the *A. argyi* extract did not change the anti-CD3-induced AP-1 activity in comparison to untreated activated AP-1 reporter cells (**Figure 3A**). In contrast, NFAT and NF-κB activity was reduced in a concentration-dependent manner by the *A. argyi* extract (**Figures 3B, C**). In summary, the reporter cell experiments pointed to a specific suppression of NFAT and NF-κB activities, but not to suppression of AP-1.

Effects of the *A. argyi* Extract on TCR-Induced Calcium Signaling

The previous experiments demonstrated that the *A. argyi* extract lowered activity of NFAT, which was induced by TCR triggering. Influx of calcium ions into the cytosol is upstream regulated of NFAT activation (Robert et al., 2011). Hence, we performed

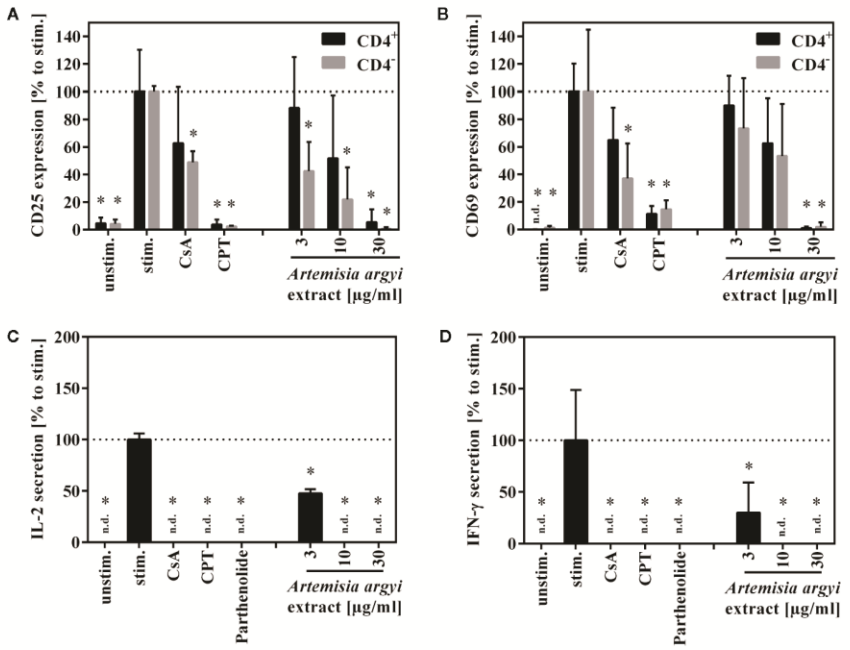

FIGURE 2 | Effects of *A. argyi* extract on the function of T lymphocytes. For **(A**, **B)**, lymphocytes (2 × 10^5) were left unstimulated (unstim.) or were activated with anti-CD3 and anti-CD28 mAbs (100 ng each and incubated for 24 h with medium (unstim., stim.), cyclosporine A (CsA; 4.16 µM), camptothecin (CPT; 300 µM), or the *A. argyi* extract. Cells were stained with anti-CD69-FITC and anti-CD4-APC **(A)** or anti-CD25-PE and anti-CD4-APC **(B)**. Expression of surface markers (CD69, CD25, CD4) was analyzed by flow cytometry, and the amounts of activated $CD4^+$ and $CD4^-$ T lymphocytes were determined. For **(C**, **D)** expanded lymphocytes (2 × 10^5) were incubated for 20 h with medium (unstim., stim.), cyclosporine A (CsA; 4.16 µM), camptothecin (CPT; 300 µM), parthenolide (20 µM) or the *A. argyi* extract. Subsequently, the cells were stimulated with PMA/Ionomycin for 4 h at 37°C. IL-2 **(C)** and IFN-γ **(D)** were quantified in the supernatants by ELISA. The results of three different experiments are summarized and are depicted as mean ± SD in relation to the untreated, stimulated control. *$p < 0.05$. n.d.= below detection limit.

calcium flux experiments to determine whether the calcium influx to the cytosol was impaired. Inhibition of calcium influx would prevent the translocation of NFAT to the nucleus and, consequently suppress NFAT activity.

Jurkat cells were stained with the calcium indicators Fluo3 and FuraRed and treated with the *A. argyi* extract. Subsequently, calcium influx was induced by TCR stimulation using an anti-CD3 mAbs. The experiments demonstrated that the treatment of the cells with the *A. argyi* extract led to a complete suppression of the calcium influx (**Figures 4A, B**).

Next, we sought to characterize the inhibition of the calcium influx. Jurkat cells were treated with the *A. argyi* extract or the calcium ion chelator EDTA to determine whether the inhibition was mediated *via* chelation of calcium. As expected, a strong calcium influx was measured for untreated cells (control) after TCR stimulation (**Figure 4C**). This influx was prevented in EDTA-treated cells but restored by the addition of calcium dichloride to the medium (**Figure 4C**). In contrast, in cells treated with the *A. argyi* extract, the calcium influx capability could not be restored with the addition of increasing concentrations of calcium dichloride (**Figure 4C**). This suggested that the *A. argyi* extract did not inhibit the calcium influx through calcium chelating properties.

Upon TCR activation by antigen binding, the opening of a calcium channel in the membrane of the ER initiates calcium release from ER stores (ER store depletion). The depletion of these intracellular calcium stores causes the formation of calcium release-activated channels (CRAC) channels, which in turn leads to a strong influx of calcium from the extracellular space to the cytosol (store-operated calcium entry, SOCE) and allows replenishment of the calcium stores in the ER (Robert et al., 2011). To discriminate between these two options, we stained Jurkat cells with Fluo3 and FuraRed in a medium supplemented with EDTA. During the staining process, the cells were treated with the *A. argyi* extract in a calcium-free setting to ensure a calcium-free, extracellular compartment. Cells were stimulated *via* TCR to induce the calcium influx. Given that the SOCE was prevented, calcium store depletion could be measured. In comparison to the untreated cells (control), treatment with the extract lowered calcium ER store depletion (**Figure 4D**). To determine whether the SOCE was also inhibited by the *A. argyi* extract, or just prevented due to the lacking depletion of ER calcium store, we stained Jurkat cells with Fluo3 and FuraRed in a medium supplemented with EDTA, and induced the calcium ER store depletion by TCR stimulation. Next, the extract and calcium dichloride were added and the SOCE was measured.

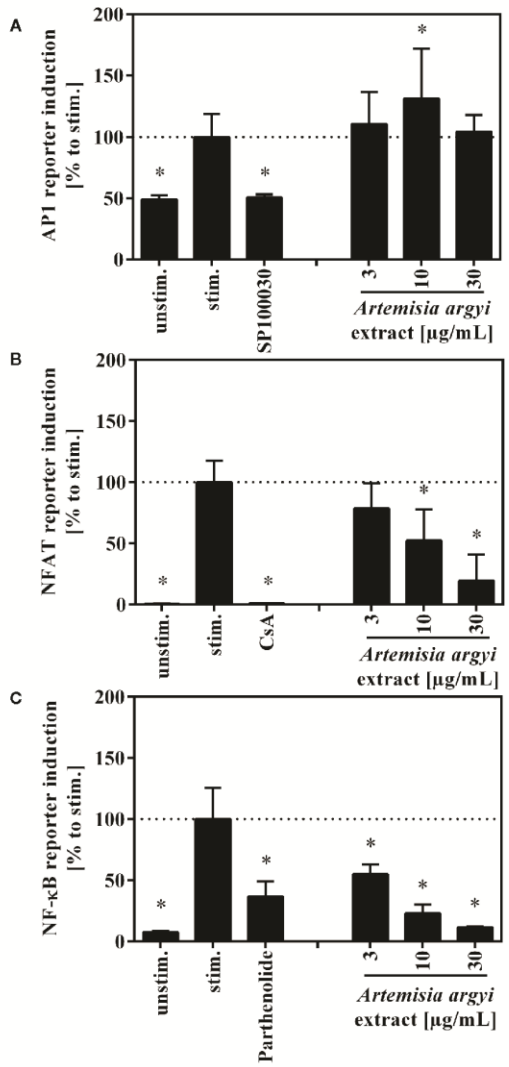

FIGURE 3 | Effect of the *A. argyi* extract on the activity of transcription factors AP-1 **(A)**, NFAT **(B)** and NFκB **(C)** in Jurkat T cells. Jurkat reporter cells (0.15×10^6) were seeded on a cell culture plate, coated with anti-CD3 mAbs, and incubated with medium, inhibitors (AP-1: 1 nM SP100030, NFAT: 4.16 µM CsA, NF-κB: 20 µM parthenolide) or the *A. argyi* extract in different concentrations for 8 (AP-1) or 24 h (NFAT and NF-κB). The GFP expression was measured by flow cytometry after incubation. The results of three independent experiments are summarized and depicted as mean ± SD. *$p < 0.05$.

The medium of control cells was supplemented with calcium dichloride directly after depletion of the intracellular calcium stores. The results showed that the *A. argyi* extract also lowered the SOCE from the extracellular space (**Figure 4D**).

In summary, the strong reduction of calcium influx upon TCR stimulation after treatment with the *A. argyi* extract resulted from suppression of the ER calcium store depletion and a reduction of the SOCE.

Effects of Isolated *A. argyi* Compounds on the Activation and Function of T Lymphocytes

We previously isolated a series of sesquiterpene lactones and flavones from the active extract (**Figure 7A**), some of which showed significant inhibitory effects on T lymphocyte proliferation (Reinhardt et al., 2019) (**Figure 1A**). Several of the most-active compounds were tested: two stereoisomeric guaianolides, artecanin and canin (**1** and **5**), artanomaloide (**2**), arteglasin A (**3**) differing from **1** and **2** in the decoration of the 7-membered ring, the moderately active flavone jaceosidin (**4**), and two stereoisomeric *seco*-guaianolides, *seco*-tanapartholides B and A (**6** and **7**) (**Figure 5**).

To better understand their contribution to the activity of the extract, their influence on activation, cytokine production, and degranulation capacity of human T lymphocytes was investigated.

The compounds **1**, **2**, **3**, **5,** and the compound mix significantly reduced the expression of CD25 in $CD4^-$ and $CD4^+$ T cells at 10 and/or 3 µg/ml. Compound **6** suppressed the CD25 expression in $CD4^+$ T cells at all tested concentration levels, while compound **7** suppressed it at 10 and 3 µg/ml. Compounds **6** and **7** had no significant effect on $CD4^-$ T cells. The isolated flavone **4** showed no effect on CD25 expression (**Figure 6A**).

All isolated compounds, with the exception of compound **4**, significantly and strongly suppressed IL-2-producing cells at 10 µg/ml. While the effect was only miniscule for the flavone (**4**), compounds **1**, **3**, **5**-**7**, and the mix also showed significant inhibition at 3 µg/ml. A similar pattern was observed for the suppression of tumor necrosis factor α-(TNFα) and IFN-γ-producing cells. The strongest suppression of IL-2- and IFN-γ-producing cells was observed from compound **6** (**Figure 6B**).

Upon release of perforin and granzymes, T lymphocytes express the lysosomal-associated membrane protein 1 (LAMP-1, CD107a) on their surface. Analysis of the LAMP-1 surface expression, showed concentration-dependent effects for the mixture of all compounds and the *A. argyi* extract (**Figure 6C**).

Effects of Isolated *A. argyi* Compounds on the Transcription Factors NFAT and NF-κB

Jurkat-based NFAT and NF-κB reporter experiments were performed to shed light on the interaction of compounds by manipulation the T lymphocyte signaling. For the sesquiterpene lactones, but not for the flavone (**4**), a concentration-dependent, suppressive effect on the NFAT pathway was found, with IC_{50} values < 10 µM (< 3 µg/ml) (**Figures 7C, D**). Likewise, NF-κB activity was significantly decreased by all compounds except compound **4** (**Figures 7B, D**). We here focused on the effects of the *A. argyi* extract and isolated compounds on the NFAT signaling pathway.

Thus we tested whether the isolated compounds were able to inhibit TCR-induced calcium signaling. To this end, we looked at both the ER calcium store depletion (**Supplement 1**, left panel) and the SOCE (**Supplement 1**, right panel), using the methodology, described above. Single compounds and a mixture of all isolated compounds were tested with the assumption that the mixture would, at least in part, mimic the activity of the whole extract.

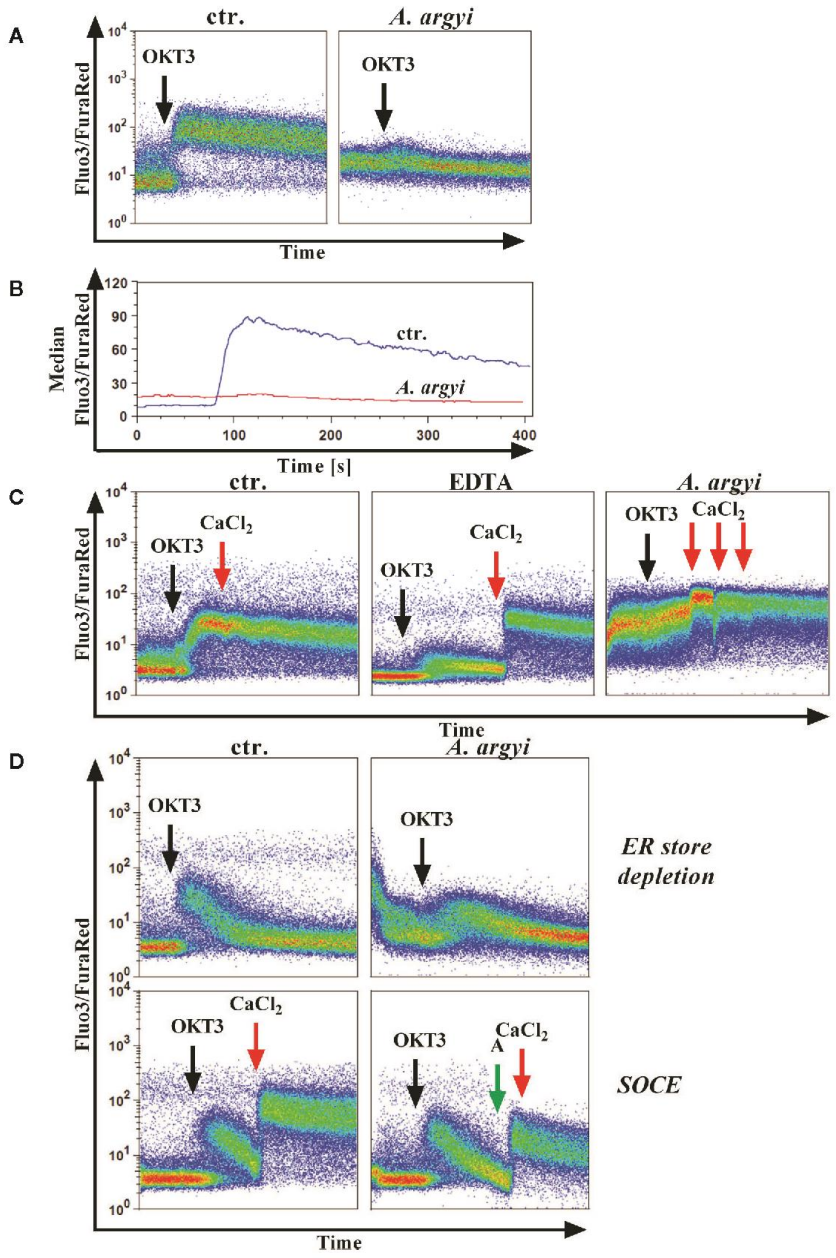

FIGURE 4 | Effect of the *A. argyi* extract on the calcium influx in Jurkat T cells. Jurkat cells (0.5 × 10^6) were stained with Fluo3 and FuraRed for 45 min at 37°C in the presence of medium, 0.6 mM EDTA or 30 µg/ml *A. argyi* extract. The results show the anti-CD3-induced (black arrows) calcium influx as the Fluo3/FuraRed ratio **(A)** and the median of this ratio **(B)** for untreated cells (ctr.) and cells treated with 30 µg/ml *A. argyi* extract. Calcium influx was induced by anti-CD3 stimulation (black arrows) of the TCR **(C)**, and, after 1 min 1 mM calcium dichloride was added (red arrows). The calcium influx (ratio Fluo3/FuraRed) of untreated cells (ctr.), cells treated with 0.6 mM EDTA, and cells treated with 30 µg/ml *A. argyi* extract are shown. The ER store depletion in presence of the *A. argyi* extract was analyzed **(D)**. Jurkat cells (0.5 × 10^6) were stained with Fluo3 and FuraRed in a calcium-free medium for 45 min at 37°C. To determine the ER calcium store depletion, 30 µg/ml *A. argyi* extract was present in the medium during staining and measurement, and the ER store depletion was triggered by TCR stimulation (black arrows). The control cells remained untreated. For determination of the SOCE, cells were stained, and the ER calcium store depletion was induced by TCR stimulation (black arrows). After 2 min 30 µg/ml *A. argyi* extract (green arrows) were added and, after another 30 s, 1 mM calcium dichloride (red arrows) was added. For the control (ctr.), 1 mM calcium dichloride was added directly after depletion of the ER calcium store. The results show the calcium influx (the ratio Fluo3/FuraRed) of the untreated cells (ctr.) and the cells treated with 30 µg/ml *A. argyi* extract.

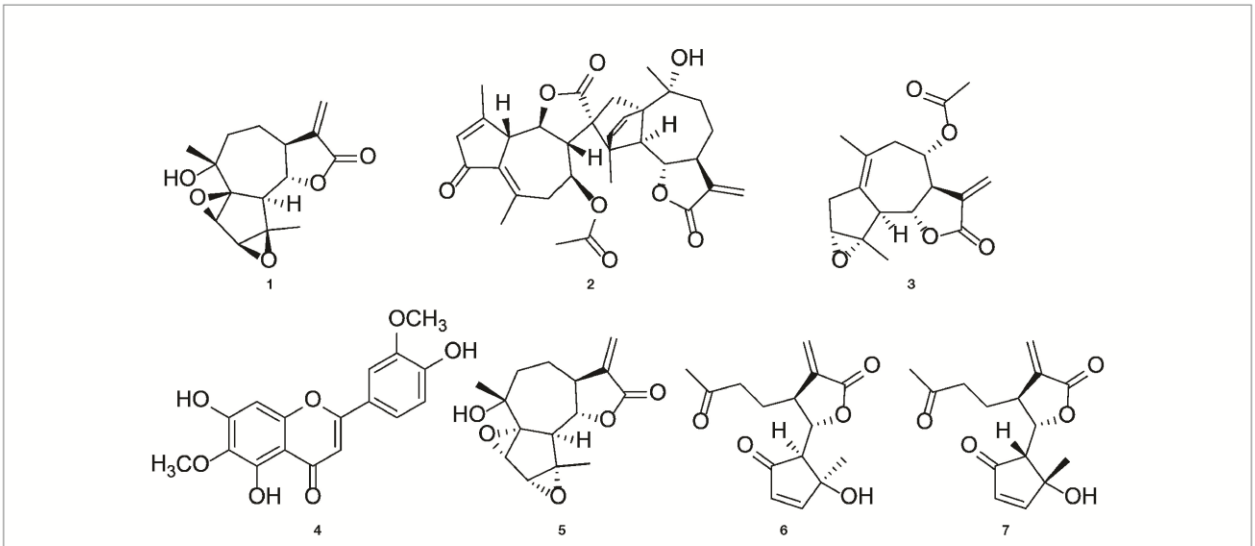

FIGURE 5 | Chemical structures of (1*S*)-artecanin **(1)**, 8-acetyl-artanomaloide **(2)**, arteglasin A **(3)**, jaceosidin **(4)**, (1*R*)-canin **(5)**, (4*S*, 5*S*, 6*S*, 7*S*)- and (4*R*, 5*R*, 6*S*, 7*S*) -*seco*-tanapartholide **(6** and **7)**.

The *A. argyi* extract was used as a control. A slight inhibition of calcium influx from the ER combined with a significant time delay was observed for compound **5**. A similar delay was observed for the compound mix and, to a lesser extent, for compounds **1**, **6**, and **7**. Compounds **2** and **3** increased the intensity of the calcium influx. However, neither the single compounds nor the compound mix inhibited the calcium influx as effectively as did the *A. argyi* extract (**Supplement 1**).

DISCUSSION

We recently found that an ethyl acetate extract of *A. argyi* suppressed the *in vitro* proliferation of human primary T lymphocytes in a concentration-dependent, non-cytotoxic manner (**Figure 1**) and we also isolated a series of compounds that were responsible for this activity (Reinhardt et al., 2019).

Stimulation of TCR promotes the surface expression of the transmembrane C-type lectin CD69 and the alpha-chain of the IL-2 receptor (CD25) on T cells (Malek, 2008). The *A. argyi* extract lowered the expression of both activation markers (**Figures 2A, B**) and of IL-2 production (**Figure 2C**) in stimulated T lymphocytes. As IL-2 is pivotal for lymphocyte proliferation, inhibition of IL-2 production could explain the observed inhibition of T cell proliferation. Further, the IFN-γ secretion was reduced after treatment with the *A. argyi* extract (**Figure 2D**). Our findings provide evidence for IL-2-mediated, anti-inflammatory properties of the extract, likely *via* IL-2-mediated T lymphocyte proliferation inhibition, and thereby corroborate the traditional use of *A. argyi* as an anti-inflammatory herbal drug (Yun et al., 2016).

The IL-2-dependent suppression of T lymphocyte proliferation by the *A. argyi* extract is linked to suppression of the transcription factors NFAT and NF-κB (**Figures 3B, C**), while AP-1 activity was not affected (**Figure 3A**). ER calcium store depletion and the SOCE were inhibited *via* a non-sequestrant mechanism (**Figures 4A–D**). Our observation that it is impossible to restore the calcium influx by generating an overage of calcium dichloride in the outer cell compartment points to an irreversible blockage of the calcium channels. Otherwise, binding and dissociation homeostasis would trigger a stronger calcium influx without binding of the active constituent(s) of the *A. argyi* extract to the calcium channels. The effect of the extract was comparable to that of the calcium chelator EDTA. Inhibition of the ER calcium store depletion and SOCE explain the observed reduced NFAT activity.

To correlate the effects found for the *A. argyi* extract to the compounds from the extract, selected T cell proliferation-inhibiting compounds were investigated analogously. Jaceosidin (**4**) showed no effect on either NFAT or NF-κB reporter cells, which is in accord with its weak inhibition of all three pro-inflammatory cytokines tested. A comparable inhibition of TNFα expression by jaceosidin (**4**) has been reported (Li et al., 2018). Thus, it is unlikely for jaceosidin to contribute significantly to the observed activity of the extract. All tested sesquiterpene lactones were shown to inhibit NFAT and NF-κB binding to the DNA. The inhibition of DNA binding of NF-κB can presumably be compared to the effects published for other sesquiterpene lactones, such as helenalin (a guaianolide) and parthenolide (a germacranolide) (García-Piñeres et al., 2001; García-Piñeres et al., 2004). Parthenolide inhibits the IκB kinase complex β (IKKβ) by alkylating a cysteine residue in its activation loop (Kwok et al., 2001). Less is known about the effect of sesquiterpene lactones on the NFAT pathway, which was the focus of this work. Only helenalin was previously shown to suppress abundance and nuclear translocation of NFATc2 (Berges et al., 2009). The stereoisomeric guaianolides artecanin (**1**) and canin (**5**), as well as the guaianolide dimer **2** and arteglasin A (**3**) showed very similar effects to the *A. argyi* extract in general. However, in the ER

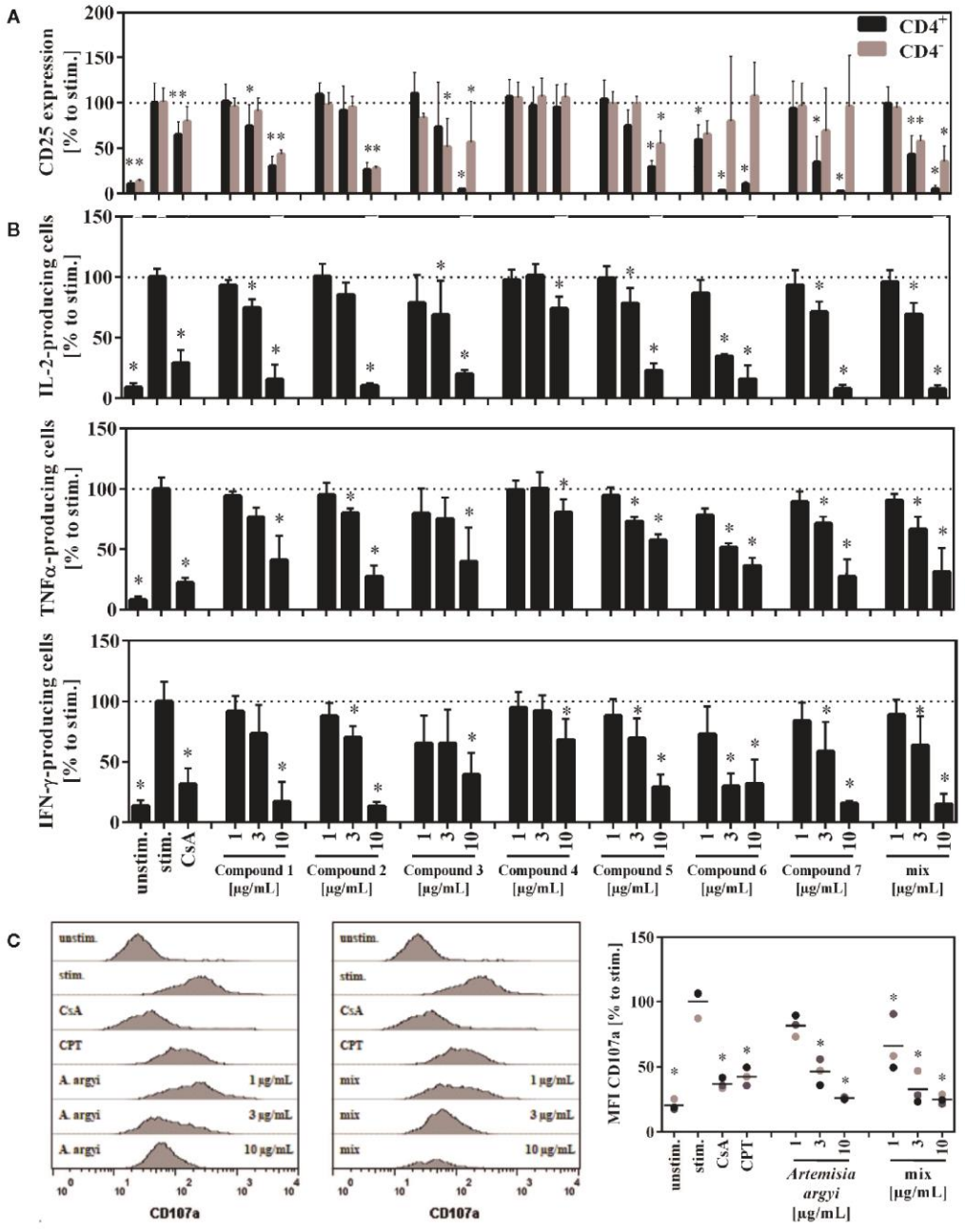

FIGURE 6 | Effect of the isolated compounds and the compound mix on activation **(A)** IL-2-, TNFα-, and IFN-γ-producing T cells **(B)** and the degranulation capacity of T cells **(C)**. For **(A),** lymphocytes (2×10^5) were stimulated with anti-CD3 and anti-CD28 mAbs (100 ng each) and incubated for 48 h with medium (unstim., stim.), cyclosporine A (CsA; 4.16 µM), the compounds, the compounds mixture, or the *A. argyi* extract **(B)**. Cells were re-stimulated with PMA (500 µg/ml) and ionomycin (500 ng/ml) and treated with GolgiPlug for 4 h. The cells were fixed, permeabilized, and stained with anti-IL-2, anti-TNFα or anti-IFN-γ mAbs. The amount of IL-2-, TNFα-, and IFN-γ-secreting cells was determined *via* flow cytometry. Results from four independent experiments were summarized and are depicted as mean ± SD in relation to the untreated, stimulated control. *$p < 0.05$. For **(C)** lymphocytes (2×10^5) were stimulated with anti-CD3 and anti-CD28 mAbs (100 ng each). Afterward, cells were incubated for 20 h with medium (unstim., stim.), cyclosporine A (CsA; 4.16 µM), camptothecin (CPT; 300 µM), the compound mixture, or the *A. argyi* extract. Cells (except the unstim. control) were restimulated with PMA (500 µg/ml) and ionomycin (500 ng/ml) for 4 h and stained with anti-CD107a-PE. The amount of degranulating T lymphocytes, as indicated by a CD107a surface expression, was determined *via* flow cytometry. Data are depicted as histogram plots, and data of three independent experiments are summarized as mean ± SD. *$p < 0.05$.

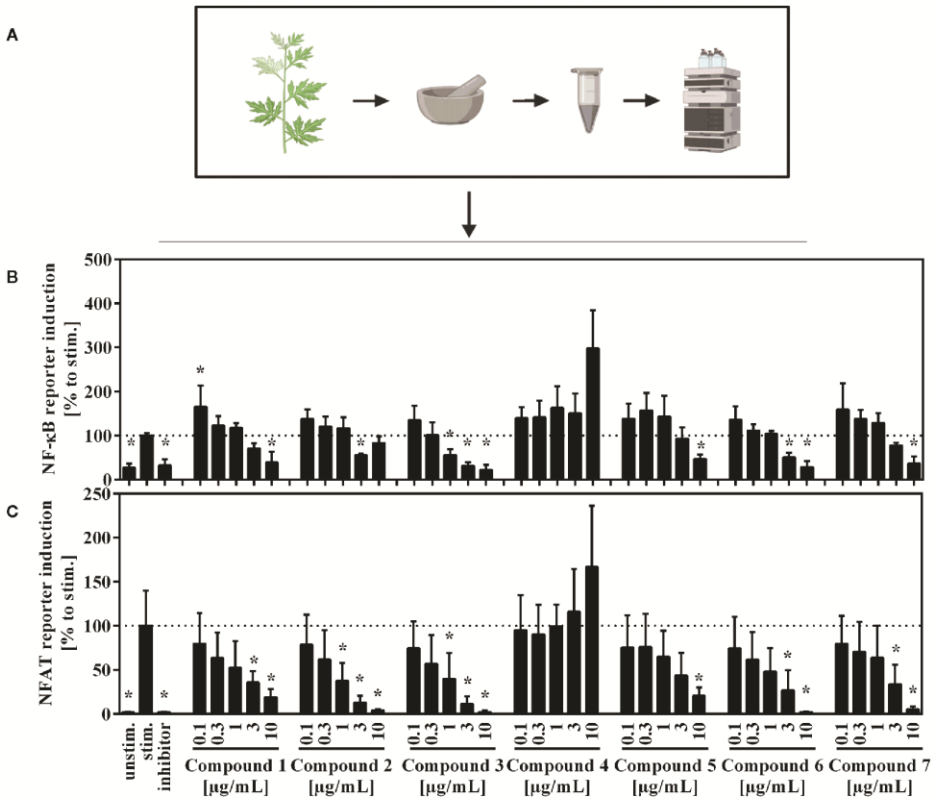

D

Compound	NF-kB IC_{50} [µg/mL]	NF-kB IC_{50} [µM]	NFAT IC_{50} [µg/mL]	NFAT IC_{50} [µM]
1	1.7	6.1	1.3	4.7
2	1.7	3.1	0.9	1.6
3	0.6	2.0	1.1	3.6
4	no inhib.	no inhib.	no inhib.	no inhib.
5	2.6	9.3	2.6	9.3
6	1.8	6.5	1.9	6.8
7	2.2	7.9	2.4	8.6

FIGURE 7 | Overview of the published fractionation process **(A)** and effect of the A. argyi compounds on NF-κB **(B)** and NFAT **(C)** activity and corresponding IC_{50} values **(D)** in Jurkart T cells. Jurkat reporter cells (0.15×10^6) were seeded on a culture plate, coated with anti-CD3 mAbs, and incubated with medium, inhibitors (NFAT: 4.16 µM CsA, NF-κB: 20 µM parthenolide) or *A. argyi* compounds in different concentrations for 24 h. The GFP expression was measured by flow cytometry. The results of three independent experiments are summarized and depicted as mean ± SD. $^*p < 0.05$ **(B, C)**. The calculated IC_{50} values are presented in µg/ml and in µM, as stated **(D)**.

store depletion and for the SOCE, the activity of the single compounds was not comparable to that of the extract. Only canin (**5**), but not its stereoisomer artecanin (**1**), showed some inhibition of ER store depletion, which did not affect the SOCE. Thus, canin (**5**) might be part of the explanation for the inhibition of the ER store depletion by the *A. argyi* extract. The specific CD25 inhibition by the two *seco*-guaianolides **6** and **7** in $CD4^+$ cells but not in$CD4^-$ cells is unusual and deserves further investigation. However, this inhibition is not reflected in the activity of the *A. argyi* extract. Although most of the observed activity from the *A. argyi* extract can be attributed to the presence of the tested guaianolides and *seco*-guaianolides, none of the isolated compounds showed sufficient inhibition of the ER calcium store depletion or the SOCE (**Supplement 1**). This was also true for a mixture of the compounds, suggesting that other, as yet unidentified compounds in the extract are responsible for this activity.

The initial screening (Reinhardt et al., 2019) included extracts from additional herbal drugs of the family Asteraceae, but none of these inhibited T cell proliferation at the concentrations tested. The lack of activity can be possibly explained, by an absence of sesquiterpene lactones from the extracts (*Carthamus tinctorius*, *Artemisia scoparia*, and *Artemisia apiacaea*). So far, sesquiterpene lactones have only been reported from *Artemisia capillaris* (Feng et al., 2017) and *Centipeda minima* (Eisenbrand and Tang, 2011), and their concentrations in the plants were very low, in the range of 0.001% in *A. capillaris* (Wu et al., 2012; Feng et al., 2017). Furthermore, the strength of T cell proliferation inhibition may also depend on the specific sesquiterpene scaffold, as significant differences were observed between eudesmanes, guaianolides, and *seco*-guaianolides (Reinhardt et al., 2019). All reported sesquiterpene lactones from *C. minima* are structurally related to helenalin, which is a known NF-κB inhibitor (Lyss et al., 1997; Eisenbrand and Tang, 2011).

We ascertained different modes of action for the capacity of the *A. argyi* extract to inhibit the proliferation of T cells. We demonstrated that the *A. argyi* extract, as well as different guaianolides isolated from it, inhibited the activity of NFAT and NF-κB. Moreover, the crude extract suppressed the TCR-induced calcium influx, but neither the isolated single compounds nor a mixture of these sesquiterpene lactones showed similar effects. This suggests that the *A. argyi* extract likely contains compounds affecting signaling on a more upstream target than the compounds isolated thus far. Our findings corroborate the notion of a multitarget effect of herbal extracts possibly resulting in pharmacological synergism (Fürst and Zündorf, 2015; Colalto, 2018). The study also demonstrates that the established cell-based screening platform approach is a powerful tool for identifying and characterizing potential immunosuppressive leads from natural product sources.

DATA AVAILABILITY STATEMENT

The datasets generated for this study are available on request to the corresponding author.

ETHICS STATEMENT

The studies involving human participants were reviewed and approved by Ethics Committee of the University of Freiburg, Engelberger Straße 21, 79106 Freiburg. The patients/participants provided their written informed consent to participate in this study.

AUTHOR CONTRIBUTIONS

AZ-K performed the experiments, analyzed the data, prepared the figures, and wrote the draft manuscript. JR prepared **Figure 5** and wrote the draft manuscript regarding results and discussion on "Effects of isolated compounds" and the discussion of other tested Asteraceae. JR, AM, WS, PS, JL, RH, MH, and CG contributed to the design, implementation of the research, and in finalizing the manuscript.

FUNDING

Gefördert durch die Deutsche Forschungsgemeinschaft (DFG) im Rahmen der Exzellenzstrategie des Bundes und der Länder – EXC – 2189 – Projektnummer 390939984. (Funded by the Deutsche Forschungsgemeinschaft (DFG, German Research Foundation) under Germany's Excellence strategy – EXC – 2189 – Project ID: 390939984.) Furthermore, this work was financially supported by the Software AG Foundation, DAMUS-DONATA e.V. and PRIAM-based foundation.

ACKNOWLEDGMENTS

We appreciate the excellent technical assistance of Kerstin Fehrenbach, Orlando Fertig and Moritz Winker, Seema Devi and Carmen Steinborn.

SUPPLEMENTARY MATERIAL

The Supplementary Material for this article can be found online at: https://www.frontiersin.org/articles/10.3389/fphar.2020.00402/full#supplementary-material

REFERENCES

Allison, A. C. (2000). Immunosuppressive drugs: the first 50 years and a glance forward. *Immunopharmacology* 47, 63–83. doi: 10.1016/S0162-3109(00)00186-7

Atanasov, A. G., Waltenberger, B., Pferschy-Wenzig, E.-M., Linder, T., Wawrosch, C., Uhrin, P., et al. (2015). Discovery and resupply of pharmacologically active plant-derived natural products: A review. *Biotechnol. Adv.* 33, 1582–1614. doi: 10.1016/j.biotechadv.2015.08.001

Bao, X., Yuan, H., Wang, C., Liu, J., and Lan, M. (2013). Antitumor and immunomodulatory activities of a polysaccharide from Artemisia argyi. *Carbohydr. Polym.* 98, 1236–1243. doi: 10.1016/j.carbpol.2013.07.018

Berges, C., Fuchs, D., Opelz, G., Daniel, V., and Naujokat, C. (2009). Helenalin suppresses essential immune functions of activated CD4+ T cells by multiple mechanisms. *Mol. Immunol.* 46, 2892–2901. doi: 10.1016/j.molimm.2009.07.004

Chaplin, D. D. (2010). Overview of the Immune Response. *J. Allergy Clin. Immunol.* 125, S3–23. doi: 10.1016/j.jaci.2009.12.980

Colalto, C. (2018). What phytotherapy needs: Evidence-based guidelines for better clinical practice. *Phytother. Res.* 32, 413–425. doi: 10.1002/ptr.5977

Eisenbrand, G., and Tang, W. (2011). *Handbook of Chinese Medicinal Plants: Chemistry, Pharmacology, Toxicology* Vol. I+II. Eds. W. Tang and G. Eisenbrand (Weinheim: Wiley-VCH), 1150. doi: 10.1002/mnfr.201190015

Fürst, R., and Zündorf, I. (2015). Evidence-Based Phytotherapy in Europe: Where Do We Stand? *Planta Med.* 81, 962–967. doi: 10.1055/s-0035-1545948

Feng, J., Jin, Y.-J., Jia, J.-J., Cao, J.-P., Wang, Y.-T., and Li, X.-P. (2017). Sesquiterpene Lactones from Artemisia capillaris*. *Chem. Nat. Compd.* 53, 978–979. doi: 10.1007/s10600-017-2176-z

Frenkel, B., White, W., and Tuckermann, J. (2015). Glucocorticoid-Induced Osteoporosis. *Adv. Exp. Med. Biol.* 872, 179–215. doi: 10.1007/978-1-4939-2895-8_8

García-Piñeres, A. J., Castro, V., Mora, G., Schmidt, T. J., Strunck, E., Pahl, H. L., et al. (2001). Cysteine 38 in p65/NF-kappaB plays a crucial role in DNA binding inhibition by sesquiterpene lactones. *J. Biol. Chem.* 276, 39713–39720. doi: 10.1074/jbc.M101985200

García-Piñeres, A. J., Lindenmeyer, M. T., and Merfort, I. (2004). Role of cysteine residues of p65/NF-kappaB on the inhibition by the sesquiterpene lactone parthenolide and N-ethyl maleimide, and on its transactivating potential. *Life Sci.* 75, 841–856. doi: 10.1016/j.lfs.2004.01.024

Gründemann, C., Koehbach, J., Huber, R., and Gruber, C. W. (2012). Do plant cyclotides have potential as immunosuppressant peptides? *J. Nat. Prod.* 75, 167–174. doi: 10.1021/np200722w

Gründemann, C., Thell, K., Lengen, K., Garcia-Käufer, M., Huang, Y.-H., Huber, R., et al. (2013). Cyclotides Suppress Human T-Lymphocyte Proliferation by an Interleukin 2-Dependent Mechanism. *PloS One* 8, e68016. doi: 10.1371/journal.pone.0068016

Gründemann, C., Lengen, K., Sauer, B., Garcia-Käufer, M., Zehl, M., and Huber, R. (2014). Equisetum arvense (common horsetail) modulates the function of inflammatory immunocompetent cells. *BMC Complement. Altern. Med.* 14, 283. doi: 10.1186/1472-6882-14-283

Her, M., and Kavanaugh, A. (2016). Alterations in immune function with biologic therapies for autoimmune disease. *J. Allergy Clin. Immunol.* 137, 19–27. doi: 10.1016/j.jaci.2015.10.023

Hogan, P. G., Lewis, R. S., and Rao, A. (2010). Molecular basis of calcium signaling in lymphocytes: STIM and ORAI. Annu. *Rev. Immunol.* 28, 491–533. doi: 10.1146/annurev.immunol.021908.132550

Jutz, S., Leitner, J., Schmetterer, K., Doel-Perez, I., Majdic, O., Grabmeier-Pfistershammer, K., et al. (2016). Assessment of costimulation and coinhibition in a triple parameter T cell reporter line: Simultaneous measurement of NF-κB, NFAT and AP-1. *J. Immunol. Methods* 430, 10–20. doi: 10.1016/j.jim.2016.01.007

Kim, J. K., Shin, E.-C., Lim, H.-J., Choi, S. J., Kim, C. R., Suh, S. H., et al. (2015). Characterization of Nutritional Composition, Antioxidative Capacity, and Sensory Attributes of Seomae Mugwort, a Native Korean Variety of Artemisia argyi H. Lév. & Vaniot. *J. Anal. Methods Chem.* 2015. doi: 10.1155/2015/916346

Kwok, B. H., Koh, B., Ndubuisi, M. I., Elofsson, M., and Crews, C. M. (2001). The anti-inflammatory natural product parthenolide from the medicinal herb Feverfew directly binds to and inhibits IkappaB kinase. *Chem. Biol.* 8, 759–766. doi: 10.1016/S1074-5521(01)00049-7

Li, S., Zhou, S., Yang, W., and Meng, D. (2018). Gastro-protective effect of edible plant Artemisia argyi in ethanol-induced rats via normalizing inflammatory responses and oxidative stress. *J. Ethnopharmacol.* 214, 207–217. doi: 10.1016/j.jep.2017.12.023

Lyss, G., Schmidt, T. J., Merfort, I., and Pahl, H. L. (1997). Helenalin, an anti-inflammatory sesquiterpene lactone from Arnica, selectively inhibits transcription factor NF-kappaB. *Biol. Chem.* 378, 951–961. doi: 10.1515/bchm.1997.378.9.951

Malek, T. R. (2008). The Biology of Interleukin-2. *Annu. Rev. Immunol.* 26, 453–479. doi: 10.1146/annurev.immunol.26.021607.090357

Moroncini, G., Calogera, G., Benfaremo, D., and Gabrielli, A. (2017). Biologics in Inflammatory Immune-mediated Systemic Diseases. *Curr. Pharm. Biotechnol.* 18, 1008–1016. doi: 10.2174/1389201019666171226152448

Myers, D. R., Wheeler, B., and Roose, J. P. (2019). mTOR and other effector kinase signals that impact T cell function and activity. *Immunol. Rev.* 291, 134–153. doi: 10.1111/imr.12796

Newman, D. J., and Cragg, G. M. (2016). Natural Products as Sources of New Drugs from 1981 to 2014. *J. Nat. Prod.* 79, 629–661. doi: 10.1021/acs.jnatprod.5b01055

Parish, C. R., Glidden, M. H., Quah, B. J. C., and Warren, H. S. (2009). "Use of the Intracellular Fluorescent Dye CFSE to Monitor Lymphocyte Migration and Proliferation," in *Current Protocols in Immunology*. Eds. J. E. Coligan, B. E. Bierer, D. H. Margulies, E. M. Shevach and W. Strober (Hoboken, NJ, USA: John Wiley & Sons, Inc.). doi: 10.1002/0471142735.im0409s84

Ramamoorthy, S., and Cidlowski, J. A. (2016). Corticosteroids-Mechanisms of Action in Health and Disease. *Rheumatol. Dis. Clin. North Am.* 42, 15–31. doi: 10.1016/j.rdc.2015.08.002

Ratzinger, F., Haslacher, H., Poeppl, W., Hoermann, G., Kovarik, J. J., Jutz, S., et al. (2014). Azithromycin suppresses CD4(+) T-cell activation by direct modulation of mTOR activity. *Sci. Rep.* 4, 7438. doi: 10.1038/srep07438

Reinhardt, J. K., Klemd, A. M., Danton, O., De Mieri, M., Smieško, M., Huber, R., et al. (2019). Sesquiterpene Lactones from Artemisia argyi: Absolute Configuration and Immunosuppressant Activity. *J. Nat. Prod.* 82, 1424–1433. doi: 10.1021/acs.jnatprod.8b00791

Robert, V., Triffaux, E., Savignac, M., and Pelletier, L. (2011). Calcium signalling in T-lymphocytes. *Biochimie* 93, 2087–2094. doi: 10.1016/j.biochi.2011.06.016

Shin, N.-R., Ryu, H.-W., Ko, J.-W., Park, S.-H., Yuk, H.-J., Kim, H.-J., et al. (2017). Artemisia argyi attenuates airway inflammation in ovalbumin-induced asthmatic animals. *J. Ethnopharmacol.* 209, 108–115. doi: 10.1016/j.jep.2017.07.033

Srikanth, S., Woo, J. S., Sun, Z., and Gwack, Y. (2017). Immunological Disorders: Regulation of Ca2+ Signaling in T Lymphocytes. *Adv. Exp. Med. Biol.* 993, 397–424. doi: 10.1007/978-3-319-57732-6_21

Sun, Z. (2012). Intervention of PKC-θ as an immunosuppressive regimen. *Front. Immunol.* 3, 225. doi: 10.3389/fimmu.2012.00225

Tedesco, D., and Haragsim, L. (2012). Cyclosporine: A review. *J. Transplant.* doi: 10.1155/2012/230386

van der Laan, S., and Meijer, O. C. (2008). Pharmacology of glucocorticoids: Beyond receptors. *Eur. J. Pharmacol.* 585, 483–491. doi: 10.1016/j.ejphar.2008.01.060

Wagner, U. (2019). Biologika in der Rheumatologie. *Internist* 60, 1036–1042. doi: 10.1007/s00108-019-00676-0

Wang, L., Wang, F.-S., and Gershwin, M. E. (2015). Human autoimmune diseases: a comprehensive update. *J. Intern. Med.* 278, 369–395. doi: 10.1111/joim.12395

Wang, Q., Jiang, H., Li, Y., Chen, W., Li, H., Peng, K., et al. (2017). Targeting NF-kB signaling with polymeric hybrid micelles that co-deliver siRNA and dexamethasone for arthritis therapy. *Biomaterials* 122, 10–22. doi: 10.1016/j.biomaterials.2017.01.008

Wiseman, A. C. (2016). Immunosuppressive Medications. *Clin. J. Am. Soc Nephrol.* 11, 332–343. doi: 10.2215/CJN.08570814

Wu, P., Su, M.-X., Wang, Y., Wang, G.-C., Ye, W.-C., Chung, H.-Y., et al. (2012). Supercritical fluid extraction assisted isolation of sesquiterpene lactones with antiproliferative effects from Centipeda minima. *Phytochemistry* 76, 133–140. doi: 10.1016/j.phytochem.2012.01.003

Yun, C., Jung, Y., Chun, W., Yang, B., Ryu, J., Lim, C., et al. (2016). Anti-Inflammatory Effects of Artemisia Leaf Extract in Mice with Contact Dermatitis In Vitro and In Vivo. *Mediators Inflammation* 2016. doi: 10.1155/2016/8027537

Zeng, K.-W., Wang, S., Dong, X., Jiang, Y., and Tu, P.-F. (2014). Sesquiterpene dimer (DSF-52) from Artemisia argyi inhibits microglia-mediated neuroinflammation via suppression of NF-κB, JNK/p38 MAPKs and Jak2/Stat3 signaling pathways. *Phytomedicine* 21, 298–306. doi: 10.1016/j.phymed.2013.08.016

Zimmermann-Klemd, A. M., Konradi, V., Steinborn, C., Ücker, A., Palanga, C. M., Woelfle, U., et al. (2019). Influence of traditionally used Nepalese plants on wound healing and immunological properties using primary human cells in vitro. *J. Ethnopharmacol.* 235, 415–423. doi: 10.1016/j.jep.2019.02.034

Conflict of Interest: The authors declare that the research was conducted in the absence of any commercial or financial relationships that could be construed as a potential conflict of interest.

3.3. *Boswellia carteri* extract and 3-O-acetyl-alpha-boswellic acid suppress T cell activation and function

Zimmermann-Klemd, A.M., Reinhardt, J.K., Nilsu, T., Morath, A., Falanga, C.M., Schamel, W.W., Huber, R., Hamburger, M., Gründemann, C., 2020. Boswellia carteri extract and 3-O-acetyl-alpha-boswellic acid suppress T cell function. Fitoterapia 146, 104694.

The resin of the *Boswellia* species has been traditionally used to treat several disorders including inflammatory diseases. This work addresses anti-inflammatory effects of a *Boswellia carteri* DCM extract on human T lymphocytes. *B. carteri* inhibits the cell division of stimulated T cells, based on a suppression of IL-2. Furthermore, the *B. carteri* extract lowered the production of IFN-γ and suppressed the degranulation capacity of stimulated T cells. HPLC-based activity profiling resulted in the identification of active compounds. A concentration-dependent inhibition of the NFAT activity, reflected by an IC_{50} of 5.6 µM, was detected for 3-O-acetyl-alpha-boswellic acid.

My contribution: I performed all experiments, except the IFN-γ and IL-2 Legendplex experiments, as well as the compound elucidation and isolation experiments. I analyzed the data of all bioassays, calculated the statistics for all bioassays, prepared the figures all bioassays, and wrote the draft manuscript.

Amy Marisa Zimmermann-Klemd

Fitoterapia 146 (2020) 104694

Contents lists available at ScienceDirect

Fitoterapia

journal homepage: www.elsevier.com/locate/fitote

Boswellia carteri extract and 3-*O*-acetyl-alpha-boswellic acid suppress T cell function

Amy M. Zimmermann-Klemd[a,1], Jakob K. Reinhardt[b,1], Thanasan Nilsu[c], Anna Morath[d,e,f,g], Chiara M. Falanga[a], Wolfgang W. Schamel[d,e,g], Roman Huber[a], Matthias Hamburger[b], Carsten Gründemann[h,*]

[a] Center for Complementary Medicine, Institute for Infection Prevention and Hospital Epidemiology, Faculty of Medicine, University of Freiburg, Freiburg, Germany
[b] Pharmaceutical Biology, Pharmacenter, University of Basel, Basel, Switzerland
[c] Kamnoetvidya Science Academy, Wang Chan, Rayong, Thailand
[d] Signalling Research Centres BIOSS and CIBSS, University of Freiburg, Freiburg, Germany
[e] Institute of Biology III, Faculty of Biology, University of Freiburg, Freiburg, Germany
[f] Spemann Graduate School of Biology and Medicine, University of Freiburg, Freiburg, Germany
[g] Center for Chronic Immunodeficiency, Medical Center Freiburg and Faculty of Medicine, University of Freiburg, Freiburg, Germany
[h] Translational Complementary Medicine, Department of Pharmaceutical Sciences, University of Basel, Basel, Switzerland

ARTICLE INFO

Keywords:
Boswellia
Immunosuppression
Interleukin-2
NFAT
T cell signaling
3-*O*-acetyl-α-boswellic acid

ABSTRACT

Resins from various *Boswellia* species have a long track record in different cultures as a treatment for inflammatory diseases. This study was designed to provide evidence for the anti-inflammatory capacity and medicinal use of *Boswellia carteri* (Burseraceae). A dichloromethane (DCM) extract of *B. carteri* gum resin and isolated compounds thereof were immunologically characterized. Flow cytometric-based analysis was performed to investigate the impact of *B. carteri* extract on proliferation, viability, and function of anti-CD3 and anti-CD28 activated human primary T cells. The secretion level of IL-2 and IFN-γ was determined by a bead array-based flow cytometric technique. HPLC-based activity profiling of the *B. carteri* extract identified active compounds. The impact of *B. carteri* extract and isolated compounds on the IL-2 transcription factor activity was addressed using specially designed Jurkat reporter cells. The extract of *B. carteri* suppressed the proliferation of human primary T lymphocytes in vitro in a concentration-dependent manner, without inducing cytotoxicity. Thereby, the *B. carteri* extract further reduced the degranulation capacity and cytokine secretion of stimulated human T cells. Transcription factor analysis showed that the immunosuppressive effects of the extract are based on specific NFAT-conditioned suppression within T cell signaling. Through HPLC-based activity profiling of the extract, 3-*O*-acetyl-alpha-boswellic acid was identified as the compound responsible for the NFAT-based mechanism. The recent study presents a scientific base for the immunosuppressive effects of *B. carteri* gum resin extract including a mode-of-action via the NFAT-conditioned suppression of T lymphocyte proliferation. The immunosuppressive effects of 3-*O*-acetyl-alpha-boswellic acid are depicted for the first time.

Abbreviations: AKBA, *o*-acetyl-11-keto-ß-boswellic; AP-1, activator protein 1; APC, allophycocyanin; ASE, accelerated Solvent Extraction; CD, cluster of differentiation; CFSE, carboxyfluorescein succinimidyl ester; CPT, camptothecin; CsA, cyclosporine A; DCM, dichloromethane; DMSO, dimethyl sulfoxide; EDTA, ethylenediaminetetraacetic acid; FA, formic acid; FACS, fluorescence-activated cell sorting; FCS, fetal bovine serum; FITC, fluorescein isothiocyanate; GFP, green fluorescent protein; HPLC, high-performance liquid chromatography; i.d., inner diameter; IFN-, interferon-; IL-, interleukin-; KBA, 1-keto-β-boswellic acid; mAb, monoclonal antibody; NFAT, nuclear factor of activated T-cells; NF-κB, nuclear factor kappa-light-chain-enhancer of activated B cells; p, *p*-value; PBMC, peripheral blood mononuclear cell; PBS, phosphate buffered saline; PE, phycoerythrin; Pen/Strep, penicillin/streptomycin; PI, propidium iodide; PMA, phorbol-12-myristat-13-acetate; RPMI 1640, Roswell Park Memorial Institute medium; SD, standard deviation; TCM, Traditional Chinese Medicine; TCR, T cell receptor

* Corresponding author at: Translational Complementary Medicine, University of Basel, Department of Pharmaceutical Sciences, Klingelbergstrasse 50, CH-4056 Basel, Switzerland.
E-mail address: carsten.gruendemann@unibas.ch (C. Gründemann).
[1] Equally contributed to this work.

https://doi.org/10.1016/j.fitote.2020.104694
Received 25 May 2020; Received in revised form 20 July 2020; Accepted 20 July 2020
Available online 24 July 2020

1. Introduction

The medical use of the *Boswellia* species (Burseraceae) has a long track record in various cultures. The resin of the *Boswellia* species was known as frankincense, or olibanum, and was used for the treatment of various disorders, including inflammatory diseases [1]. In Ayurvedic medicine, the resin of *Boswellia serrata* Roxb. ex Colebr. is used, whereas the resin of *Boswellia sacra* Flueck. (*B. carteri* Birdw.) and other species are employed in traditional Chinese medicine (TCM). *B. serrata* and *B. carteri* resins are complex mixtures of triterpenoids; mono-, sesqui-, and diterpenoids; and polysaccharide gum [2,26].

The anti-inflammatory properties of *Boswellia* resins have already been investigated to a certain extent. For example, cultured, lipopolysaccharide (LPS)-stimulated, peripheral blood monocytes (PBMCs) showed a reduced secretion of tumor necrosis factor α (TNFα), interleukin-1ß (IL-1ß), interleukin-6 (IL-6), and interleukin-8 (IL-8), following treatment with *B. serrata* extract [11,12]. Additionally, the downregulation of Th1 cytokines interferon-γ (IFN-γ) and interleukin-12 (IL-12) and an upregulation of Th2 cytokines interleukin-4 (IL-4) and interleukin-10 (IL-10) were observed upon treatment of PBMCs with *B. serrata* extract [11]. Further in vitro studies using polymorph mononuclear neutrophil leukocytes (PMNLs) confirmed an inhibitory effect of *B. serrata* on mediators of the arachidonic acid cascade [25]. *B. carteri* gum resin is studied less, but in mouse splenocytes a suppression of the Th1 cytokine production, and an enhanced Th2 cytokine production was observed [6].

Previous investigations identified boswellic acids, especially 11-keto-β-boswellic acid (KBA) and *O*-acetyl-11-keto-β-boswellic acid (AKBA), as compounds responsible for the anti-inflammatory properties of *Boswellia* resin [1]. There is evidence that boswellic acids suppress the immune response via inhibition of the NF-κB activity in LPS activated monocytes (Syrovets et al., 2005a), and the immune suppressive effects were confirmed in an autoimmune model for psoriasis in rodents [30].

In autoimmune diseases, the immune cells lose their ability to distinguish between self and nonself structures [31]. This in turn leads to an overreaction of the immune system, including an enhanced proliferation, activation and mediator secretion of T lymphocytes.

We here focus on other, not yet investigated, aspects of *B. carteri* extract with relation to an overwhelming immune system, such as the proliferation, activation, and function of T cells. The results indicate a mode-of-action of *B. carteri* gum resin extract and boswellic acids via NFAT-conditioned immune suppression. 3-*O*-acetyl-alpha-boswellic acid was found to be at least partly responsible for the observed effects on the NFAT activity.

2. Materials and methods

2.1. Ethics statement

All experiments conducted with human material were approved by the Ethics Committee of the University of Freiburg (55/14; 11.02.2014), and all methods used were compliant with the regulations of the Ethics Committee.

2.2. Preparation of B. carteri dichloromethane (DCM) extract

B. carteri gum resin extract was prepared using Accelerated Solvent Extraction (ASE). For this, the ground gum resin of *B. carteri* (Lian Chinaherb AG, Wollerau, Switzerland, Article Nr. 2174, charge M08201004A; a voucher specimen with the number 00969 has been

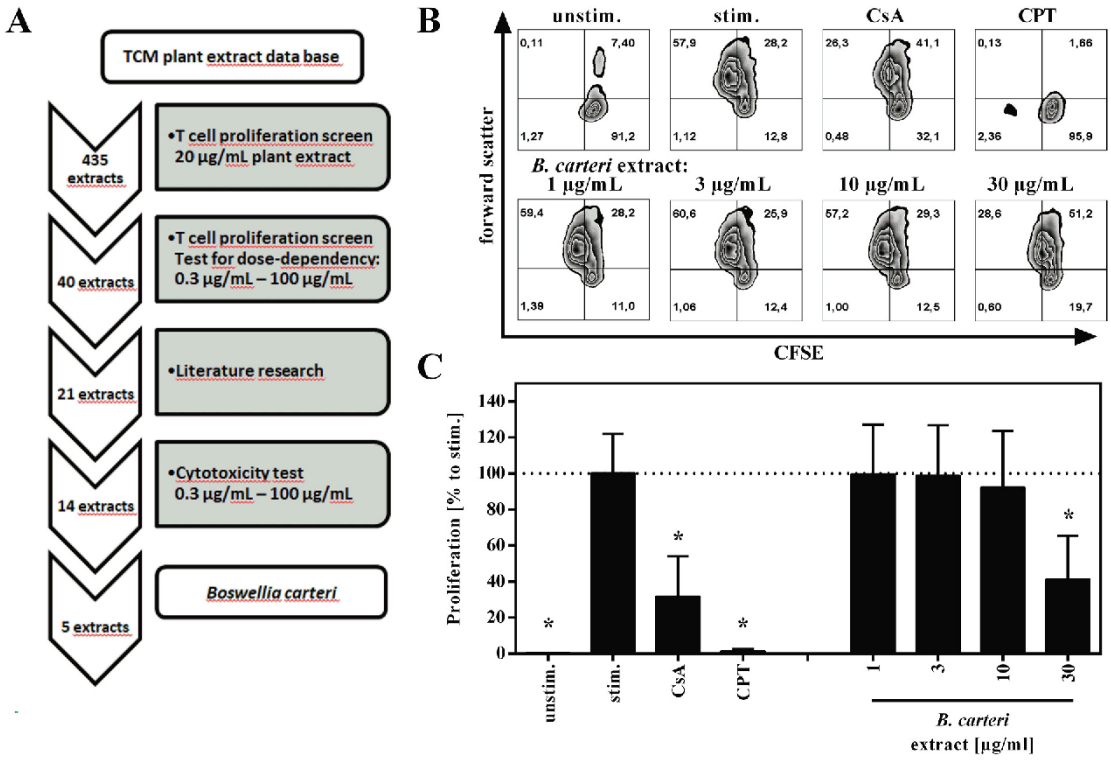

Fig. 1. Inhibitory effects of *B. carteri* extract on the proliferation of T lymphocytes. (A) Flowchart of the screening process. (B, C) Human PBMCs ($2*10^5$) were stained with CFSE and stimulated with anti-CD3 and anti-CD28 mAbs (100 ng/mL each). Unstimulated cells (unstim.) served as a control. Afterwards, anti-CD3 and anti-CD28 activated cells were incubated for 72 h in the presence of medium (stim.), cyclosporine A (CsA; 4.16 µM), camptothecin (CPT; 300 µM), or the *B. carteri* gum resin extract. Cell division was analyzed by flow cytometry. Data are depicted as zebra plots (B). Numbers indicate the percentage of quadrants. The percentage of proliferating cells was compared and normalized to the stimulated control and depicted as mean ± standard deviation (C). $n = 3$; $*p < .05$.

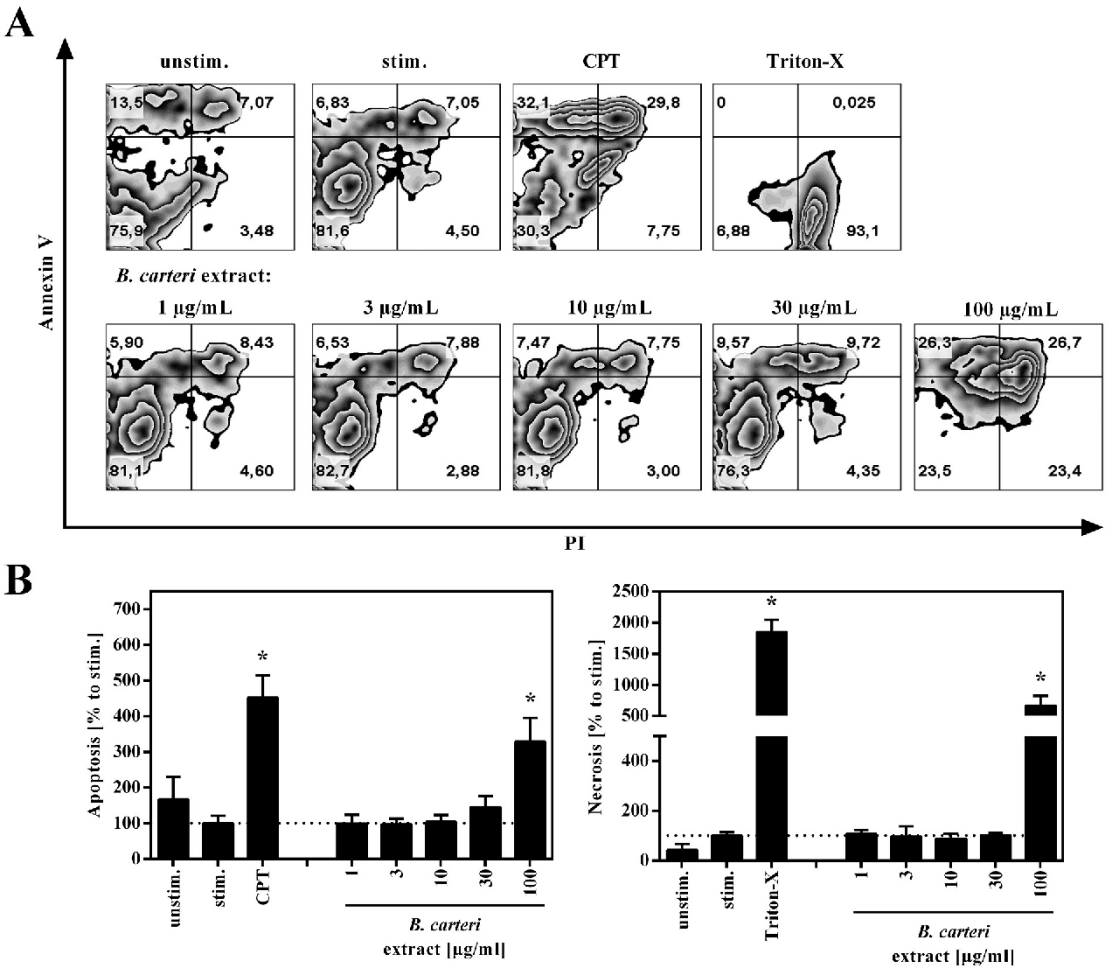

Fig. 2. Effect of *B. carteri* extract on the viability of T lymphocytes. Human PBMCs ($2*10^5$) were stimulated with anti-CD3 and anti-CD28 mAbs antibodies (100 ng/mL each). Unstimulated cells served as a control (unstim.). Afterwards, anti-CD3 and anti-CD28 activated cells were incubated for 48 h with medium (stim.), camptothecin (CPT; 300 µM), Triton-X 100 (0.5%) or *B. carteri* gum resin extract. Annexin V-FITC and PI double staining was performed. The proportions of viable, necrotic and apoptotic cells were analyzed via flow cytometry. Data are depicted as zebra plots (A). Numbers indicate the percentage of quadrants. The amount of apoptotic/necrotic lymphocytes compared to the stimulated control was determined and depicted as mean ± standard deviation (B). $n = 3$; $*p < .05$.

deposited at the Division of Pharmaceutical Biology, University of Basel, Switzerland), was extracted with redistilled, technical grade, dichloromethane (DCM) for three cycles with an ASE 200 extraction system with solvent module (Dionex) at 70 °C and 120 bar. The HPLC profile of the extract is shown in Fig. S1. The extracts from all cycles were combined and dried in vacuo yielding a crude extract with approx. 19% yield.

2.3. Preparation and cultivation of human peripheral lymphocyte

Preparation and cultivation of human peripheral lymphocytes was performed as indicated in [32]. Briefly, lymphocytes were isolated from the blood of healthy adult donors obtained from the Blood Transfusion Centre (Medical Centre – University of Freiburg) via sugar gradient separation and were finally cultured in RPMI 1640 full medium. Lymphocytes were stimulated with anti-CD3- and anti-CD28 mAbs and treated as described in the figure legends and already by our group [32]. After cultivation, the cells were assessed in biological tests as indicated.

2.4. Determination of apoptosis and necrosis of T cells

Cells were treated for 48 h, as described in 2.3. Cultured cells were washed with PBS and stained with Annexin V-FITC and propidium iodide using the Apoptosis Detection kit (eBioscience, Frankfurt, Germany) according to manufacturer's instructions. Apoptosis and necrosis rates were determined by flow cytometric analysis using a FACS analysis. Cell populations were described as follows: viable (annexinV^-/PI^-), early (annexinV^+/PI^-) and late apoptotic (annexinV^+/PI^+) and necrotic (annexinV^-/PI^+). In graphs, early and late apoptotic cells were summarized as apoptotic cells.

2.5. Determination of T cell proliferation

The proliferation of T lymphocytes was determined via carboxyfluorescein diacetate succinimidyl ester (CFSE) staining, as described earlier [13,21].

2.6. Analysis of activation marker of T cells

The activation state of T lymphocytes was determined via cell surface analysis of CD25 and CD69, as as previously reported [14].

2.7. Determination of cytokines

Cells were treated for 20 h, as described in 2.3, and restimulated

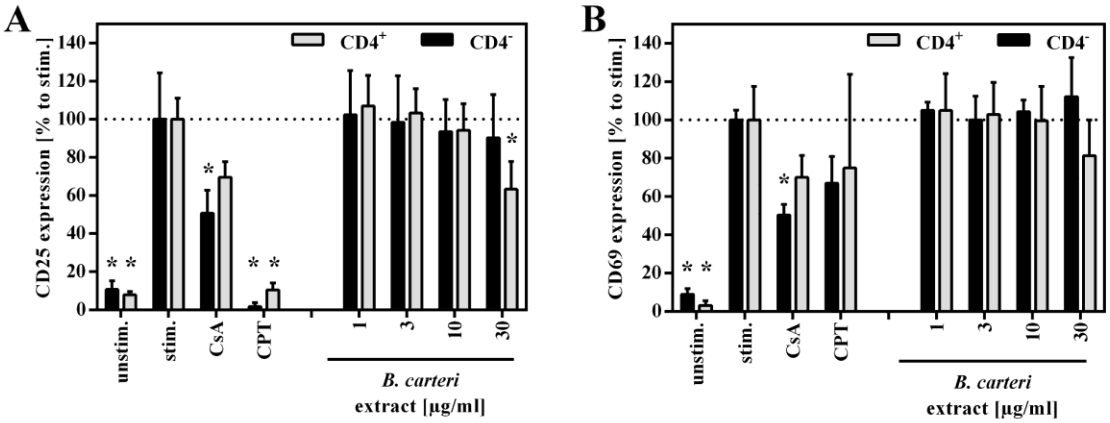

Fig. 3. Effects of *B. carteri* extract on the activation of T cells. Human PBMCs ($2*10^5$) were left unstimulated (unstim.), or stimulated with anti-CD3 and anti-CD28 mAbs (100 ng/mL each). Afterwards, anti-CD3 and anti-CD28 activated cells were incubated for 24 h with or without (stim.) the addition of cyclosporine A (CsA; 4.16 µM), camptothecin (CPT; 300 µM), or the *B. carteri* gum resin extract. Cells were stained with anti-CD25-PE (A) or anti-CD69-FITC (B) and anti-CD4-APC and analyzed by flow cytometry. Bar diagrams depict the percentage of $CD4^+$ and $CD4^-$ T lymphocytes that express CD25 or CD69 in relation to the untreated, stimulated control ± standard deviation. n = 3; *p < .05.

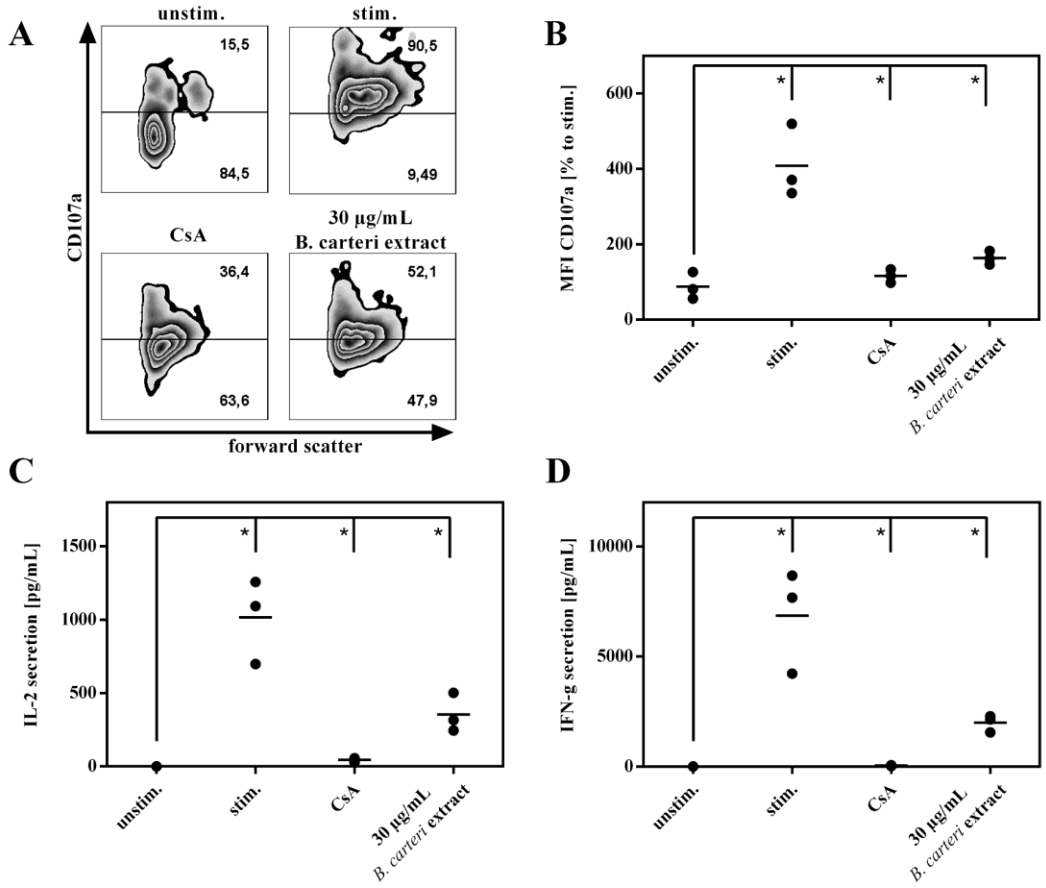

Fig. 4. Effects of *B. carteri* extract on the degranulation capacity of T lymphocytes and on IL-2 and IFN-γ secretion. Human PBMCs ($2*10^5$) were stimulated with anti-human CD3 and anti-human CD28 mAbs (100 ng/mL each) or left unstimulated (unstim.). Anti-CD3 and anti-CD28 activated cells were incubated for 20 h with medium (stim.), cyclosporine A (CsA; 4.16 µM) or *B. carteri* gum resin extract. Cells (except the unstim. control) were re-stimulated with PMA (50 ng/mL) and ionomycin (500 ng/mL) for 4 h. (A, B) Cells were stained with CD107a-PE, and CD107a surface expression was determined via flow cytometry. Data are depicted in zebra plots (A). The mean fluorescence intensity (MFI) of CD107a was determined and is depicted in relation to the stimulated control (B). n = 3, *p < .05. (C, D) The amounts of IL-2 (C) and IFN-γ (D) were determined in the supernatant by LEGENDplex™. Results are depicted as mean ± standard deviation in relation to the untreated, stimulated control. n = 3; *p < .05.

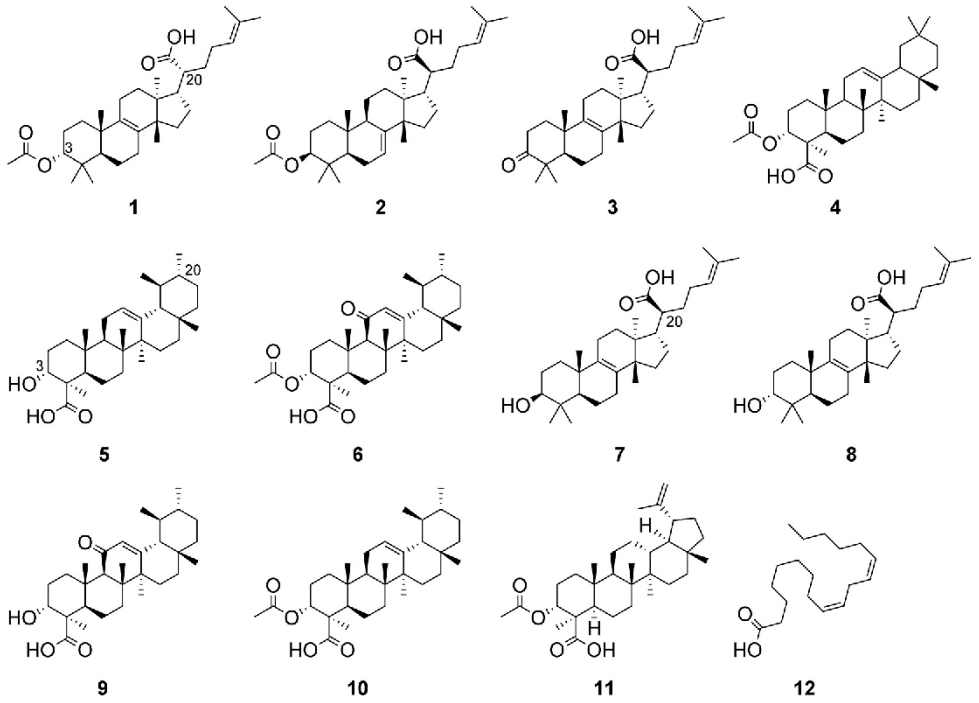

Fig. 5. Isolated compounds **1–12**.

with PMA (50 ng/mL; Sigma-Aldrich, Taufkirchen, Germany) and ionomycin (500 ng/mL; Sigma-Aldrich, Taufkirchen, Germany) for additional 4 h at 37 °C. Supernatants were harvested by centrifugation and stored at −20 °C. The amount of cytokines was determined using LEGENDplex™ according to the manufacturer's instructions (BioLegend, San Diego, CA).

2.8. Analysis of T cell degranulation

A CD107a surface staining was performed, as described [15], to determine the T cell degranulation capacity.

2.9. Reporter cell experiments for the determination of NFAT-, NF-κB- and AP-1 activity

A 96 well F-bottom cell culture plate was coated with anti-human CD3 monoclonal antibodies (mAbs) (clone OKT3, 1 μg/mL, 50 μL/well) or phosphate buffered saline (unstim.). Here we used individual designed human Jurkat T cell reporter cells, where the response elements for NF-κB, NFAT and AP-1 drive the expression of each fluorescent proteins (CFP, eGFP and mCherry, respectively. Reporter cells [17] were seeded in 5% FCS RPMI 1640 cell culture medium ($0.15*10^6$ cells in 200 μL/ well) and treated with inhibitors (1 nM SP100030 for AP-1, 5 μg/mL cyclosporine A for NFAT and 20 μM parthenolide for NF-κB), gum resin extract or isolated compounds from *B. carteri* or remained untreated (unstim., stim.). Cells were incubated at 37 °C for 8 h (AP-1) or 24 h (NFAT and NF-κB). The expression of eGFP was determined by FACS analysis.

2.10. Isolation and identification of compounds 1–12

Extraction and isolation of compounds **1–12** from *B. carteri* gum resin DCM extract is described in detail in the supplementary information. NMR data were recorded on a Bruker Avance II NMR spectrometer operating at 500.13 MHz for ^{1}H and 125.77 MHz for ^{13}C nuclei. ^{1}H NMR data and COSY, HSQC, HMBC, and ROESY spectra were measured at 18 °C in a 1 mm TXI probe with a z-gradient. ^{13}C NMR/DEPTQ spectra were recorded at 23 °C in 3 mm tubes with a 5 mm BBI probe. Spectra were analyzed by Bruker TopSpin 3.0 and ACDLabs Spectrus Processor. Samples were measured in $CDCl_3$ (Sigma-Aldrich).

2.11. Analysis of data

For statistical analysis, data was processed with Microsoft Excel and SPSS software (Version 22.0, IBM, Armonk, USA). Statistical significance was determined with the SPSS software by a one-way ANOVA followed by Dunnett's post hoc pairwise comparisons. Values are presented as mean ± standard deviation (SD) for the indicated number of independent experiments. The asterisks represent significant differences from controls (*$p < .05$).

3. Results and discussion

3.1. Effects of B. carteri extract on the proliferation capacity of activated human T lymphocytes

Autoimmune diseases are characterized by an overwhelming immune system with an enhanced proliferation of T cells. In a search for extracts and natural products that might suppress the proliferation of physiological (anti-CD3 and anti-CD28) activated human T lymphocytes, we screened a library of 435 extracts from plants used in TCM (Fig. 1A). An initial screening of extracts was performed at a concentration of 20 μg/mL, and active extracts were then tested in a concentration range of 0.3–100 μg/mL using cell division analysis. A shortlist of promising candidate extracts was established based on a literature search and the testing of extracts for the absence of cytotoxicity. A DCM extract of *B. carteri* gum resin inhibited the proliferation of activated T lymphocytes in a concentration-dependent manner (IC_{50} of 27 μg/mL) (Fig. 1B and C), without inducing cytotoxicity. These results are in line with previous findings where a concentration-dependent proliferation inhibition of stimulated murine spleen cells from non-immunized mice was reported [27].

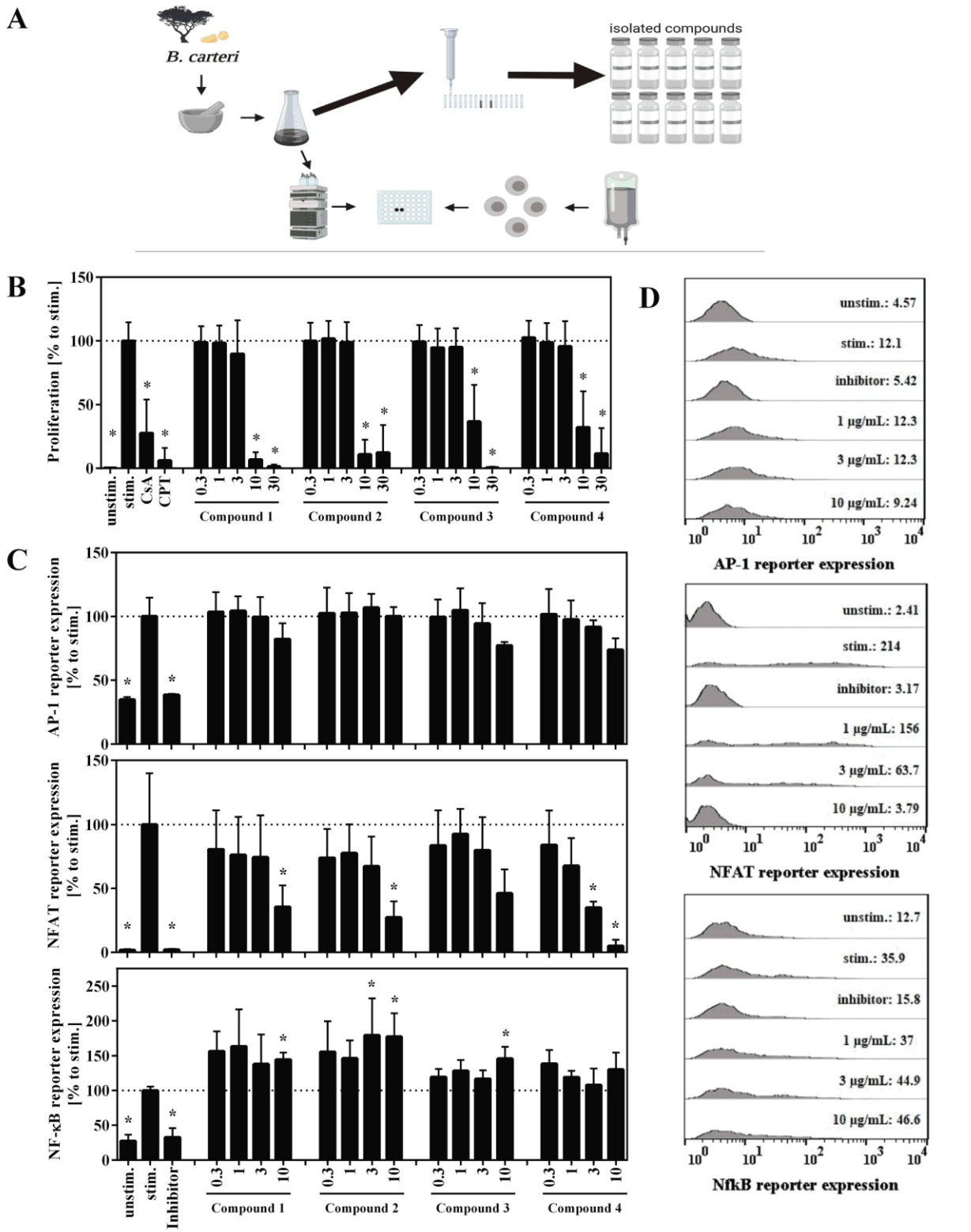

(caption on next page)

Fig. 6. Effects of *B. carteri* boswellic acids on T cell proliferation and *il-2* gene transcription factor induction. (A) Schematic overview of the HPLC-based activity profiling process. (B) Human PBMCs ($2*10^5$) were stained with CFSE, and stimulated with anti-CD3 and anti-CD28 mAbs (100 ng/mL each). One control remained unstimulated (unstim.). Afterwards, anti-CD3 and anti-CD28 activated cells were incubated for 72 h with medium (stim.), cyclosporine A (CsA; 4.16 μM), camptothecin (CPT; 300 μM), or compounds isolated from *B. carteri*. Cell division rate was determined via flow cytometric analysis. Data are depicted as mean ± standard deviation. n = 3, *p < .05. (C, D) Jurkat reporter cells ($0.15*10^6$) were seeded on an anti-CD3-coated cell culture plate and incubated with medium, inhibitors (AP-1: 1 nM SP100030, NFAT: 4.16 μM CsA, NF-κB: 20 μM parthenolide) or *B. carteri* compounds for 8 (AP-1) or 24 h (NFAT, NF-κB). After incubation GFP expression was quantified by flow cytometry. The percentage of cells was compared and normalized to the stimulated control and depicted as mean ± standard deviation (C). n = 3, *p < .05. Data are depicted as histogram plots of controls and indicated concentrations of 4 (D). Numbers indicate the MFI of the reporter expression.

3.2. Effects of the B. carteri extract on the induction of apoptosis and necrosis in human T lymphocytes

To evaluate whether the observed immunosuppressive activity of the extract was not due to general cytotoxicity, we determined the non-toxic concentration. Annexin V and PI double stainings were performed to detect the apoptosis and necrosis rates of cells. Only at the highest extract concentration of 100 μg/mL were apoptosis and necrosis observed, while concentrations of 30 μg/mL and lower were not harmful (Fig. 2A and B). For further mechanistic studies concentrations non-toxic concentrations were used.

3.3. Effects of the B. carteri extract on the upregulation of activation markers by activated human T lymphocytes

Following TCR stimulation, T cells become activated and thereby express the activation markers CD25 and CD69 on their surface. Hence, phenotyping of the cell surface using fluorescence-coupled antibodies against CD25 and CD69 allows quantifying their activation state via flow cytometry. The results did not point to an influence of *B. carteri* gum resin extract on the activation state of T cells (Fig. 3A and B). Solely the CD25 expression of $CD4^+$ T cells was slightly reduced after treatment with 30 μg/mL of extract (Fig. 3A).

3.4. Effects of the B. carteri extract on the degranulation and cytokine production of activated human T lymphocytes

Next, we analyzed whether the extract affected T lymphocyte function, in particular the release of perforin and granzymes. Therefore, analysis of the lysosomal-associated membrane protein 1 (LAMP-1, CD107a) showed a significantly reduced degranulation of activated T cells after treatment with 30 μg/mL of extract (Fig. 4A and B). The secretion of the pro-inflammatory cytokines, interleukin-2 (IL-2), and IFN-γ upon T cell receptor (TCR) stimulation is an important function of T cells. The treatment of stimulated T lymphocytes with 30 μg/mL of extract significantly lowered the secretion of IL-2 and IFN-γ (Fig. 4C and D). Our data corroborate earlier findings of a concentration-dependent inhibition of IL-2 and IFN-γ production of murine splenocytes by a *B. carteri* gum resin extract [6]. The inhibition of IL-2 production in turn leads to an inhibition of the proliferation and differentiation of T lymphocytes [24].

3.5. Isolated compounds

Plant extracts consist of a complex mixture of compounds. Compounds **1**–**12** (Fig. 5) were identified by fractionation of the extract of *B. carteri* gum resin guided by activity testing (Fig. 6A) [22]. The extraction of the compounds is described in the supplementary information. The triterpenes were identified by comparison with reported NMR data as 3-*O*-acetyl-8,24-dienetirucallic acid (**1**) [18], 3-*O*-acetyl-7,24-dienetirucallic acid (**2**) [29], 3-oxo-8,24-dienetirucallic acid (**3**) [29], 3-*O*-acetyl-α-boswellic acid (**4**) [4], β-boswellic acid (**5**) [8], 3-*O*-acetyl-11-keto-β-boswellic acid (**6**) [7], 3-β-8,24-dienetirucallic acid (**7**) [33], 3-α-8,24-dienetirucallic acid (**8**) [34], 11-keto-β-boswellic acid (**9**) [16], 3-*O*-acetyl-β-boswellic acid (**10**) [4], 3-acetyl-20(29)-lupene-24-oic acid (**11**) [3], and linoleic acid (**12**) [19]. Of these, compounds **1**–**4** suppressed the proliferation of stimulated T lymphocytes in a defined concentration range of 10–30 μg/mL (Fig. 6B). In case of compound **2**, the activity was not certain as ca. 30% of unknown impurities were present. With respect to antiproliferative activity, **9** (KBA) and **6** (AKBA) have been predominantly investigated previously [1]. Interestingly, **6** was inactive in this assay at the test concentrations used, and **9** inhibited T cell proliferation via an induction of apoptosis (Fig. S2).

3.6. Impact of B. carteri compounds on the transcription factors AP-1, NFAT, and NF-κB

To better understand the mode of action by which the triterpenoids exert their immunosuppressive activity, their effect on T cell signaling was investigated, specifically on the transcription factors of the *il-2* gene, activator protein 1 (AP-1), the nuclear factor of activated T cells (NFAT), and the nuclear factor kappa-light-chain-enhancer of activated B cells (NF-κB). These transcription factors bind to the *il-2* gene and enable the transcription and secretion of IL-2 [20]. IL-2 is crucial for the immune response and can be linked to immune overreactions because it autocrinely stimulates T cell proliferation. We used reporter cell lines [17,23] to investigate the effects on the *il-2* transcription factors. No inhibitory effect of the compounds on AP-1 or NF-κB activity was observed (Fig. 6C and D). However, the NFAT activity was significantly and concentration-dependently suppressed by compound **4**, with an IC_{50} of 5.6 μM (2.8 μg/mL). The compound also showed a comparable IC_{50} of 17.9 μM (8.9 μg/mL) for T cell proliferation inhibition (Fig. 6B) and is thus of interest for further investigation. The inhibition of NFAT activity by a boswellic acid is here reported for the first time, but has been described for other triterpenes [9,10].

Compound **6** has been previously shown to reduce the NF-κB activity in activated monocytes via inhibition of IκB kinase activity [28]. In vivo studies using a psoriasis mouse model confirmed the suppression by **6** of NF-κB in macrophages [30]. In contrast to **6**, **4** did not inhibit the NF-κB activity. The major structural difference between **6** and **4** is the presence of an 11-keto group in **6** which constitutes a polar moiety in an otherwise rather lipophilic structure, and enables hydrogen bond formation. This may play a role for a differential interaction with proteins leading to different bioactivity.

4. Conclusion

Our study demonstrates that a lipophilic extract of *B. carteri* gum resin inhibited the proliferation, degranulation capacity and secretion of inflammatory mediators of physiologically relevant anti-CD3 and anti-CD28 activated human T lymphocytes in a non-toxic concentration range. In an activity-guided isolation approach eleven triterpenoids and linoleic acid were isolated, whereby 3-*O*-acetyl-alpha-boswellic acid (**4**) suppressed NFAT activity in a significant and concentration-dependent manner.

Acknowledgments

Gefördert durch die Deutsche Forschungsgemeinschaft (DFG) im Rahmen der Exzellenzstrategie des Bundes und der Länder – EXC – 2189 – Projektnummer 390939984. (Funded by the Deutsche

Forschungsgemeinschaft (DFG, German Research Foundation) under Germany's Excellence strategy – EXC – 2189 – Project ID: 390939984.), and by a PRIAM-based consortium of foundations. Jurkat reporter cell lines were kindly provided by Peter Steinberger, Medical Univerity Vienna. The excellent technical assistance of Kerstin Fehrenbach und Orlando Fertig is gratefully acknowledged.

Declaration of Competing Interest

The authors declare no competing interests.

Appendix A. Supplementary data

Supplementary data to this article can be found online at https://doi.org/10.1016/j.fitote.2020.104694.

References

[1] H.P.T. Ammon, Boswellic extracts and 11-keto-ß-boswellic acids prevent type 1 and type 2 diabetes mellitus by suppressing the expression of proinflammatory cytokines, Phytomedicine 63 (2019) 153002, https://doi.org/10.1016/j.phymed.2019.153002.

[2] S. Basar, Phytochemical Investigations on Boswellia Species, https://ediss.sub.uni-hamburg.de/, (2005).

[3] K. Belsner, B. Büchele, U. Werz, T. Simmet, Structural analysis of 3-α-acetyl-20(29)-lupene-24-oic acid, a novel pentacyclic triterpene isolated from the gum resin of Boswellia serrata, by NMR spectroscopy, Magn. Reson. Chem. 41 (2003) 629–632, https://doi.org/10.1002/mrc.1212.

[4] K. Belsner, B. Büchele, U. Werz, T. Syrovets, T. Simmet, Structural analysis of pentacyclic triterpenes from the gum resin of Boswellia serrata by NMR spectroscopy, Magn. Reson. Chem. 41 (2003) 115–122, https://doi.org/10.1002/mrc.1138.

[6] M.R. Chevrier, A.E. Ryan, D.Y.-W. Lee, M. Zhongze, Z. Wu-Yan, C.S. Via, Boswellia carterii extract inhibits TH1 cytokines and promotes TH2 cytokines in vitro, Clin. Diagn. Lab. Immunol. 12 (2005) 575–580, https://doi.org/10.1128/CDLI.12.5.575-580.2005.

[7] R. Csuk, A. Barthel-Niesen, D. Ströhl, R. Kluge, C. Wagner, A. Al-Harrasi, Oxidative and reductive transformations of 11-keto-β-boswellic acid, Tetrahedron 71 (13) (2015) 2025–2034.

[8] G. Culioli, C. Mathe, P. Archier, C. Vieillescazes, A Lupane triterpene from frankincense (Boswellia sp., Burseraceae), Phytochemistry 62 (2003) 537–541, https://doi.org/10.1016/s0031-9422(02)00538-1.

[9] N.T. Dat, I.S. Lee, X.F. Cai, G. Shen, Y.H. Kim, Oleanane triterpenoids with inhibitory activity against NFAT transcription factor from Liquidambar formosana, Biol. Pharm. Bull. 27 (2004) 426–428, https://doi.org/10.1248/bpb.27.426.

[10] J.M. Escandell, M.C. Recio, S. Máñez, R.M. Giner, M. Cerdá-Nicolás, R. Gil-Benso, J.-L. Ríos, Dihydrocucurbitacin B inhibits delayed type hypersensitivity reactions by suppressing lymphocyte proliferation, J. Pharmacol. Exp. Ther. 322 (2007) 1261–1268, https://doi.org/10.1124/jpet.107.122671.

[11] B. Gayathri, N. Manjula, K.S. Vinaykumar, B.S. Lakshmi, A. Balakrishnan, Pure compound from Boswellia serrata extract exhibits anti-inflammatory property in human PBMCs and mouse macrophages through inhibition of TNFα, IL-1β, NO and MAP kinases, Int. Immunopharmacol. 7 (2007) 473–482, https://doi.org/10.1016/j.intimp.2006.12.003.

[12] P. Governa, M. Marchi, V. Cocetta, B. De Leo, P. Saunders, D. Catanzaro, E. Miraldi, M. Montopoli, M. Biagi, Effects of Boswellia Serrata Roxb. And Curcuma longa L. in an in vitro intestinal inflammation model using immune cells and Caco-2, Pharmaceuticals 11 (2018) 126, https://doi.org/10.3390/ph11040126.

[13] C. Gründemann, J. Koehbach, R. Huber, C.W. Gruber, Do plant cyclotides have potential as immunosuppressant peptides? J. Nat. Prod. 75 (2012) 167–174, https://doi.org/10.1021/np200722w.

[14] C. Gründemann, K. Lengen, B. Sauer, M. Garcia-Käufer, M. Zehl, R. Huber, Equisetum arvense (common horsetail) modulates the function of inflammatory immunocompetent cells, BMC Complement. Altern. Med. 14 (2014) 283, https://doi.org/10.1186/1472-6882-14-283.

[15] C. Gründemann, K. Thell, K. Lengen, M. Garcia-Käufer, Y.-H. Huang, R. Huber, D.J. Craik, G. Schabbauer, C.W. Gruber, Cyclotides suppress human T-lymphocyte proliferation by an interleukin 2-dependent mechanism, PLoS One 8 (2013) e68016, , https://doi.org/10.1371/journal.pone.0068016.

[16] J. Jauch, J. Bergmann, An efficient method for the large-scale preparation of 3-O-Acetyl-11-oxo-β-boswellic acid and other Boswellic acids, Eur. J. Org. Chem. 2003 (2003) 4752–4756, https://doi.org/10.1002/ejoc.200300386.

[17] S. Jutz, J. Leitner, K. Schmetterer, I. Doel-Perez, O. Majdic, K. Grabmeier-Pfistershammer, W. Paster, J.B. Huppa, P. Steinberger, Assessment of costimulation and coinhibition in a triple parameter T cell reporter line: simultaneous measurement of NF-κB, NFAT and AP-1, J. Immunol. Methods 430 (2016) 10–20, https://doi.org/10.1016/j.jim.2016.01.007.

[18] C.-N. Lin, Y.-F. Fann, M.-I. Chung, Steroids of formosan Ganoderma tsugae, Phytochemistry 46 (1997) 1143–1146, https://doi.org/10.1016/S0031-9422(97)00387-7.

[19] R.G. Marwah, M.O. Fatope, M.L. Deadman, Y.M. Al-Maqbali, J. Husband, Musanahol: a new aureonitol-related metabolite from a Chaetomium sp, Tetrahedron 63 (2007) 8174–8180, https://doi.org/10.1016/j.tet.2007.05.119.

[20] D.R. Myers, B. Wheeler, J.P. Roose, mTOR and other effector kinase signals that impact T cell function and activity, Immunol. Rev. 291 (2019) 134–153, https://doi.org/10.1111/imr.12796.

[21] C.R. Parish, M.H. Glidden, B.J.C. Quah, H.S. Warren, Use of the intracellular fluorescent dye CFSE to monitor lymphocyte migration and proliferation, in: J.E. Coligan, B.E. Bierer, D.H. Margulies, E.M. Shevach, W. Strober (Eds.), Current Protocols in Immunology, John Wiley & Sons, Inc., Hoboken, NJ, USA, 2009, , https://doi.org/10.1002/0471142735.im0409s84.

[22] O. Potterat, M. Hamburger, Combined use of extract libraries and HPLC-based activity profiling for Lead discovery: potential, challenges, and practical considerations, Planta Med. 80 (2014) 1171–1181, https://doi.org/10.1055/s-0034-1382900.

[23] F. Ratzinger, H. Haslacher, W. Poeppl, G. Hoermann, J.J. Kovarik, S. Jutz, P. Steinberger, H. Burgmann, W.F. Pickl, K.G. Schmetterer, Azithromycin suppresses CD4(+) T-cell activation by direct modulation of mTOR activity, Sci. Rep. 4 (2014) 7438, https://doi.org/10.1038/srep07438.

[24] S.H. Ross, D.A. Cantrell, Signaling and function of Interleukin-2 in T lymphocytes, Annu. Rev. Immunol. 36 (2018) 411–433, https://doi.org/10.1146/annurev-immunol-042617-053352.

[25] H. Safayhi, S.E. Boden, S. Schweizer, H.P. Ammon, Concentration-dependent potentiating and inhibitory effects of Boswellia extracts on 5-lipoxygenase product formation in stimulated PMNL, Planta Med. 66 (2000) 110–113, https://doi.org/10.1055/s-2000-11136.

[26] S. Seitz, Isolierung und Strukturaufklärung von entzündungshemmenden Inhaltsstoffen aus Weihrauchharz, https://publikationen.sulb.uni-saarland.de, (2008).

[27] M.L. Sharma, A. Kaul, A. Khajuria, S. Singh, G.B. Singh, Immunomodulatory activity of Boswellic acids (Pentacyclic triterpene acids) from Boswellia serrata, Phytother. Res. 10 (1996) 107–112, https://doi.org/10.1002/(SICI)1099-1573(199603)10:2<107::AID-PTR780>3.0.CO;2-3.

[28] T. Syrovets, B. Büchele, C. Krauss, Y. Laumonnier, T. Simmet, Acetyl-Boswellic acids inhibit lipopolysaccharide-mediated TNF-α induction in monocytes by direct interaction with IκB kinases, J. Immunol. 174 (2005) 498–506, https://doi.org/10.4049/jimmunol.174.1.498.

[29] M. Verhoff, S. Seitz, M. Paul, S.M. Noha, J. Jauch, D. Schuster, O. Werz, Tetra- and pentacyclic triterpene acids from the ancient anti-inflammatory remedy frankincense as inhibitors of microsomal prostaglandin E(2) synthase-1, J. Nat. Prod. 77 (2014) 1445–1451, https://doi.org/10.1021/np500198g.

[30] H. Wang, T. Syrovets, D. Kess, B. Büchele, H. Hainzl, O. Lunov, J.M. Weiss, K. Scharffetter-Kochanek, T. Simmet, Targeting NF-κB with a natural triterpenoid alleviates skin inflammation in a mouse model of psoriasis, J. Immunol. 183 (2009) 4755–4763, https://doi.org/10.4049/jimmunol.0900521.

[31] L. Wang, F.-S. Wang, M.E. Gershwin, Human autoimmune diseases: a comprehensive update, J. Intern. Med. 278 (2015) 369–395, https://doi.org/10.1111/joim.12395.

[32] A.M. Zimmermann-Klemd, V. Konradi, C. Steinborn, A. Ücker, C.M. Falanga, U. Woelfle, R. Huber, G. Jürgenliemk, M. Rajbhandari, C. Gründemann, Influence of traditionally used Nepalese plants on wound healing and immunological properties using primary human cells in vitro, J. Ethnopharmacol. 235 (2019) 415–423, https://doi.org/10.1016/j.jep.2019.02.034.

[33] F.A. Badria, B.R. Mikhaeil, G.T. Maatooq, M.M.A. Amer, Immunomodulatory Triterpenoids from the Oleogum Resin of Boswellia carterii Birdwood, Zeitschrift für Naturforschung C 58 (7–8) (2003) 505–516.

[34] A.J. Mora, G. Delgado, G. Díaz de Delgado, A. Usubillaga, N. Khouri, A. Bahsas, 3alpha-Hydroxytirucalla-7,24-dien-21-oic acid: a triterpene from Protium crenatum Sandwith, Acta Crystallogr. C 57 (Pt 5) (2001) 638–640.

3.4. Influence of traditionally used Nepalese plants on wound healing and immunological properties using primary human cells in vitro

Zimmermann-Klemd, A.M., Konradi, V., Steinborn, C., Ücker, A., Falanga, C.M., Woelfle, U., Huber, R., Jürgenliemk, G., Rajbhandari, M., Gründemann, C., 2019. Influence of traditionally used Nepalese plants on wound healing and immunological properties using primary human cells in vitro. Journal of Ethnopharmacology 235, 415–423.

Nepal has a long-lasting tradition of using medicinal plants. Extracts of nine different plants, which were traditionally used for the treatment of inflammatory skin injuries, were investigated for their immune modulatory effects and their capacity to support wound healing. An ethyl acetate extract of *Gmelina arborea* was shown to improve the wound closure of human keratinocytes and fibroblasts. Furthermore, the *G. arborea* extract and an ethyl acetate extract of *Bassia longifolia* suppressed the proliferation, the IL-2 and IFN-γ secretion, and the degranulation capability of stimulated T lymphocytes. Finally, an increase in the IL-8 secretion by stimulated DCs for both plant extracts was detected.

My contribution: I designed all experiments and supervised a medical student to perform the experiments. I analyzed all data, calculated the statistics and prepared all figures. Finally, I wrote the draft manuscript. This work also yielded the doctoral dissertation of Viktoria Konradi.

Amy Marisa Zimmermann-Klemd

Journal of Ethnopharmacology 235 (2019) 415–423

Contents lists available at ScienceDirect

Journal of Ethnopharmacology

journal homepage: www.elsevier.com/locate/jethpharm

Influence of traditionally used Nepalese plants on wound healing and immunological properties using primary human cells in vitro

Amy M. Zimmermann-Klemd[a], Viktoria Konradi[a], Carmen Steinborn[a], Annekathrin Ücker[a], Chiara Madlen Falanga[a], Ute Woelfle[b], Roman Huber[a], Guido Jürgenliemk[c], Meena Rajbhandari[d], Carsten Gründemann[a,*]

[a] Centre for Complementary Medicine, Institute for Infection Prevention and Hospital Epidemiology, Faculty of Medicine, University of Freiburg, Breisacher Straße 115 B, 79106 Freiburg, Germany
[b] Research Centre skinitial, Department of Dermatology, University Medical Center, Hauptstraße 7, 79104 Freiburg, Germany
[c] University of Regensburg, Pharmaceutical Biology, Faculty of Chemistry and Pharmacy, Universitätsstr. 31, 93053 Regensburg, Germany
[d] Research Centre for Applied Science and Technology (RECAST), Tribhuvan University, Kirtipur, Kathmandu, Nepal

ARTICLE INFO

Classifications:
Skin

Keywords:
Immunomodulation
Inflammation
Lymphocytes
Traditional medicine Asia & Oceania
Wound healing

ABSTRACT

Ethnopharmacological relevance: The improvement of wound healing has always been an important issue for both ethnopharmacological and modern medical research. In this study, we used state-of-the-art methods to investigate extracts of plants used traditionally in Nepal for more than 1000 years to treat inflammatory injuries.
Aim of the study: We focused on the potential of the plant extracts to ameliorate wound healing and to influence immune modulatory properties.
Materials and methods: Nine Nepalese plant extracts in three different solvents (methanol, ethyl acetate, petroleum ether) were immunologically characterised. Water-soluble tetrazolium (WST-1) assays and scratch assays were performed to determine their impact on viability and wound healing capacity of human keratinocytes and fibroblasts. Effects on proliferation, viability and function of physiologically relevant anti-CD3 and anti-CD28 stimulated primary human T lymphocytes were assessed using carboxyfluorescein succinimidyl ester (CFSE), annexin V/propidium iodide staining assays and flow cytometry–based surface receptor characterisation. The secretion level of interleukin-2 (IL-2) was analysed with the ELISA technique. Dendritic cells were generated out of peripheral blood mononuclear cells (PBMC) by $CD14^+$ magnetic bead selection. Flow cytometry-based surface receptor characterisation and ELISA-based technique were used to evaluate the DC activation state and the interleukin-8 (IL-8) secretion level.
Results: We demonstrate that an ethyl acetate extract of *Bassia longifolia* and of *Gmelina arborea* have anti-inflammatory capacities, indicated by reduced proliferation, inhibition of IL-2 secretion and degranulation capacity of activated human T cells, when compared with adequate concentrations of synthetic positive drug controls. Furthermore, *Gmelina arborea* improved the wound healing of keratinocytes and fibroblasts and has tendency to increase the secretion of IL-8 by human primary dendritic cells.
Conclusion: With this preliminary screening, we offer a scientific basis for the immunomodulatory properties of the two Nepalese medicinal plants *Bassia longifolia* and *Gmelina arborea*. However, further detailed studies regarding the responsible compounds are necessary.

1. Introduction

The skin is the largest organ of the human body and performs a range of functions. Aside from barrier functions based on mechanical resilience, the skin also provides immunological protection against environmental toxins and microbes (Braun-Falco, 2005; Matejuk, 2018). Injury to the skin therefore produces a decay of this function and can lead to unimpeded infiltration of pathogens (Singer and Clark, 1999). Research on pharmaceuticals that could improve the wound-healing process and thereby ameliorate this dysregulation of the immune system is therefore essential. The quest for new agents without harmful side effects has been extended to the field of natural products over the past few decades (Xie et al., 2015); with the continuous historical use of plants for medicinal purposes in many cultures,

* Corresponding author.
E-mail address: carsten.gruendemann@uniklinik-freiburg.de (C. Gründemann).

https://doi.org/10.1016/j.jep.2019.02.034
Received 30 October 2018; Received in revised form 13 February 2019; Accepted 17 February 2019
Available online 19 February 2019
0378-8741/

ethnobotanical research is an excellent choice for the development of drugs which could be applied in modern medicine (Kunwar et al., 2013).

Phytomedicine has a long tradition in Nepal and is still practised in rural communities (Malla et al., 2015; Manandhar, 1998; Shrestha et al., 2016). Nepal is a rich source of knowledge of medicinal plants that could be used for the treatment of inflammatory skin injuries (Kunwar et al., 2013). In the north-west Himalayan region, the juice of *Anaphalis busua* leaves is applied to cuts and wounds (Raturi et al., 2012), as well as the bark paste of *Bassia longifolia*, which can be used to treat cuts and wounds due to its anti-inflammatory abilities (Singh and Hamal, 2013). *Coccinia grandis, a precious medicinal plant with anti-oxidant capacities*, has edible fruits that also exhibit antibacterial activity against a range of gram positive and gram negative bacteria (Lee et al., 2015; Shaheen, 2009). Moreover, the leaves of *Coccinia grandis* contribute to the medical adaptability. Studies substantiate their antimicrobial activity (Bhattacharya et al., 2010) and anticancer activity on Swiss albino mice (Bhattacharya et al., 2011). A paste of *Drymaria diandra* can help to relief gastric problems with an inflammatory potential of the mucosa (Manandhar, 2002). Another plant with a variety of medical purposes is *Gmelina arborea*. Studies have noted anti-hyperglycaemic effects (Attanayake et al., 2013), while others have identified gastro-protective features against ethanol-induced ulcer of the stem bark in rats, based on antioxidative activity (Lawrence et al., 2016b). *Gmelina arborea* has also been shown to have anti-inflammatory properties on carrageenan-induced paw oedema in rats. This effect is likely related to an inhibition of the production or activity of inflammatory prostaglandins (Kulkarni et al., 2013; Lawrence et al., 2016a) and, in an animal model, dried leaves of *Gmelina arborea* have been shown to evoke a reduced inflammatory wound-healing response (Shirwaikar et al., 2003). The juice of *Hypericum cordifolium*, a plant that is barely investigated, can be used to treat gastrointestinal complaints (Manandhar, 2002). *Inula cappa* is relatively well-examined, and used in Chinese folk medicine for treating a variety of disorders, such as inflammatory immune disorders (Xie et al., 2007), and recent studies have described anti-inflammatory and immunomodulatory properties of the *Inula cappa* root (Kalola et al., 2017). Nepalese communities also widely exploit the plant *Rumex nepalensis*; orally taken roots can be used against gastro-intestinal complaints (Giday et al., 2009). Externally applied *Rumex nepalensis* root paste improves inflammation at the gum side (Manandhar, 2002). Another traditionally used plant is *Smilax ovalifolia*, which is edible and whose roots are used by rural people from Nepal for medicinal purposes. *Smilax ovalifolia* is applied in the treatment of inflammatory skin problems and overwhelming immune disorders (Shah, 2015).

In the current study, we investigated defined extracts of traditionally used plants from Nepal for the treatment of inflammatory wounds, to evaluate their potential for improving wound healing and the modulation of inflammatory immune dysfunction. The collection sites for the plants used can be seen in the map of Nepal (Fig. 1). Cell-based in vitro assays with human primary immune cells were used to screen and clarify the biological activity.

2. Materials and methods

2.1. Plant material and collection sites

Plants were collected from different parts of Nepal at the end of 2015 and the beginning of 2016. The plants were authenticated by Professor Sangeeta Rajbhandari, Central Department of Botany, Tribhuvan University. Voucher specimens were deposited at the Research Centre for Applied Science and Technology (RECAST), Tribhuvan University, Kathmandu, Nepal. The names of the plants, respective families, local names, parts used, collection dates and voucher numbers are given below.

Species and life form	Family	Local name	Part used	Collection site	Voucher number
Anaphalis busua, Herb	Compositae	Taptap mhendo	Whole plant	Nagarkot	AB-16-MR
Bassia longifolia, Tree	Sapotaceae	Mauwa	Bark	Kailali	BL-16-DPP
Coccinia grandis, Climbing herb	Cucurbitaceae	Golkakri	Aerial part	Dhading	CG-15-TPK
Drymaria diandra, Diffuse herb	Carylophyllaceae	Abijalo	Aerial part	Bhaktapur	DD-16-SK
Gmelina arborea, Tree	Verbenaceae	Khamari	Bark	Jhapa	GA-16-DB
Hypericum cordifolium, Shrub	Guttiferae	Areli	Flower	Nagarkot	HC-16-MR
Inula cappa, Shrub	Compositae	Gaitihare	Leaf	Dhading	IC-15-TPK
Rumex nepalensis, Herb	Polygonaceae	Halhale	Leaf	Shivapuri	RN-16-MR
Smilax ovalifolia, Twining shrub	Smilacaceae	Kukurdiano	Root	Kailali	SM-16-DPP

Plant names, families, local names, parts used, collection sites and voucher numbers.

2.2. Plant extraction

Each plant was mixed with sea sand (1 + 1), placed in glass columns (35 × 5 cm) and subsequently percolated with 1 L petroleum ether (PE), 1.8 L ethyl acetate (EA) and 2.3 L methanol (ME) and then eluted at room temperature to get a lipophilic, middle polar and polar extract of each drug. All extracts were dried with a rotary evaporator and by lyophilisation. *Anaphalis busua* herb (25.62 g) yielded 0.38 g PE, 0.21 g EA and 0.67 g ME extract; *Bassia longifolia* bark (67.82 g) yielded 0.86 g PE, 0.15 g EA and 9.24 g ME extract; *Coccinia grandis* herb (54.17 g) yielded 1.1 g PE, 0.53 g EA and 4.81 g ME extract; *Drymaria diandra* herb (35.64 g) yielded 0.36 g PE, 0.86 g EA and 6.76 g ME extract; *Gmelina arborea* bark (75.38 g) yielded 3.15 g PE, 0.99 g EA and 17.6 g ME extract; *Hypericum cordifolium* flowers (67.62 g) yielded 4.8 g PE, 2.17 EA and 13.98 g ME extract; *Inula cappa* leaves (51.52 g) yielded 1.99 g PE, 1.29 g EA and 6.14 g ME extract; *Rumex nepalensis* leaves (54.95 g) yielded 0.68 g PE, 0.45 g EA and 7.72 g ME extract; *Smilax ovalifolia* roots (44.30 g) yielded 0.09 g PE, 0.2 g EA and 1.84 g ME extract.

2.3. Ethics statement

All experiments conducted on human material were approved by the ethics committee of the University of Freiburg (235/11; 22.06.11). The present study was performed according to international, national and institutional rules considering animal experiments, clinical studies and biodiversity rights.

2.4. Keratinocytes and fibroblast cell culture

The spontaneously immortalized human keratinocyte cell line HaCaT (from CLS, Heidelberg, Germany) was cultured in Dulbecco's modified essential medium DMEM (Invitrogen GmbH, Karlsruhe, Germany) containing 10% foetal calf serum (FCS; PAA, Pasching, Austria) at 37 °C in a humified atmosphere with 5% CO_2Normal human

Fig. 1. Map of Nepal with collection sites of plants.

dermal fibroblasts (NHDF) were isolated from human foreskin as described (Heinemann et al., 2011) and routinely used between passage 3 and 6.

2.5. WST assay

WST assays were performed with keratinocytes and fibroblasts (4×10^5/ml). Attachment of the cells was enabled by 24 h cultivation at 37 °C, after which, plant extracts in different concentrations (1.23 µg/ml, 3.7 µg/ml, 11.11 µg/ml, 100 µg/ml) or control substances were added. After another 24 h incubation at 37 °C, the cells were washed with PBS and stained with 100 µl WST-1 solution (Roche, Indianapolis, IN) per well. Cells were further incubated for 2 h at 37 °C and analysed with an ELISA Reader (Tecan Reader Infinite M 200) at 450 nm. An untreated sample (NC), a sample treated with camptothecin (CPT, 300 µM) (control for apoptosis) and a sample treated with Triton-X 100 (0.5%) (control for necrosis) served as controls.

2.6. Scratch assay

Scratch assays adjusted according to Jonkman et al. (2014) were performed with the keratinocyte cell line HaCaT and primary human fibroblasts. Two confluent cell layers were cultivated in 2 well silicone micro inserts with a defined cell-free gap (ibidi GmbH, Martinsried, Germany) 70 µl cell suspension (8×10^5 cells/ml for HaCaT cells and 5.7×10^5 cells/ml for fibroblasts)were poured into each well. After 24 h incubation at 37 °C, plant extracts (20 µg/ml) in medium were added. The size of the gap between the two cell layers was determined by microscopy camera until the cell-cell contacts were recovered. An untreated sample (negative control, NC) and a sample treated with PDGF (50 ng/ml) (positive control, PC) were used as controls

2.7. Preparation and cultivation of human peripheral lymphocytes

Peripheral blood mononuclear cells (PBMCs) were isolated from the blood of healthy adult donors obtained from the Blood Transfusion Centre (University Medical Centre, Freiburg, Germany). Venous blood was centrifuged on a LymphoPrep gradient (density: 1.077 g/cm3, 20 min, 500 × *g*, 20 °C; Progen, Heidelberg, Germany). After centrifugation, cells were washed twice with PBS and subsequently cultured in RPMI 1640 medium supplemented with 10% heat-inactivated foetal calf serum, 2 mM L-glutamine, 100 U/ml penicillin and 100 U/ml streptomycin (all from Life Technologies, Paisley, UK). The cells were cultured at 37 °C in a humidified incubator with a 5% CO_2/ 95% air atmosphere.

2.8. Activation and treatment of lymphocytes

Lymphocytes were stimulated with anti-human CD3 (clone HIT3a) and anti-human CD28 (clone 28.2) mAbs (each 100 ng/ml; both from eBioscience, Frankfurt, Germany) as indicated by the presence of the medium, ciclosporin A (CsA; 5 µg/ml; Sandimmun 50 mg/ml, Novartis Pharma, Basel, Switzerland), camptothecin (CPT; 300 µM: Tocris, Bristol, UK), 0.5% Triton-X 100 or plant extracts in different concentrations. After cultivation, the cells were assessed in biological tests as described.

2.9. Determination of apoptosis and necrosis of T cells

Cells were treated for 48 h. Cultured cells were washed with PBS and stained with annexin V-FITC using an apoptosis detection kit (eBioscience, Frankfurt, Germany), according to manufacturer instructions. Propidium iodide (PI; eBioscience, Frankfurt, Germany) was then added and the cells were stained for 15 min at room temperature in the dark. Apoptosis and necrosis rates were determined by flow cytometric analysis using a FACSCalibur analyser (BD Biosciences, Becton Dickinson, Franklin Lakes, NJ).

2.10. Determination of T cell proliferation

The proliferation of T lymphocytes was determined using CFSE-stainings, as described earlier (Parish et al., 2009; Gründemann et al., 2012). For the determination of cell proliferation, lymphocytes were isolated, washed twice in cold PBS and resuspended in PBS at a concentration of 5×10^6 cells/ml. Cells were stained for 10 min at 37 °C with carboxyfluorescein diacetate succinimidyl ester (CFSE; 5 µM:

Sigma-Aldrich, St. Louis, MO). The staining reaction was stopped by washing twice with complete medium. Stained cells were treated for 72 h. The cell division progress was analysed by flow cytometric analysis using a FACSCalibur analyser (BD Biosciences, Becton Dickinson, Franklin Lakes, NJ).

2.11. Analysis of activation markers of T cells

The activation state of T lymphocytes can be determined via cell surface analysis of CD25 and CD69, as depicted in Gründemann et al. (2014). Cells were treated for 24 h. Cultured cells were washed with PBS and stained with PE-labelled anti-human CD25 mAbs, FITC-labelled anti-human CD69 and, for the differentiation of $CD4^+$ and $CD8^+$ T cells, with APC-labelled anti-human CD4 mAb (all from eBioscience, Frankfurt, Germany) for 20 min at 4 °C. Afterwards, the cells were washed twice with PBS, resuspended and transferred into FACS vials. The expression of the IL-2 surface receptor α-chain CD25 and CD69 was measured for $CD4^+$ and $CD8^+$ T cells, respectively, by FACS analysis using a FACSCalibur analyser (BD Biosciences, Becton Dickinson, Franklin Lakes, NJ).

2.12. Cytokine determination of T cells

Cells were treated for 20 h and re-stimulated with PMA (50 ng/ml) and ionomycin (500 ng/ml) for an additional 4 h. Supernatants were harvested by centrifugation and were stored at − 20 °C. The amount of cytokines was measured and quantified using the ELISA technique according to the manufacturer's instructions (Affymetrix, Frankfurt, Germany).

2.13. Analysis of T cell degranulation

A CD107a surface staining was performed, as described in Gründemann et al. (2013), to determine the T cell degranulation capacity. Cells were treated for 20 h and re-stimulated for 4 h with PMA (50 ng/ml) and ionomycin (500 ng/ml). To each well containing 200 µl of cell suspension, 2.5 µl PE-conjugated anti-CD107a mAb (eBioscience, Frankfurt, Germany) was added. After incubation at 37 °C for 1 h, 2 µl of 1/10 diluted GolgiStop (Becton Dickinson, Franklin Lakes, NJ) was added per well, and the plates were incubated for another 3 h. Samples were analysed with a FACSCalibur analyser (BD Biosciences, Becton Dickinson, Franklin Lakes, NJ).

2.14. Generation and maturation of immature monocyte-derived dendritic cells (DC)

Immature DCs were generated, after $CD14^+$ positive selection using the EasySep $CD14^+$ positive selection kit, together with the EasySep magnet, as instructed by the manufacturer (all products from StemCell Technologies, Grenoble, France) and described previously (Steinborn et al., 2017). For generation of DCs, the cells were cultured in serum-free CellGro DC medium (CellGenix, Freiburg, Germany), supplemented with 800 U/ml recombinant human IL-4 (PeproTech, Hamburg, Germany) and 1000 U/ml recombinant human GM-CSF (Leukine [sargramostim]; Bayer, Leverkusen, Germany). DCs were cultivated at a density of 1.6×10^6 cells/ml with medium (NC), parthenolide (20 µM) or plant extracts for 96 h at 37 °C in a 5% CO_2/ 95% air atmosphere. DCs (DC Stim) were stimulated after 24 h using a maturation cocktail (500 ng/ml LPS; Sigma-Aldrich, Taufkirchen, Germany); 50 ng/ml TNFα and 10 ng/ml IL-1β (both from PeproTech, Hamburg, Germany). After 96 h of cultivation, supernatants were harvested by centrifugation and were stored at − 20 °C. Cells were assessed in biological tests as described.

2.15. Surface receptor analysis of DCs

The effects of plant extracts and controls on DC maturation were determined by measuring surface receptor expression (anti-human CD83 mAbs; both from eBioscience, Frankfurt, Germany; anti-human HLA-DR; BD Biosciences, Heidelberg, Germany) using live cell gating in flow cytometric analysis with a FACSCalibur flow cytometer (BD Biosciences, Becton Dickinson, Franklin Lakes, NJ) and BD CellQuest Pro software, as performed in Steinborn et al. (2017).

2.16. Cytokine determination of DCs

The mediator IL-8 and were detected and analysed in the supernatants of cultured cells using the ELISA technique (Affymetrix, Frankfurt, Germany) or a LEGENDplex™ assay (Biolegend, San Diego) according to the manufacturer's instructions.

2.17. Analysis of data

For statistical analysis, data was processed with Microsoft Excel and SPSS software (IBM, Version 22.0, Armonk, USA). Statistical significance was determined with the SPSS software by a one-way ANOVA, followed by Dunnett's post hoc pairwise comparisons or by paired two-sample *t*-tests. For not normally distributed data statistical significance was calculated with the SPSS software using the Mann-Whitney-*U* test for independent samples or the Kruskal-Wallis test for independent samples with more than two values. Values are presented as mean ± SD for the indicated number of independent experiments. The asterisks represent significant differences from controls (*$p < 0.05$, **$p < 0.01$, ***$p < 0.001$).

3. Results

3.1. Impact of Nepalese plant extracts on wound-healing properties of human keratinocytes and fibroblasts

All nine Nepalese plant extracts screened in this study have been described as possessing wound-healing properties. We therefore addressed the possible wound-healing promoting effects on the human HaCaT keratinocyte cell line and primary human fibroblasts using a scratch assay. Results demonstrated no improvement in wound healing by most of the tested plant extracts (Supplementary Figs. A and B). However, the ethyl acetate extract of *Gmelina arborea* displayed a distinct wound-healing effect, in comparison with the synthetic PDGF positive control used for the human cells (Fig. 2). The effects for keratinocytes reached significance, as well as the effects of the other setting with fibroblasts (Figs. 2 and 3). The results indicate that toxic influence can be widely excluded, since no effects of the used extract concentrations on cell viability, expressed by mitochondrial activity (Supplementary Figs. C and D), could be identified. Considering the capacity to improve the wound healing of keratinocytes and fibroblasts, as well as the absence of cytotoxicity, the *Gmelina arborea* ethyl acetate extract was shown to be the most promising candidate for further investigation.

3.2. Effects of Nepalese plant extracts on proliferation capacity of human activated lymphocytes

To analyse the impact of the plant extracts on proliferation capacity of human T lymphocytes, cell division assays were performed (Supplementary Fig. E). Double stainings with annexin V and PI showed that immunosuppressive effects were based on either induction of apoptosis or necrosis (Supplementary Fig. E, F and G). *Gmelina arborea*, and a second plant, *Bassia longifolia*, decreased T lymphocyte proliferation in a non-cytotoxic concentration range (Fig. 4).

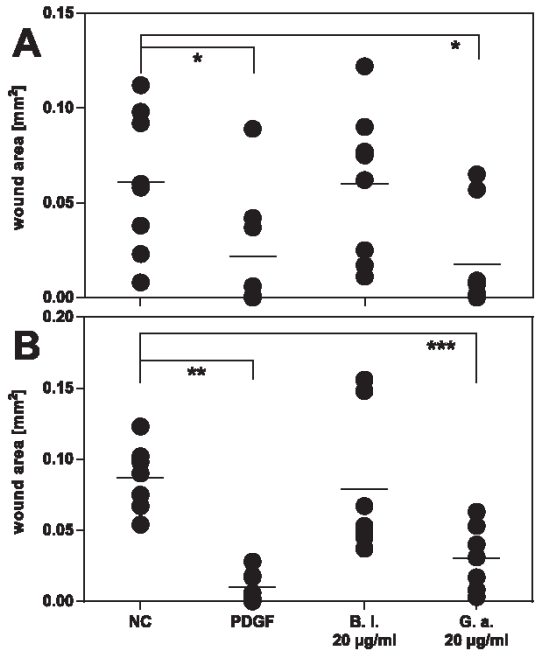

Fig. 2. Effects of *Gmelina arborea* ethyl acetate extract on migration and proliferation of keratinocytes (A) and fibroblasts (B). Cells (5.7×10^5 cells/ml) were cultivated in two confluent cell layers using micro-inserts. After 24 h of cultivation, the micro-inserts were removed and either *Bassia longifolia* (B. l.) or *Gmelina arborea* (G. a.) ethyl acetat extract [20 µg/ml each] and medium were added. An untreated sample (NC) and a sample treated with PDGF (50 ng/ml, PC) were used as controls. Microscopic image acquisition of eight independent experiments was performed after 18–30 h. *p < 0.05, **p < 0.01, ***p < 0.001.

3.3. Influence of Bassia longifolia and Gmelina arborea on function of human primary T lymphocytes

Further immunological characterisation of the impact on T cell activation was performed, based on non-cytotoxic concentrations of *Bassia longifolia* and *Gmelina arborea*. Stimulation of T lymphocytes by antigen binding of the T cell receptor activates the T cells and gives rise to expression of specific activation markers (e.g. CD25 or CD69) on the cell surface (Malek, 2008; Sancho et al., 2005). Flow cytometric–based phenotyping of these markers on T cells showed a significant difference between untreated cells and cells treated with extracts of 100 µg/ml *Bassia longifolia* or *Gmelina arborea* (Fig. 5). For *Gmelina arborea* this

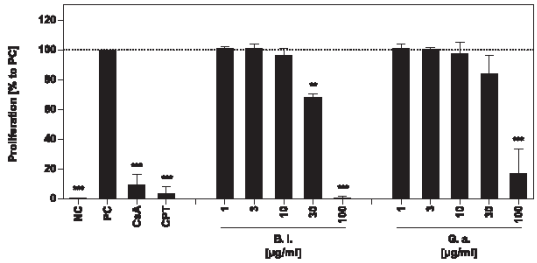

Fig. 4. Inhibitory effects of *Bassia longifolia* and *Gmelina arborea* ethyl acetate extracts on the proliferation of T lymphocytes. Lymphocytes were stained with CFSE, activated with anti-human CD3/CD28 mAb (100 ng/ml each) and incubated for 72 h with medium (positive control, PC), ciclosporin A (5 µg/ml, CsA), camptothecin (300 µM, CPT), either *Bassia longifolia* (B. l.) or *Gmelina arborea* (G. a.) ethyl acetate extract in different concentrations. Flow cytometric analysis of the cell division was performed after incubation. Data from three independent tests were summarised and are depicted as mean ± standard deviation in relation to the untreated, stimulated control (PC; = 100% ± SD). **p < 0.01, ***p < 0.001.

reduction reaches significance CD69 marker und $CD4^+$ T cells.

We therefore sought to determine if *Bassia longifolia* or *Gmelina arborea* extracts affected T lymphocyte functionality, specifically by the release of perforin and granzymes. The analysis of the lysosomal-associated membrane protein 1 (LAMP-1, CD107a) showed a weak dose-dependent impact of *Bassia longifolia* on degranulation capacity of activated T cells (Fig. 6). The influence of *Gmelina arborea* was stronger and reached significance in a concentration of 30 µg/ml.

T lymphocytes react to activation with the secretion of the pro-inflammatory, autocrine growth factor interleukin 2 (IL-2), which promotes interaction with its surface receptor, which in turn is expressed on the surface of activated T cells (Malek, 2008). This means that, besides IL-2 receptor expression, T cell proliferation is regulated by endogenous release of IL-2, and the inhibition of its production may explain the immunosuppressive effects. Enzyme-linked immunosorbent assays were performed and the results showed a dose-dependent reduction of IL-2 secretion for both *Bassia longifolia* and *Gmelina arborea* extracts (Fig. 7).

3.4. Influence of Bassia longifolia and Gmelina arborea on function of human primary DCs

IL-8 is secreted by mature DCs after skin injuries, to increase the cell migration rate of keratinocytes (Jiang et al., 2012). We therefore examined the influence of *Bassia longifolia* and *Gmelina arborea* extracts on maturation and mediator release status, expressed by higher surface expression of CD83 level of secretion of IL-8 by human primary DCs.

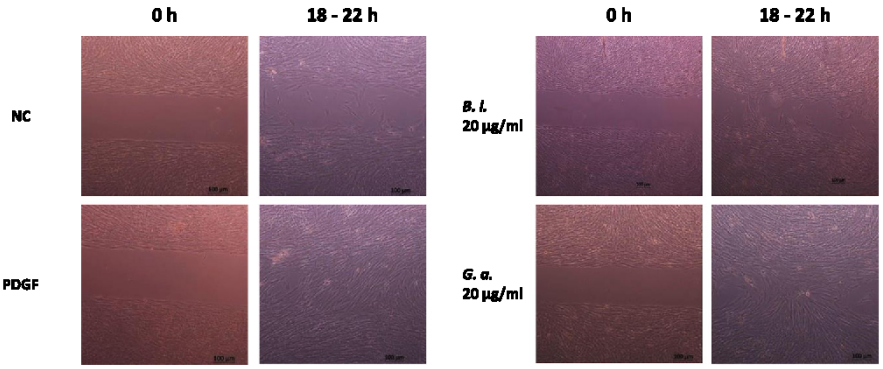

Fig. 3. Microscopic images (5 × objective magnification) of the fibroblast wound healing. Pictures were taken at different time points after addition of *Bassia longifolia* or *Gmelina arborea* ethyl acetate extract (20 µg/ml) or PDGF, compared with an untreated control (NC).

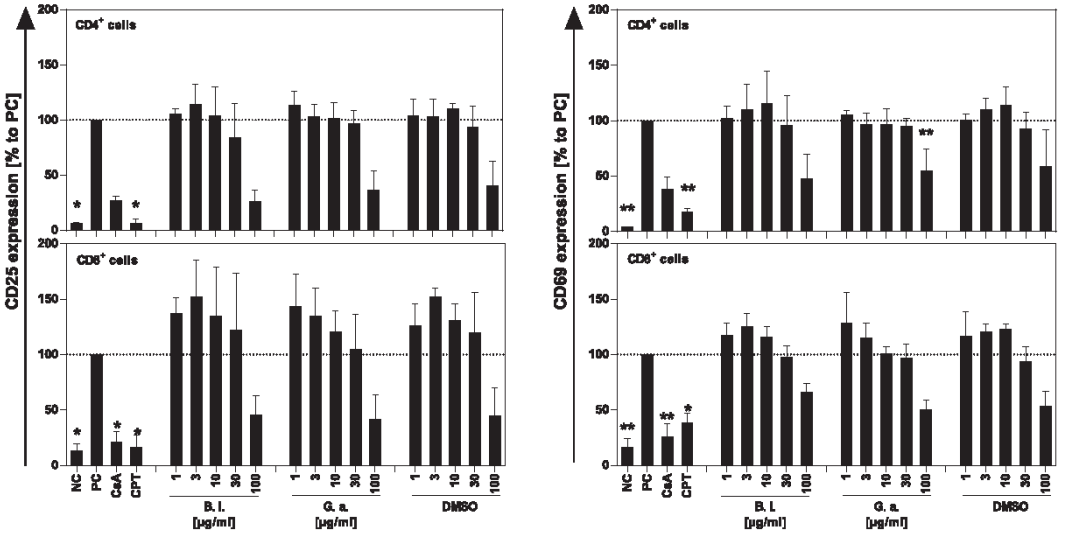

Fig. 5. Effects of *Bassia longifolia* and *Gmelina arborea* ethyl acetate extracts on the activation of $CD4^+$ and $CD8^+$ T lymphocytes. Lymphocytes were activated with anti-human CD3/CD28 mAb (100 ng/ml each) and incubated for 24 h with medium (PC), ciclosporin A (5 µg/ml, CsA), camptothecin (300 µM, CPT), and either *Bassia longifolia* (B. l.) or *Gmelina arborea* (G. a.) ethyl acetate extract or DMSO in relatively correlated concentrations. Cells were stained with CD69-FITC, CD25-PE and CD4-APC after incubation. Expression of surface markers (CD69, CD25, CD4) was analysed using flow cytometry. The amounts of activated $CD4^+$ and $CD8^+$ T lymphocytes were determined in three independent experiments. Results were summarised and are depicted as mean ± standard deviation in relation to the untreated, stimulated control. *p < 0.05, **p < 0.01.

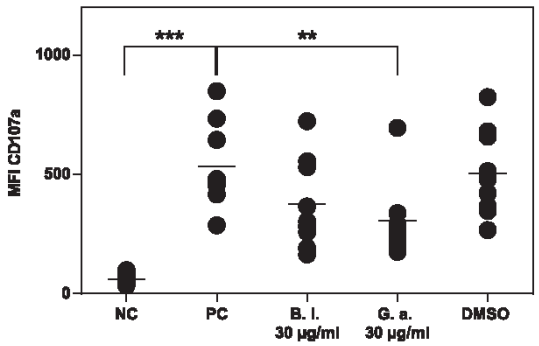

Fig. 6. Effects of *Bassia longifolia* and *Gmelina arborea* ethyl acetate extracts on the degranulation of T lymphocytes. Lymphocytes were activated with anti-human CD3/CD28 mAb (100 ng/ml each) and incubated for 20 h with medium (PC), camptothecin (300 µM, CPT), Triton-X 100 (3,3%) and either *Bassia longifolia* (B. l.) or *Gmelina arborea* (G. a.) ethyl acetate extract or DMSO in a relatively correlated concentration. Cells were re-stimulated with PMA (50 ng/ml) and ionomycin (500 ng/ml) for 4 h, stained with CD107a-PE after incubation, and the expression was analysed using flow cytometry. The amount of degranulating T lymphocytes was determined in eight independent experiments. Results were summarised and are depicted as mean ± standard deviation in relation to the untreated, stimulated control. **p < 0.01, ***p < 0.001.

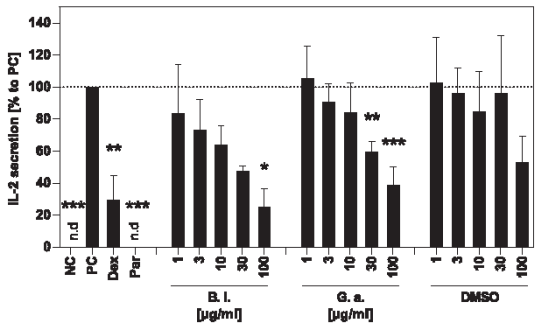

Fig. 7. Effects of *Bassia longifolia* and *Gmelina arborea* ethyl acetate extracts on the secretion of IL-2 by T cells. Lymphocytes were activated with anti-human CD3/CD28 mAb (100 ng/ml each) and incubated for 20 h with medium (PC), dexamethasone (10^{-4} M, Dex), parthenolide (20 µM, Par) and either *Bassia longifolia* (B. l.) or *Gmelina arborea* (G. a.) ethyl acetate extract or DMSO in relatively correlated concentrations. Cells were re-stimulated with PMA (50 ng/ml) and ionomycin (500 ng/ml) for 4 h, and supernatants were frozen. The supernatants were used to determine the IL-2 secretion via ELISA. Results of three independent experiments were summarised and are depicted as mean ± standard deviation in relation to the untreated, stimulated control. *p < 0.05, **p < 0.01, ***p < 0.001.

Treatment of DCs with extracts did not yield any changes of the activation marker CD83, indicating that there was no effect of *Bassia longifolia* or *Gmelina arborea* extract on the maturation status of DCs (Fig. 8). Experiments showed a weak increased IL-8 secretion for both extracts (Fig. 9). However, these effects did not reach significance.

4. Discussion

Phytomedicine has a long tradition in the treatment of inflammatory disorders, like poorly healing cuts and wounds, and so we investigated nine different traditionally applied Nepalese plants to ascertain whether there is a rational basis for their use. For this purpose, we addressed wound healing and immune modulatory effects in cell-based assays using the human keratinocyte cell line HaCaT, primary human fibroblasts or immunocompetent cells.

Our screen demonstrated that an ethyl acetate extract of *Gmelina arborea* improved the wound-healing response of human keratinocytes and fibroblasts after treatment (Figs. 2 and 3), where cytotoxicity of the applied concentrations was excluded (Supplementary Figs. C and D).

When tissue damage occurs, the immune system needs to prevent wound infection and, in parallel, initiate repair mechanisms for the affected skin area. We therefore addressed the potential parallel immune modulatory effects of the investigated Nepalese plants. An efficient wound-healing response requires both a pro-inflammatory

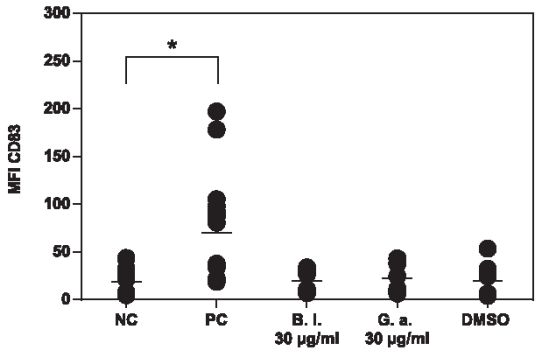

Fig. 8. Effects of *Bassia longifolia* and *Gmelina arborea* ethyl acetate extracts on the activation of dendritic cells. DCs derived from CD14$^+$ monocytes were incubated with medium (NC) and either *Bassia longifolia* (B. l.) or *Gmelina arborea* (G. a.) ethyl acetate extract or DMSO in a relatively correlated concentration. PC was stimulated with LPS, TNFα and IL1β. DC activation was determined by flow cytometric analysis of CD83. Results of eight independent experiments were summarised and are depicted as mean ± standard deviation in relation to the untreated, unstimulated control. *p < 0.05.

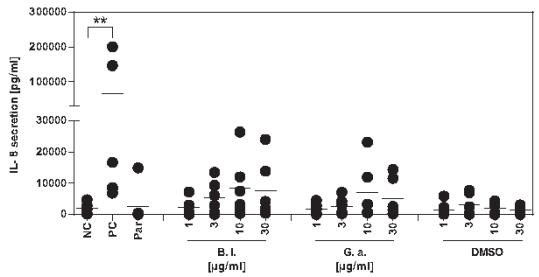

Fig. 9. Effects of *Bassia longifolia* and *Gmelina arborea* ethyl acetate extracts on the IL-8 secretion of dendritic cells. DCs derived from CD14$^+$ monocytes were incubated with medium (NC) and either parthenolide (20 µM, Par), *Bassia longifolia* (B. l.) or *Gmelina arborea* (G. a.) ethyl acetate extract or DMSO in relatively correlated concentrations. PC was stimulated with LPS, TNFα and IL1β. After maturation, supernatants were taken and frozen. The supernatants were used to determine IL-8 secretion. Results of six independent experiments were summarised and are depicted as mean ± standard deviation in relation to the untreated, unstimulated control. **p < 0.01.

feedback loop, to ensure pathogen removal, and an anti-inflammatory control loop, which avoids a fatal inflammatory response (Sen and Roy, 2008). We first examined the T cell proliferation-inhibiting potential of the extracts to address their ability to intervene in the anti-inflammatory feedback loop.

Our data showed that *Bassia longifolia* and *Gmelina arborea* extracts inhibited proliferation of activated T cells, without cytotoxic effects such as apoptosis and necrosis (Fig. 4 and Supplementary Figs. F and G).

Stimulation of the T cell receptor promotes the surface expression of the human transmembrane C-type lectin protein CD69 and the autocrine growth factor IL-2 (Malek, 2008). We found that *Bassia longifolia* and *Gmelina arborea* only have a weak influence on the activation of T cells, when measured by surface expression of activation markers CD69 and CD25 (Fig. 5). Activation of T cells also leads to the release of endogenous IL-2, which interacts with its surface receptor to promote T cell proliferation. Our results showed that both extracts reduced IL-2 cytokine production (Fig. 7). As IL-2 is pivotal for lymphocyte proliferation, the demonstrated inhibition of its production by the defined extracts could explain the observed inhibition of T cell proliferation.

To examine the pro-inflammatory T cell response, we investigated the degranulation capacity of T cells after treatment with both extracts by checking the expression of the lysosomal-associated membrane protein 1 (LAMP-1, CD107a), a surface marker present on degranulating lymphocytes. It was found that the *Bassia longifolia* and *Gmelina arborea* extracts have an influence on the degranulation of activated T cells (Fig. 6). Taking these results together, both extracts have anti-inflammatory capacity on human T cells.

Since DCs are crucial for effective wound healing, we then focused upon verifying the impact of the extracts on activation and function of human primary DCs. We found that treatment with the extracts did not change DC maturation/activation (Fig. 8). After injuries, IL-8 is secreted by DCs to increase the cell migration rate of keratinocytes (Jiang et al., 2012). We therefore concentrated on the function of DCs in producing IL-8. Our results revealed a weak positive influence of both extracts on the IL-8 secretion of DCs (Fig. 9), possibly explaining, at least partially, the wound-healing properties of the *Gmelina arborea* extract.

Wound healing is a very complex process requiring some highly regulated steps. Consequently, there are multiple avenues for plant extracts to improve wound healing. Both, *Bassia longifolia* and *Gmelina arborea*, extracts appear to restore the barrier function of the skin by facilitating re-epithelisation. The extracts marginally increased the IL-8 secretion of DCs, and thereby have the capacity to promote the migration of keratinocytes from the wound margin (O'Toole, 2001). For *Gmelina arborea*, our findings are consistent with the results by Shirwaikar et al. (2003), who reported increased re-epithelisation time and decreased collagen deposition following treatment with *Gmelina arborea* leaf extract. The findings of Kulkarni et al. (2013) suggested that *Gmelina arborea* possesses significant anti-inflammatory properties, as displayed in a Wistar rat inflammation model.

Bassia longifolia extract was also shown to improve immune suppressive properties, for the purpose of maintaining the balance of bacterial clearance and inflammation. A study from 2009 also described an anti-inflammatory effect of *Bassia longifolia*, reflected in a significant reduction of oedema in a carrageenan-induced inflammation model after treatment with an ethanol extract of *Bassia longifolia* seeds; this effect was verified in a formaldehyde-induced pain model and a cotton pellet granuloma model (Gaikwad et al., 2009). Another study postulated an improvement in wound healing due to a reduction of the epithelisation time, using *Bassia longifolia* bark extract (Akshatha et al., 2013).

The advantage of using plant extracts that have multi-component characteristics for the treatment of wounds and cuts lies in the combination of the chemical structures of the active compounds and their pharmacodynamic effects on the unbalanced skin area of a wound. Many different compounds can act together in synergy, thereby improving their efficacy (Colalto, 2018; Fürst and Zündorf, 2015). It is known from the literature that many plant compounds, such as flavonoids, given either orally or systemically, are absorbed and eliminated very quickly in humans (Scholz and Williamson, 2007). However, the extracts screened in the current study are traditionally used externally for poorly healing wounds. It may be possible, therefore, that relevant concentrations remain locally in the tissue for some time and continue to display their immunomodulatory properties. Furthermore, our investigations show that the concentrations of the used extracts can potentially be considered as clinically relevant, because the doses which were effective *in vitro* could be administered locally by topical application.

However, our study had some limitations. Up to now, we do not have determined the bioactive compounds which are responsible for the described effects of *Bassia longifolia* and Gmelina *arborea*. Thus, a subject for a following study would be the isolation and characterisation of bioactive compounds from *Bassia longifolia* and *Gmelina arborea* to confirm a compound-effect-relationship. Besides, *in vivo* experiments are needed to approve the observed effects of the plants in animals and humans.

5. Conclusion

In the present study, we screened for wound-healing properties of nine different plants. The plants have been applied as local therapy by the rural people of Nepal for more than 1000 years. For the *Bassia longifolia* and *Gmelina arborea* extracts, we can provide a potential mechanism that explains, at least partially, their traditional use in the treatment of wounds. However, further detailed studies regarding the identification of bioactive compounds will be necessary.

Acknowledgements

We thank Top Prasad Kapri, Saroj Kafle, Deepak Bhattarai and Damaru Prasad Paneru for helping to collect the plants and Vera Salwey and Martin Nagel for technical support.

Appendix information

List of authors

Author's name	Postal address	E-mail	Phone	Fax
Carsten Gründemann	Centre for Complementary Medicine, Institute for Infection Prevention and Hospital Epidemiology, Faculty of Medicine, University of Freiburg, Breisacher Straße 115 B, 79106 Freiburg, Germany	carsten.gruendemann@uniklinik-freiburg.de	++49(0)761/27083170	++49(0)761/27083210
Amy Marisa Zimmermann-Klemd		amy.klemd@uniklinik-freiburg.de	++49(0)761/27083220	++49(0)761/27083210
Viktoria Konradi		viktoria-konradi@gmx.de	++49(0)761/27083220	++49(0)761/27083210
Carmen Steinborn		carmen.steinborn@uniklinik-freiburg.de	++49(0)761/27083130	++49(0)761/27083210
Annekathrin Ücker		annekathrin.uecker@uniklinik-freiburg.de	++49(0)761/27083120	++49(0)761/27083210
Chiara Madlen Falanga		chiara.madlen.falanga@uniklinik-freiburg.de		
Roman Huber		roman.huber@uniklinik-freiburg.de	++49(0)761/27082010	++49(0)761/27083210
Ute Woelfle	Research Centre skinitial, Department of Dermatology, University Medical Centre of Freiburg, Hauptstraße 7, 79104 Freiburg, Germany	ute.woelfle@uniklinik-freiburg.de	++49(0)761/27068250	++49(0)761/27067831
Guido Jürgenliemk	University of Regensburg, Pharmaceutical Biology, Universitätsstraße 31, 93053 Regensburg, Germany	guido.juergenliemk@chemie.uni-regensburg.de	++49(0)941/9434758	++49(0)941/9434990
Meena Karmacharya	Research Centre for Applied Science and Technology, Tribhuvan University, Kathmandu, Nepal	Karmacharyameena@gmail.com	0097714330348	–

Appendix A. Supplementary material

Supplementary data associated with this article can be found in the online version at doi:10.1016/j.jep.2019.02.034.

References

Attanayake, A., Jayatilaka, K.P.W., Pathirana, C., Mudduwa, L.B., 2013. Study of anti-hyperglycaemic activity of medicinal plant extracts in alloxan induced diabetic rats. Anc. Sci. Life 32, 193–198. https://doi.org/10.4103/0257-7941.131970.

Braun-Falco, O., 2005. Dermatologie und Venerologie. Springer, Heidelberg.

Colalto, C., 2018. What phytotherapy needs: evidence-based guidelines for better clinical practice. Phytother. Res. PTR 32, 413–425. https://doi.org/10.1002/ptr.5977.

Fürst, R., Zündorf, I., 2015. Evidence-based phytotherapy in Europe: where do we stand? Planta Med. 81, 962–967. https://doi.org/10.1055/s-0035-1545948.

Gaikwad, R.D., Ahmed, M.L., Khalid, M.S., Swamy, P., 2009. Anti-inflammatory activity of Madhuca longifolia seed saponin mixture. Pharm. Biol. 47, 592–597. https://doi.org/10.1080/13880200902902513.

Gründemann, C., Koehbach, J., Huber, R., Gruber, C.W., 2012. Do plant cyclotides have potential as immunosuppressant peptides? J. Nat. Prod. 75, 167–174. https://doi.org/10.1021/np200722w.

Gründemann, C., Thell, K., Lengen, K., Garcia-Käufer, M., Huang, Y.-H., Huber, R., Craik, D.J., Schabbauer, G., Gruber, C.W., 2013. Cyclotides suppress human T-lymphocyte proliferation by an interleukin 2-dependent mechanism. PLoS One 8, e68016. https://doi.org/10.1371/journal.pone.0068016.

Gründemann, C., Lengen, K., Sauer, B., Garcia-Käufer, M., Zehl, M., Huber, R., 2014. Equisetum arvense (common horsetail) modulates the function of inflammatory immunocompetent cells. BMC Complement Altern. Med. 14, 283. https://doi.org/10.1186/1472-6882-14-283.

Heinemann, A., He, Y., Zimina, E., Boerries, M., Busch, H., Chmel, N., Kurz, T., Bruckner-Tuderman, L., Has, C., 2011. Induction of phenotype modifying cytokines by FERMT1 mutations. Hum. Mutat. 32, 397–406. https://doi.org/10.1002/humu.21449.

Jiang, W.G., Sanders, A., Ruge, F., Harding, K.G., 2012. Influence of interleukin-8 (IL-8) and IL-8 receptors on the migration of human keratinocytes, the role of PLC-γ and potential clinical implications. Exp. Ther. Med. 3, 231–236. https://doi.org/10.3892/etm.2011.402.

Jonkman, J.E.N., Cathcart, J.A., Xu, F., Bartolini, M.E., Amon, J.E., Stevens, K.M., Colarusso, P., 2014. An introduction to the wound healing assay using live-cell microscopy. Cell Adhes. Migr. 8, 440–451. https://doi.org/10.4161/cam.36224.

Kalola, J., Shah, R., Patel, A., Lahiri, S.K., Shah, M.B., 2017. Anti-inflammatory and immunomodulatory activities of Inula cappa roots (Compositae). J. Complement. Integr. Med. 14. https://doi.org/10.1515/jcim-2016-0083.

Kulkarni, Y.A., Panjabi, R., Patel, V., Tawade, A., Gokhale, A., 2013. Effect of Gmelina arborea Roxb in experimentally induced inflammation and nociception. J. Ayurveda Integr. Med. 4, 152–157. https://doi.org/10.4103/0975-9476.118697.

Kunwar, R.M., Mahat, L., Acharya, R.P., Bussmann, R.W., 2013. Medicinal plants, traditional medicine, markets and management in far-west Nepal. J. Ethnobiol. Ethnomed. 9, 24. https://doi.org/10.1186/1746-4269-9-24.

Lawrence, L., Menon, S., K, D.M., Sivaram, V.P., Padikkala, J., 2016a. Inhibition of dimethylbenz(a)anthracene (DMBA) - croton oil-induced mouse skin tumorigenesis by Gmelina arborea with potential anti-inflammatory activity. J. Environ. Pathol. Toxicol. Oncol. Off. Organ Int. Soc. Environ. Toxicol. Cancer 35, 263–272. https://doi.org/10.1615/JEnvironPatholToxicolOncol.2016014572.

Lawrence, L., Menon, S., Vincent, S., Sivaram, V.P., Padikkala, J., 2016b. Radical scavenging and gastroprotective activity of methanolic extract of Gmelina arborea stem bark. J. Ayurveda Integr. Med. 7, 78–82. https://doi.org/10.1016/j.jaim.2016.06.003.

Lee, Y.H., Choo, C., Watawana, M.I., Jayawardena, N., Waisundara, V.Y., 2015. An appraisal of eighteen commonly consumed edible plants as functional food based on their antioxidant and starch hydrolase inhibitory activities: edible plants as functional food. J. Sci. Food Agric. 95, 2956–2964. https://doi.org/10.1002/jsfa.7039.

Malla, B., Gauchan, D.P., Chhetri, R.B., 2015. An ethnobotanical study of medicinal plants used by ethnic people in Parbat district of western Nepal. J. Ethnopharmacol. 165, 103–117. https://doi.org/10.1016/j.jep.2014.12.057.

Malek, T.R., 2008. The biology of interleukin-2. Annu. Rev. Immunol. 26, 453–479. https://doi.org/10.1146/annurev.immunol.26.021607.090357.

Manandhar, N.P., 2002. Plants and People of Nepal. Timber Press, Portland, OR.

Matejuk, A., 2018. Arch. Immunol. Ther. Exp. 66, 45. https://doi.org/10.1007/s00005-017-0477-3.

Giday, M., Asfaw, Z., Woldu, Z., 2009. Medicinal plants of the Meinit ethnic group of

Ethiopia: an ethnobotanical study. J. Ethnopharmacol. 124, 513–521. https://doi.org/10.1016/j.jep.2009.05.009.
N. Akshatha, K., Murthy, S., Lakshmidevi, N., 2013. Ethnomedical uses of Madhuca longifolia – A review. Int. J. Life Sci. Pharma Res. 3.
O'Toole, E.A., 2001. Extracellular matrix and keratinocyte migration. Clin. Exp. Dermatol. 26, 525–530.
Parish, C.R., Glidden, M.H., Quah, B.J.C., Warren, H.S., 2009. Use of the Intracellular Fluorescent Dye CFSE to Monitor Lymphocyte Migration and Proliferation. In: Coligan, J.E., Bierer, B.E., Margulies, D.H., Shevach, E.M., Strober, W. (Eds.), Current Protocols in Immunology. John Wiley & Sons, Inc, Hoboken, NJ, USA (https://doi.org/10.1002/0471142735.im0409s84).
Raturi, R., Sati, S.C., Singh, H., Sati, M.D., Badoni, P.P., 2012. Phytochemical examination of Anaphalis Busua leaves. In: Khemani, L.D., Srivastava, M.M., Srivastava, S. (Eds.), Chemistry of Phytopotentials: Health, Energy and Environmental Perspectives. Springer, Berlin, pp. 105–106 (https://doi.org/10.1007/978-3-642-23394-4_22).
Sancho, D., Gómez, M., Sánchez-Madrid, F., 2005. CD69 is an immunoregulatory molecule induced following activation. Trends Immunol. 26, 136–140. https://doi.org/10.1016/j.it.2004.12.006.
Scholz, S., Williamson, G., 2007. Interactions affecting the bioavailability of dietary polyphenols in vivo. Int. J. Vitam. Nutr. Res. 77 (3), 224–235. https://doi.org/10.1024/0300-9831.77.3.224.
Sen, C.K., Roy, S., 2008. Redox signals in wound healing. Biochim. Biophys. Acta 1780, 1348–1361. https://doi.org/10.1016/j.bbagen.2008.01.006.
Shah, R.K., 2015. A review on ethnobotanical uses of Smilax ovalifolia. Int. J. Herb. Med. 3 (2), 16–19.
Shrestha, N., Shrestha, S., Koju, L., Shrestha, K.K., Wang, Z., 2016. Medicinal plant diversity and traditional healing practices in eastern Nepal. J. Ethnopharmacol. 192, 292–301. https://doi.org/10.1016/j.jep.2016.07.067.
Shirwaikar, A., Ghosh, S., Rao, P.G.M., 2003. Effects of Gmelina arborea Roxb. leaves on wound healing in rats. J. Nat. Rem. 3, 45–48.
Singer, A.J., Clark, R.A.F., 1999. Cutaneous wound healing. N. Engl. J. Med. 341, 738–746. https://doi.org/10.1056/NEJM199909023411006.
Singh, A.G., Hamal, J.P., 2013. Traditional phytotherapy of some medicinal plants used by Tharu and Magar communities of western Nepal against dermatological disorders. Sci. World 11, 81–89. https://doi.org/10.3126/sw.v11i11.8558.
Steinborn, C., Klemd, A.M., Sanchez-Campillo, A.-S., Rieger, S., Scheffen, M., Sauer, B., Garcia-Käufer, M., Urech, K., Follo, M., Ücker, A., Kienle, G.S., Huber, R., Gründemann, C., 2017. Viscum album neutralizes tumor-induced immunosuppression in a human in vitro cell model. PLoS One 12, e0181553. https://doi.org/10.1371/journal.pone.0181553.
Xie, H.-G., Chen, H., Cao, B., Zhang, H.-W., Zou, Z.-M., 2007. Cytotoxic germacranolide sesquiterpene from Inula cappa. Chem. Pharm. Bull. (Tokyo) 55, 1258–1260.

Glossary

C: Celsius
CFSE: carboxyfluorescein succinimidyl ester
CPT: camptothecin
CsA: ciclosporin A
DC: dendritic cell
DMSO: dimethyl sulfoxide
DMEM: Dulbecco's modified Eagle medium
EDTA: ethylenediaminetetraacetic acid
EGF: epidermal growth factor
ELISA: enzyme-linked immunosorbent assay
FACS: fluorescence-activated cell sorting
FCS: foetal bovine serum
GM-CSF: granulocyte-macrophage colony-stimulating factor
h: hour
IFN-: interferon-
IGF-1: insulin-like growth factor 1
IL-: interleukin
KGF: keratinocyte growth factor
LPS: lipopolysaccharide
mg: milligram
ml: millilitre
ng: nanogram
mAb: monoclonal antibody
MACS: magnetic cell sorting
NC(s): negative control (s)
p: p-value
Par: parthenolide
PBMC: peripheral blood mononuclear cell
PBS: phosphate buffered saline
PC(s): positive control (s)
PDGF: platelet-derived growth factor
PE: phycoerythrin
Pen/Strep: penicillin/streptomycin
PI: propidium iodide
PMA: phorbol-12-myristat-13-acetate
RPMI: Roswell Park Memorial Institute medium
SD: standard deviation
TGF-ß: transforming growth factor beta
TNF-α: tumour necrosis factor alpha
µg: microgram
VEGF: vascular endothelial growth factor
WST-1: water-soluble tetrazolium

4. Conclusion and outlook

This work presents an established cell-based screening platform for the initial investigation of natural products. Three examples demonstrated that this platform is a powerful tool for identifying and characterizing potential novel leads from natural product sources.

TCM is a millennia-old medical concept that includes external practices (acupuncture, acupressure, cupping, and moxibustion), exercises (meditation, tai chi chuan, and qigong), and herbal and dietary therapies (Efferth et al., 2019). The success of the TCM concept is largely experienced-based; hence, evidence-based scientific research is needed to provide proof of the success of TCM applications (Efferth et al., 2019). Consequently, screening for the anti-inflammatory effects of extracts from plants, which have been applied in TCM for thousands of years, constitutes the central part of this study.

Proliferation of T lymphocytes follows a number of signal transduction steps, which are initiated upon stimulation of the cell via TCR. Proliferation inhibition is therefore a robust marker for anti-inflammatory effects. For this reason, proliferation inhibition was used as an initial parameter to screen plants for their anti-inflammatory capacity.

This study found that an ethyl acetate extract of *A. argyi* inhibited the proliferation of T lymphocytes in a concentration-dependent manner, with an IC_{50} of 16.2 µg/mL. Ideally, toxicity can be excluded for a defined bioactive concentration range (Liu, 2008). Induced apoptosis and necrosis was excluded as a cause of the anti-proliferative effects of *A. argyi* extract, suggesting a functional inhibition of T cell proliferation. The anti-proliferative capacity of *A. argyi* could be further defined as IL-2-dependent, since a concentration-dependent inhibition of the IL-2 secretion was observed upon treatment with *A. argyi* extract. The pro-inflammatory cytokine IL-2 autocrinely stimulates the proliferation and differentiation of T cells (Ross and Cantrell, 2018) and its inhibition therefore prevents proliferation.

The next steps of the research approach focused on the signaling transduction of activated T cells (described in 1.2). First, the impact of *A. argyi* extract on the activity of the *il-2* transcription factors NFAT, AP-1, and NF-κB was analyzed. Since an influence on the AP-1 activity could be excluded, an impact on the factors of the AP-1 signaling cascade seemed unlikely and was therefore not addressed. Investigation of relevant factors, downstream to upstream of NFAT, was performed, in order to relate the inhibition of NFAT activity to the reduced calcium flux of stimulated T cells upon treatment with *A. argyi* extract. It can be assumed that *A. argyi* has a direct impact on the calcium flux, because inhibition of factors upstream of the calcium flux, such as Lck, ZAP70, LAT, or PLCγ1, would also affect AP-1. However, IP3 and the IP3 receptors are qualified as targets and the impact of *A. argyi* on them should be a subject of prospective tests.

A more precise characterization of the calcium flux inhibition by *A. argyi* extract could also be investigated in the future. A question to be answered is whether *A. argyi* directly interferes with the

cell membrane channels that mediate the calcium flux. The most popular channel, regarding calcium flux, is the TCR inducible CRAC channel, but voltage-gated calcium channels and channels of the P2X family also play a role in calcium flux induction (Kliem et al., 2012; Yip et al., 2009). The use of specific channel agonists in combination with calcium flux experiments, as in this study, should help to evaluate a specific influence on any calcium channel. In addition, some efforts should be made to elucidate the suppression of the NF-κB activity by *A. argyi* extract.

Aside from research regarding the mode of action of *A. argyi*, HPLC-based activity profiling yielded six bioactive sesquiterpene lactone compounds (three guaianolides, two seco-guaianolides, and a guaianolide dimer) and a moderately active flavone jaceosidin. These seven compounds appear to be responsible for the anti-proliferative capacity of *A. argyi* (Reinhardt et al., 2019a). In plant extracts, many different compounds may act in combination and, thereby, add up to overall efficacy (Colalto, 2018; Fürst and Zündorf, 2015). These multi-component characteristics are very specific, and the elucidation of the compound interaction is extremely interesting; therefore, the NFAT and NF-κB transcription factor analysis was repeated for the isolated compounds. Except jaceosidin, all the compounds inhibited the activity of NFAT and NF-κB. The influence of sesquiterpene lactones on NF-κB has been thoroughly described (García-Piñeres et al., 2001; García-Piñeres et al., 2004); therefore, investigation of the impact of the sesquiterpene lactone compounds of *A. argyi* on the NFAT signaling pathway was preferred. Nevertheless, it is already known that the sesquiterpene lactone helenalin suppresses the abundance and nuclear translocation of NFATc2 (Berges et al., 2009). In contrast to the *A. argyi* crude extract, none of the compounds, and no mixture of all compounds, including jaceosidin, showed any influence on the calcium flux of activated Jurkat T cells. These results point towards different modes of action of the crude extract and the isolated compounds, whereby the crude extract might affect cell biology through a more upstream level than the single isolated components.

Further examination should aim at describing the mode of action of the compounds. The target of the isolated compounds is expected to be downstream of the calcium flux and upstream of NFAT activity, because calcium flux was not affected but NFAT activity significantly suppressed. An impact of *A. argyi* active compounds on calmodulin seems unlikely, since calmodulin is composed of EF-hand domains, and the superfamily of EF-hand calcium binding proteins regulates diverse cellular activities, including metabolism, transcription, and cell proliferation (Bhattacharya et al., 2004; Carafoli and Krebs, 2016; Eldik and Watterson, 2012; Oku et al., 2017). Inhibition would imply massive toxic effects on the cells, which were not measurable with the crude plant extract. The phosphatase calcineurin would be a possible target; its activity can be addressed by either Western blot analysis of the phosphorylation state of NFAT or by using a commercial colorimetric test kit.

Further research would include the analysis of compounds that are responsible for the calcium inhibition of the *A. argyi* crude extract. HPLC-based activity profiling would need to be repeated, with microfractionation combined with calcium flux assays, rather than proliferation assays.

Moreover, pharmacological research should examine substance intake and metabolization and, finally, *in vivo* studies in a suitable model organism are required.

The initial screening of TCM plants revealed that, aside from the *A. argyi* ethyl acetate extract, a DCM extract of *B. carteri* suppressed the proliferation of activated T cells dose-dependently with an IC_{50} of 27.0 µg/mL. Induced apoptosis and necrosis was excluded as a cause of proliferation inhibition; however, a functional, IL-2 mediated inhibition was shown to be responsible for the observed effects.

HPLC-based activity profiling was performed and led to the identification of four bioactive compounds (3-O-acetyl-8,24-dienetirucallic acid, 3-O-acetyl-7,24-dienetirucallic acid, 3-oxo-8,24-dienetirucallic acid, and 3-O-acetyl-α-boswellic acid) with T cell proliferation inhibitory capacity. Transcription factor analysis of NFAT, AP-1, and NF-κB resulted in a reduction of the NFAT activity by all four compounds; AP-1 and NF-κB were not affected. The strongest activity suppression was registered for 3-O-acetyl-α-boswellic acid, making this compound the first choice for further research.

The exact mode of action of *B. carteri* extract and 3-O-acetyl-α-boswellic acid remains unknown and should be addressed by future studies. Possible targets here are IP3 or the IP3 receptor, as well as calcium flux or calcineurin, and their investigation should be done systematically.

Autoimmune diseases affect roughly 5% of the population and the incidence rate is rising, emphasizing the need for appropriate therapy options (Khan and Ghazanfar, 2018; Murphy and Weaver, 2016). Because available medications are attended by severe side effects or high costs, constant research on novel treatments is ongoing. Research on plant extracts has great potential for the development of innovative drugs, because the high number of plant species worldwide produces a variety of bioactive compounds with different, evolutionarily-optimized chemical scaffolds (Atanasov et al., 2015). Due to the vast number of plant species and related scaffolds a systematic and well-planned approach for plant-based drug discovery is required. Guidelines and exemplary studies may be very helpful in this context; hence, this study presents a procedure for basic plant-based drug discovery on the basis of *A. argyi* and *B. carteri*.

Aside from autoimmune diseases, the complex regulation of inflammatory reactions is also critical for the process of wound healing. For satisfactory wound healing, a balance of pathogen clearance by inflammatory feedback loops, and regulatory mechanisms to prevent fatal inflammatory responses, is essential (Sen and Roy, 2008). Nepal has a long-standing tradition of using medicinal plants for the

treatment of inflammatory skin injuries and, therefore, offers a promising field for wound-healing medication and drug discovery (Kunwar et al., 2013). The potential for improving wound healing and the modulation of inflammatory immune dysfunction of defined extracts from Nepalese plants, which are traditionally used to improve wound healing, was addressed in an *in vitro* study (Zimmermann-Klemd et al., 2019).

Ethyl acetate extracts of *B. longifolia* and *G. arborea* inhibited the proliferation of activated T lymphocytes concentration-dependently, without showing cytotoxic effects such as apoptosis and necrosis (Zimmermann-Klemd et al., 2019). The observed suppression of T cell proliferation could be linked to a decreased secretion of IL-2 (Zimmermann-Klemd et al., 2019). The degranulation capacity of stimulated T cells was shown to be reduced by treatment with 30 µg/mL of either *B. longifolia* or *G. arborea* extract, evidencing the anti-inflammatory potential of both extracts (Zimmermann-Klemd et al., 2019).

Generally, wound healing can be separated into four different phases, starting with the exudation phase, followed by the resorption phase and, finally, the proliferation and reparative phases. The exudation phase is characterized by the initiation of an inflammatory reaction (Diegelmann and Evans, 2004). The resorption phase starts with the secretion of pro-inflammatory cytokines to prevent the entry of bacteria (Guo and Dipietro, 2010). The proliferation phase and the reparative phase conduce the formation of granulation tissue, angiogenesis, and re-epithelization, followed by remodeling (Lippert et al., 2012; O'Toole, 2001). This step is distinguished by reduced proliferation and inflammatory activity (DiPietro, 1995). A prolonged inflammation phase usually implies a delayed remodeling process and matrix synthesis, indicating retarded wound closure and a higher pain level. Both extracts could help to improve wound healing when applied after the completed exudation and resorption phases. A possible field of application may also be for the treatment of chronic wounds, since those often stall in the inflammation phase (Frykberg and Banks, 2015).

In addition to the anti-inflammatory capacity, the study addressed the wound healing capacity of the Nepalese plant extract. The results showed that the ethyl acetate extract of *G. arborea* improved the wound-healing response of human keratinocytes and fibroblasts. Cytotoxicity of the applied concentrations was excluded (Zimmermann-Klemd et al., 2019). The wound healing capacity of *G. arborea* could be linked to a slightly enhanced secretion of IL-8 by DCs, which in turn increased the cell migration rate of keratinocytes (Jiang et al., 2012). This effect was observed for *G. arborea* ethyl acetate extract, as well as for *B. longifolia* ethyl acetate extract.

Taken together, the study presents two promising extracts with wound healing and anti-inflammatory capacity, but the characterization of bioactive compounds from *B. longifolia* and *G. arborea*, and

confirmation of compound–effect relationships, should be addressed in further studies. An additional topic that needs to be addressed is the route of administration. The extracts that were investigated in this study are traditionally applied topically to improve wound healing. A topical application may be favorable, since many plant compounds, such as flavonoids, are characterized by a low bioavailability when given orally (Thilakarathna and Rupasinghe, 2013). *In vivo* studies are needed to ascertain whether the applied concentrations act local and whether the *in vitro* observed effects can be seen *in vivo*.

There is a high demand for novel and innovative drugs, due to the limitations of currently available pharmaceuticals, including various side effects, nonresponding the development of bacterial or viral resistance, and high costs (Allison, 2000; Aslam et al., 2018; Daubert et al., 2017; Mathur and Hoskins, 2017; Río et al., 2009). Ethnobotanical research is an excellent choice for drug discovery, because plants have been historically used in many cultures (Kunwar et al., 2013). A well-planned, multidisciplinary research approach is essential; hence, this study provides the principles for a well-planned, multidisciplinary drug discovery approach based on three recent, promising examples, and thereby serves as a basis for future research projects.

References

Allison, A.C., 2000. Immunosuppressive drugs: the first 50 years and a glance forward. Immunopharmacology 47, 63–83.

Aslam, B., Wang, W., Arshad, M.I., Khurshid, M., Muzammil, S., Rasool, M.H., Nisar, M.A., Alvi, R.F., Aslam, M.A., Qamar, M.U., Salamat, M.K.F., Baloch, Z., 2018. Antibiotic resistance: a rundown of a global crisis. Infection and Drug Resistance 11, 1645–1658.

Atanasov, A.G., Waltenberger, B., Pferschy-Wenzig, E.-M., Linder, T., Wawrosch, C., Uhrin, P., Temml, V., Wang, L., Schwaiger, S., Heiss, E.H., Rollinger, J.M., Schuster, D., Breuss, J.M., Bochkov, V., Mihovilovic, M.D., Kopp, B., Bauer, R., Dirsch, V.M., Stuppner, H., 2015. Discovery and resupply of pharmacologically active plant-derived natural products: A review. Biotechnology Advances 33, 1582–1614.

Berges, C., Fuchs, D., Opelz, G., Daniel, V., Naujokat, C., 2009. Helenalin suppresses essential immune functions of activated $CD4^+$ T cells by multiple mechanisms. Molecular Immunology 46, 2892–2901.

Bhattacharya, S., Bunick, C.G., Chazin, W.J., 2004. Target selectivity in EF-hand calcium binding proteins. BBA-Biochimica Biophysica Acta 1742, 69–79.

Carafoli, E., Krebs, J., 2016. Why calcium? How calcium became the best communicator. Journal of Biological Chemistry 291, 20849–20857.

Colalto, C., 2018. What phytotherapy needs: Evidence-based guidelines for better clinical practice. Phytotherapy Research 32, 413–425.

Daubert, C., Behar, N., Martins, R.P., Mabo, P., Leclercq, C., 2017. Avoiding non-responders to cardiac resynchronization therapy: a practical guide. European Heart Journal 38, 1463–1472.

Diegelmann, R., F., 2004. Wound healing: an overview of acute, fibrotic and delayed healing. Frontiers in Bioscience 9, 283.

DiPietro, L.A., 1995. Wound healing: the role of the macrophage and other immune cells. Shock 4, 233–240.

Efferth, T., Xu, A.-L., Lee, D.Y.W., 2019. Combining the wisdoms of traditional medicine with cutting-edge science and technology at the forefront of medical sciences. Phytomedicine 64, 153078.

Eldik, L.J.V., Watterson, D.M., 2012. Calmodulin and signal transduction, 1st ed. Elsevier, Amsterdam.

Frykberg, R.G., Banks, J., 2015. Challenges in the treatment of chronic wounds. Advances in Wound Care 4, 560–582.

Fürst, R., Zündorf, I., 2015. Evidence-based phytotherapy in Europe: Where do we stand? Planta Medica 81, 962–967.

García-Piñeres, A.J., Castro, V., Mora, G., Schmidt, T.J., Strunck, E., Pahl, H.L., Merfort, I., 2001. Cysteine 38 in p65/NF-κB plays a crucial role in DNA binding inhibition by sesquiterpene lactones. Journal of Biological Chemistry 276, 39713–39720.

García-Piñeres, A.J., Lindenmeyer, M.T., Merfort, I., 2004. Role of cysteine residues of p65/NF-κB on the inhibition by the sesquiterpene lactone parthenolide and N-ethyl maleimide, and on its transactivating potential. Life Sciences 75, 841–856.

Guo, S., DiPietro, L.A., 2010. Factors affecting wound healing. Journal of Dental Research 89, 219–229.

Jiang, W.G., Sanders, A.J., Ruge, F., Harding, K.G., 2012. Influence of interleukin-8 (IL-8) and IL-8 receptors on the migration of human keratinocytes, the role of PLC-γ and potential clinical implications. Experimental and Therapeutic Medicine 3, 231–236.

Khan, U., Ghazanfar, H., 2018. T lymphocytes and autoimmunity, in: International review of cell and molecular biology. Elsevier, Amsterdam, 125–168.

Kliem, C., Merling, A., Giaisi, M., Köhler, R., Krammer, P.H., Li-Weber, M., 2012. Curcumin suppresses T cell activation by blocking Ca^{2+} mobilization and nuclear factor of activated T cells (NFAT) activation. Journal of Biological Chemistry 287, 10200–10209.

Kunwar, R.M., Mahat, L., Acharya, R.P., Bussmann, R.W., 2013. Medicinal plants, traditional medicine, markets and management in far-west Nepal. Journal of Ethnobiology and Ethnomedicine 9, 24.

Lippert, H. (Ed.), 2012. Wundatlas: Kompendium der komplexen Wundbehandlung, 3rd ed. Georg Thieme Verlag, Stuttgart.

Liu, Z., 2008. Preparation of botanical samples for biomedical research. Endocrine, Metabolic & Immune Disorders-Drug Targets 8, 112–121.

Mathur, S., Hoskins, C., 2017. Drug development: Lessons from nature. Biomedical Reports 6, 612–614.

Murphy, K., Weaver, C., 2016. Janeway's Immunobiology, 9th ed. Garland Science, New York, NY.

Oku, A., Imanishi, M., Noshiro, D., Murayama, T., Takeuchi, T., Nakase, I., Futaki, S., 2017. Calmodulin EF-hand peptides as Ca^{2+} -switchable recognition tags: Calmodulin EF-Hand Peptides. Biopolymers 108.

O'Toole, E.A., 2001. Extracellular matrix and keratinocyte migration. Clinical and Experimental Dermatology 26, 525–530.

Río, J., Comabella, M., Montalban, X., 2009. Predicting responders to therapies for multiple sclerosis. Nature Reviews Neurology 5, 553–560.

Ross, S.H., Cantrell, D.A., 2018. Signaling and function of interleukin-2 in T lymphocytes. Annual Review of Immunology 36, 411–433.

Scholz, S., Williamson, G., 2007. Interactions affecting the bioavailability of dietary polyphenols *in vivo*. International Journal for Vitamin and Nutrition Research 77, 224–235.

Sen, C.K., Roy, S., 2008. Redox signals in wound healing. BBA-Biochimica et Biophysica Acta 1780, 1348–1361.

Thilakarathna, S.H., Rupasinghe, H.P.V., 2013. Flavonoid bioavailability and attempts for bioavailability enhancement. Nutrients 5, 3367–3387.

Yip, L., Woehrle, T., Corriden, R., Hirsh, M., Chen, Y., Inoue, Y., Ferrari, V., Insel, P.A., Junger, W.G., 2009. Autocrine regulation of T cell activation by ATP release and P2X 7 receptors. The FASEB Journal 23, 1685–1693.

Zimmermann-Klemd, A.M., Konradi, V., Steinborn, C., Ücker, A., Falanga, C.M., Woelfle, U., Huber, R., Jürgenliemk, G., Rajbhandari, M., Gründemann, C., 2019. Influence of traditionally used Nepalese plants on wound healing and immunological properties using primary human cells in vitro. Journal of Ethnopharmacology 235, 415–423.

5. Acknowledgments

An erster Stelle möchte ich mich bei meinem Doktorvater Herrn Prof. Dr. Carsten Gründemann bedanken. Lieber Carsten, ich danke dir sehr für deine Unterstützung und das Vertrauen, das du mir stets entgegengebracht hast. Durch die Freiheit, die du mir bei der Durchführung meiner Arbeit gewährt hast, und die inspirierenden Gespräche habe ich gelernt, auf eigenen Beinen zu stehen und den Mut zu haben, meinem eigenem Urteil zu vertrauen.

Auch möchte ich mich bei Herrn Prof. Dr. Matthias Hamburger, meinem Zweitgutachter, bedanken. Lieber Professor Herr Hamburger, vielen Dank dafür, dass Sie stets ein offenes Ohr für mich hatten und sich immer Zeit für ein sorgfältiges, produktives Feedback genommen haben.

Außerdem geht mein Dank an Herrn Prof. Dr. Roman Huber für die Möglichkeit, meine Doktorarbeit in seiner Arbeitsgruppe am Uni-Zentrum Naturheilkunde anzufertigen. Lieber Roman, deine Wertschätzung und dein Vertrauen in mein Urteil haben mich in dieser Zeit oft bestärkt.

Bei Herrn Prof. Dr. Hajo Grundmann als Institutsleiter möchte ich mich für die Möglichkeit, meine Doktorarbeit am Institut für Infektionsprävention und Krankenhaushygiene zu erstellen, bedanken.

Herr Prof. Dr. Jörg Heilmann hat sich netterweise bereit erklärt, die Position des externen Experten anzunehmen. Vielen Dank dafür.

Ohne die Unterstützung meiner Kollaborationspartner wäre diese Arbeit nicht möglich gewesen.

Zunächst möchte ich hier Jakob Reinhardt nennen. Lieber Jakob, vielen Dank für die tolle Kooperation und deine zuverlässige, fachlich sehr gute Arbeit. Danke auch für die schöne und lustige Zeit bei unseren gemeinsamen Konferenzen und Treffen, deine geduldigen Versuche, mir – für mich – hoch komplexe Methoden zu erklären und dafür, dass du des Öfteren irgendwelche Zettel für mich irgendwo abgegeben hast. Ich finde, wir waren ein gutes Team!

Außerdem möchte ich mich ganz herzlich bei Herrn Prof. Dr. Wolfgang Schamel für die Möglichkeit, einige Versuche in seinem Labor am BIOSS Centre For Biological Signalling Studies durchzuführen, bedanken. Lieber Wolfgang, vielen Dank für auch die hilfreichen fachlichen Ratschläge und Diskussionen. Sie waren für mich sehr wertvoll und inspirierend. Ich weiß deine umfangreiche Unterstützung und dein Interesse an der Naturstoffforschung sehr zu schätzen.

Frau Dr. Anna Morath war mir bei meinen Versuchen am BIOSS Centre For Biological Signalling Studies eine wunderbare Hilfe. Liebe Anna, ich weiß, dass die Promotion eine wirklich sehr anstrengende Zeit ist. Vielen Dank, dass du mich trotz der Arbeit an deiner eigenen Dissertation so humorvoll und mit genialen Ratschlägen unterstützt hast.

Für die inspirierende Kooperation im Rahmen des Nepal-Projektes möchte ich mich auch bei Meena Karmacharya, Guido Jürgenliemk und Ute Woelfle bedanken. Und ein ganz besonderes Dankeschön geht an Viktoria Konradi, die im Rahmen ihrer medizinischen Doktorarbeit für einen Teil der Arbeiten verantwortlich ist.

Viel Sorge und Freude haben mir bei meiner Arbeit drei Reporterzelllinien bereitet, für deren Generierung ich mich ganz herzlich bei Dr. Peter Steinberger und Dr. Judith Leithner bedanken möchte.

Und selbstverständlich haben die vielen wundervollen Kollegen, die mich die letzten fünf Jahre hier am Uni-Zentrum Naturheilkunde begleitet haben, stark zur Aufrechterhaltung meiner Motivation beigetragen: Carmen Steinborn, Annekathrin Ücker, Viktoria Konradi, Gabriela Rentsch, Seema Devi, Chiara Falanga und Moritz Winker. Leute, ihr ahnt gar nicht, wie viel mir die vielen Kaffee-Pausen, die Bastel-Sessions, die vielen Gespräche – die ernsthaften und die weniger ernsthaften-, eure aufbauenden Worte und eure umfangreiche Unterstützung bedeuten!

Bei meinen Eltern und Geschwistern möchte ich mich ganz besonders bedanken. Lieber Papa, liebe Mama, lieber Noah, liebe Cara, danke, dass ihr mir zugehört habt, euch mit mir gefreut, mich getröstet und mir so viel Mut und Vertrauen geschenkt habt, meinen eigenen Weg zu gehen.

Zu guter Letzt möchte ich mich bei meinem Mann bedanken. Lieber Peter, ich bin dir unglaublich dankbar für deine Liebe und uneingeschränkte Unterstützung. Du hast mir die letzten fünf Jahre Mut gemacht, an mich geglaubt, hast mich in den Arm genommen und getröstet, hattest Verständnis für meine (oft hungerbedingten) Launen, hast dich mit mir geärgert und gefreut, hast mit mir große fachliche Diskussionen geführt, hast mit mir am Wochenende im Labor gestanden (insgeheim habe ich es doch gemocht), hast mit mir die Nadel im Heuhaufen gesucht, hast mir Ablenkung verschafft, hast mich manchmal gezwungen, mir Auszeiten zu nehmen und zu lernen, wie wichtig dies ist. Vielen Dank, dass du bei allen Aufs und Abs in dieser Zeit mit so viel Geduld und Liebe für mich da warst.

Curriculum vitae

PERSONAL DATA

Name:	Zimmermann-Klemd
First Name:	Amy Marisa
E-Mail:	amy_klemd@web.de
Mobile phone:	+49(0)17682099454
Date of birth:	20.03.1992
Nationality:	deutsch

EDUCATION

03/2017 – 04/2020	PhD Thesis (Division of Pharmaceutical Biology, Department of Pharmaceutical Sciences, University of Basel, Switzerland), Title: Effects of selected natural products on human immunocompetent cells
03/2017 – 04/2020	Doctoral studies (University of Basel, Switzerland)
03/2016 – 12/2016	Master Thesis (Center for Complementary Medicine, Institute for Infection Prevention and Hospital Epidemiology, Faculty of Medicine, University of Freiburg, Freiburg, Germany), Title: Einfluss von *Artemisia argyi* auf die Funktion von humanen Immunzellen, grade: 1.0
10/2014 – 12/2016	Master of Science (MSc) in Biology (University of Freiburg, Germany), grade: 1.4
03/2014 – 06/2014	Bachelor Thesis (Max Planck Institute for Terrestrial Microbiology, Faculty of Biology, University of Marburg, Marburg, Germany), Title: Funktion einer α-L-Arabinofuranosidase in *Ustilago* maydis, grade: 14 of 15 points
10/2011 – 06/2014	Bachelor of Science (BSc) in Biology (University of Marburg, Germany), grade: 2.0

WORK EXPERIENCE

07/2013 – 10/2013	Activity as a working student in the molecular research of the KWS SAAT SE & Co. KGaA (Einbeck, Germany)

ADDITIONAL QUALIFICATIONS

07/2018	Fortbildung Literaturrecherche, 10 Fortbildungseinheiten, Universitätsklinikum Freiburg, Studienzentrum
10/2019	Skills for Supervising Bachelor and Master Theses; Thesis-Supervision Skills: The Solution-Focus Approach, Graduate Center, University of Basel

LANGUAGES

German	Native language
English	Fluent
French	Basic knowledge

PUBLICATIONS, SHORT LECTTURES, POSTER PRESENTATIONS

Publications

Reinhardt, J.K., **Klemd, A.M.**, Danton, O., De Mieri, M., Smieško, M., Huber, R., Bürgi, T., Gründemann, C., Hamburger, M., 2019. Sesquiterpene lactones from *Artemisia argyi*: Absolute configuration and immunosuppressant activity. Journal of Natural Products 82, 1424–1433.

Zimmermann-Klemd, A.M., **Reinhardt, J.K.**, Morath, A., Schamel, W.W., Steinberger, P., Leitner, J., Huber, R., Hamburger, M., Gründemann, C., 2020. Immunosuppressive activity of *Artemisia argyi* extract and isolated compounds. Frontiers in Pharmacology 11.

Zimmermann-Klemd, A.M., Reinhardt, J.K., Nilsu, T., Morath, A., Falanga, C.M., Schamel, W.W., Huber, R., Hamburger, M., Gründemann, C., 2020. *Boswellia carteri* extract and 3-O-acetyl-alpha-boswellic acid suppress T cell function. Fitoterapia 146, 104694.

Zimmermann-Klemd, A.M., Konradi, V., Steinborn, C., Ücker, A., Falanga, C.M., Woelfle, U., Huber, R., Jürgenliemk, G., Rajbhandari, M., Gründemann, C., 2019. Influence of traditionally used Nepalese plants on wound healing and immunological properties using primary human cells *in vitro*. Journal of Ethnopharmacology 235, 415–423.

Gründemann, C., Arnhold, M., Meier, S., Bäcker, C., Garcia-Käufer, M., Grunewald, F., Steinborn, C., **Klemd, A.M.**, Wille, R., Huber, R., Lindequist, U., 2016. Effects of *Inonotus hispidus* extracts and compounds on human immunocompetent cells. Planta Medica 82, 1359–1367.

Steinborn, C., **Klemd, A.M.**, Sanchez-Campillo, A.-S., Rieger, S., Scheffen, M., Sauer, B., Garcia-Käufer, M., Urech, K., Follo, M., Ücker, A., Kienle, G.S., Huber, R., Gründemann, C., 2017. *Viscum album* neutralizes tumor-induced immunosuppression in a human *in vitro* cell model. PLoS ONE 12, e0181553.

Stadlbauer, S., Steinborn, C., **Klemd, A.**, Hattori, F., Ohmori, K., Suzuki, K., Huber, R., Wolf, P., Gründemann, C., 2018. Impact of green tea catechin ECG and its synthesized fluorinated analogue on prostate cancer cells and stimulated immunocompetent cells. Planta Medica 84, 813–819.

Rentsch, G., Steinborn, C., **Klemd, A.M.**, Kienle, G.S., Gründemann, C., Huber, R., 2018. Investigations on the constitutional types under consideration of anthropometric data, autonomic regulation and immunological parameters. Complementary Therapies in Medicine 40, 133–144.

Lederer, A.-K., Hannibal, L., Hettich, M., Behringer, S., Spiekerkoetter, U., Steinborn, C., Gründemann, C., **Zimmermann-Klemd, A.M.**, Müller, A., Simmet, T., Schmiech, M., Maul-Pavicic, A., Samstag, Y., Huber, R., 2019. Vitamin B12 status upon short-term intervention with a vegan diet - a randomized controlled trial in healthy participants. Nutrients 11, 2815.

Chilczuk, T., Steinborn, C., Breinlinger, S., **Zimmermann-Klemd, A.M.**, Huber, R., Enke, H., Enke, D., Niedermeyer, T.H.J., Gründemann, C., 2019. Hapalindoles from the *Cyanobacterium Hapalosiphon sp.* inhibit T cell proliferation. Planta Medica 86, 96-103.

Lederer, A.-K., Maul-Pavicic, A., Hannibal, L., Hettich, M., Steinborn, C., Gründemann, C., **Zimmermann-Klemd, A.M.**, Müller, A., Sehnert, B., Salzer, U., Klein, R., Voll, R.E., Samstag, Y., Huber, R., 2020. Vegan diet reduces neutrophils, monocytes and platelets related to branched-chain amino acids - A randomized, controlled trial. Clinical Nutrition. Published online: February 24, 2020

Short lectures

09/2019	Young Researchers Workshop of 67th International Congress and Annual Meeting of the Society for Medicinal Plant and Natural Product Research (GA), Innsbruck, Austria
10/2017	12th Freiburg Immunology Meeting (FIM)

Poster Presentations

09/2019	67th International Congress and Annual Meeting of the Society for Medicinal Plant and Natural Product Research (GA), Innsbruck, Austria
06/2018	Phytotherapiekongress, Vienna, Austria
09/2017	65th Annual Meeting of the Society for Medicinal Plant and Natural Product Research (GA), Basel, Switzerland